2018

DETERMINATION OF LIPID BILAYER AFFINITIES FOR SMALL MOLECULES USING CAPILLARY ELECTROPHORESIS AND COPOLYMER – STABILIZED LIPID BILAYER NANODISCS

William Michael Penny

DETERMINATION OF LIPID BILAYER AFFINITIES FOR SMALL MOLECULES USING CAPILLARY ELECTROPHORESIS AND COPOLYMER – STABILIZED LIPID BILAYER NANODISCS

By

William Michael Penny

Bachelor of Science with Honors in Chemistry, Seton Hall University, South Orange, New Jersey, 2012

Dissertation

Presented in partial fulfillment of the requirements for the degree of

Doctor of Philosophy in Analytical Chemistry

The University of Montana

Missoula, MT

August 2018

Approved by:

Scott Whittenburg, Dean of the Graduate School

Graduate School

Christopher P. Palmer, Ph.D.

Department of Chemistry and Biochemistry

Orion B. Berryman, Ph.D.

Department of Chemistry and Biochemistry

Michael D. DeGrandpre, Ph.D.

Department of Chemistry and Biochemistry

J.B. Alexander Ross, Ph.D.

Department of Chemistry and Biochemistry

J. Stephen Lodmell, Ph.D.

Division of Biological Sciences

Penny, William, Ph.D., August 2018 Analytical Chemistry

DETERMINATION OF LIPID BILAYER AFFINITIES FOR SMALL MOLECULES USING CAPILLARY ELECTROPHORESIS AND COPOLYMER – STABILIZED LIPID BILAYER NANODISCS

Advisor: Christopher Palmer

Chairperson: Michael DeGrandpre

Electrokinetic chromatography is a variation of capillary electrophoresis that allows for the separation of nonionic analytes by selective interaction with an ionic pseudostationary phase dissolved in the background electrolyte. The utility of electrokinetic chromatography to characterize pseudostationary phases and pseudostationary phase–solute interactions has been recognized since its introduction. The objective of this dissertation was to use electrokinetic chromatography and copolymer stabilized lipid bilayer nanodiscs as a pseudostationary phase to characterize small molecule-lipid bilayer interactions.

Styrene-maleic acid copolymers were used to stabilize cylindrical sections of lipid bilayer in solution, forming nanodiscs. The nanodiscs are formed based on strong hydrophobic interactions between the styrene moiety, on the copolymer, and the alkyl tails of the lipids. Using the nanodisc pseudostationary phase, the affinity of the bilayer structure for probe solutes was characterized. Linear solvation energy relationship analysis was employed to characterize the changes in solvent environment of the nanodiscs of varied copolymer to lipid ratio, copolymer chemistry and molecular weight, and lipid composition. Increases in the lipid to copolymer ratio resulted in smaller, more cohesive nanodiscs with greater electrophoretic mobility. Nanodisc structures with copolymers of different chemistry and molecular weight were compared and showed changes in solvent characteristics and selectivity. Seven phospholipid and sphingomyelin nanodiscs of different lipid composition were characterized. Changes in lipid head group structure had a significant effect on bilayer-solute interactions. In most cases, changes in alkyl tail structure had no discernible effect on solvation environment.

The nanodisc pseudostationary phase was also used to study sphingomyelin stereochemistry. Various studies have produced conflicting results regarding whether interactions with lipid bilayers are or can be stereoselective. Using sphingomyelin nanodiscs stereoselective interactions between a pair of atropisomers, R-(+)/(S)-(−) 1,1′-Bi-2-naphthol, were demonstrated.

Finally the dissociation constants between sphingomyelin nanodiscs and solvochromatic analytes were measured and then validated using steady state fluorescence. Using nanodisc affinity capillary electrophoresis, dissociation constants were derived on the same order of magnitude as the dissociation constants derived using the fluorescent technique. Future directions of this project will be to study peptide and protein interactions with lipid bilayers of interest.

Acknowledgements

Overall, my experience at the University of Montana has been an amazing one. I never could have imagined that my research project would have been as productive and as enjoyable, as it has been. My advisor Chris Palmer has been a phenomenal mentor; he set me up with a project that I became passionate about, provided thoughtful advice throughout the research process, and helped me secure a postdoc position with a respected professor in our field. I would like to also thank Sandy Ross, without his initial collaboration, I would not have a dissertation project. As well as the rest of my committee, whose constructive advice has guided me throughout my time at the University of Montana.

I would also like to thank Jesse, Julie, Virginia, Hannah, and Beth for making the Palmer lab a great work environment. Having supportive coworkers, who took the time to talk through research problems, made the research process less intimidating. I would also like to thank Asia, Dan, and Vanessa, graduate students, who have become my Montana family. By best friends were also a tremendous help, Grecia, who took the time to edit parts of my dissertation, and Marilyn and Nicole who provided amazing advice and emotional support throughout my time at the University of Montana.

Finally, I could not have accomplished any of this without the support of my family. My parents, Bill and Pat, have been an amazing support system prior to and during my time in Montana. Ryan and Allison, my siblings, have been instrumental in shaping me into the person that I am today.

Table of Contents

List of Figures

List of Tables

List of Equations

Abbreviations

ACE- Affinity Capillary Electrophoresis

BGE- Background Electrolyte

CE- Capillary Electrophoresis

EKC- Electrokinetic Chromatography

FA- Frontal Analysis

K_D- Dissociation Constant

LSER- Linear Solvation Energy Relationship Analysis

NACE- Nanodisc Affinity Capillary Electrophoresis

NEKC- Nanodisc Electrokinetic Chromatography

PSP- Pseudostationary Phase

SMA- Styrene-Maleic Acid

14:0 CL- cardiolipin

14:0 PC- 1,2-dimyristoyl-sn-glycero-3-phosphocholine

14: 1 PC- 1,2-dimyristoleoyl-sn-glycero-3-phosphocholine

14: 0 PE- 1,2-dimyristoyl-sn-glycero-3-phosphoethanolamine

14:0 PS- 1,2-dimyristoyl-sn-glycero-3-phospho-L-serine

16:0 PC- 1,2-dipalmitoyl-sn-glycero-3-phosphocholine

16:0 SM- Sphingomyelin, N-hexadecanoyl-D-e*rythro*-sphingosylphosphorylcholine

16:0-18:1 PC- 1-palmitoyl-2-oleoyl-glycero-3-phosphocholine

Chapter 1: Introduction to Capillary Electrophoresis, Lipid Bilayers and Biomimetic Systems Background and Theory

1. Overview

The objective of this dissertation research was to characterize the solvent environment of copolymer-stabilized lipid bilayer nanodiscs, utilizing electrokinetic chromatography. Copolymer stabilized nanodiscs consist of a cylindrical section of lipid bilayer stabilized by a styrene-maleic acid copolymer. These nanodiscs were originally developed for the spectroscopic study of membrane bound proteins.[1] Nanodiscs have been adapted for use in capillary electrophoresis as a pseudostationary phase for the first time. The future directions of the project are to study novel interactions between lipid bilayers of interest and small molecules, peptides, and proteins. However, before those noncovalent interactions can be studied and quantified, the nanodisc pseudostationary phase needed to be validated as a biomimetic system in electrokinetic chromatography. In order to study nanodisc pseudostationary phase solvent properties, I developed six research questions:

1. Will copolymer-stabilized nanodiscs be compatible as a pseudostationary phase?
2. How does the ratio of copolymer to lipid affect the nanodisc solvent environment?
3. How does copolymer chemistry affect the nanodisc solvent environment?
4. Does lipid bilayer chemistry affect nanodisc-solute interactions?
5. What role does stereochemistry play in lipid bilayer chemistry?
6. Can dissociation constants between nanodiscs and small molecules be accurately measured?

The answers to these questions are detailed in Chapters 3-7 of my dissertation.

1.1 Development of Capillary Electrophoresis (CE)

In 1937 Arne Tiselius demonstrated that the electrophoretic mobility of horse serum globulin protein was pH dependent because the pH of the horse serum globulin solution influenced the charge on the protein.[2] This discovery was subsequently followed by a series of experiments where alpha, beta, and gamma horse serum globulin proteins were separated based on their unique electrophoretic mobilities.[3] This groundbreaking work on electrophoresis resulted in a Nobel Prize for Tiselius in 1948.[4] In addition to a Nobel Prize, this work also laid the groundwork for the eventual development of capillary electrophoresis. In 1967, electrophoresis was performed for the first time in a 300 µm glass tube using UV absorbance for the detection of analytes.[5] Modern Capillary Electrophoresis (CE) was developed by Jorgenson and Lukacs in 1981 where the separations of amino acids and dipeptides occurred in glass capillaries with 75 µm internal diameters.[6] It was demonstrated that the small diameter of the capillary would reduce the effects of joule heating that resulted from the application of high voltages.[6] The optimization by Jorgenson and Lukacs led capillary electrophoresis instrumentation to become a valuable separation technique for analytical and bioanalytical chemists. As shown in Figure 1-1, the number of articles that contain the concept of capillary electrophoresis has increased dramatically since the article published by Jorgenson and Lukacs in 1981. Since CE is still a relatively new form of instrumentation new techniques are constantly

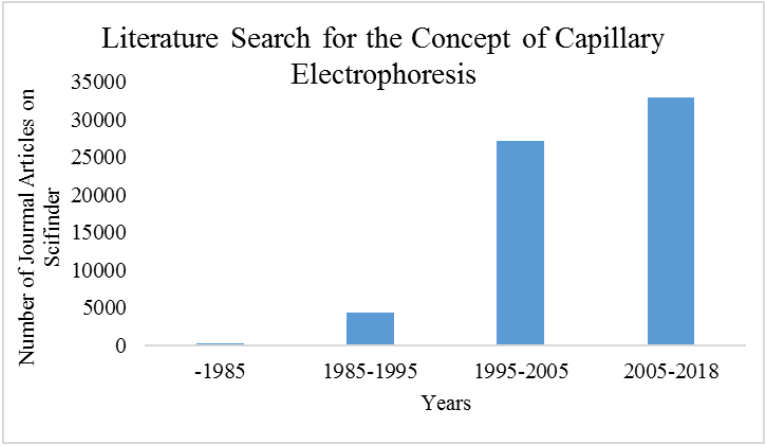

Figure 1-1. Number of times the concept of CE has been mentioned in the literature.

being developed that utilized CE to solve novel challenges in analytical and bioanalytical chemistry

1.1.1 Capillary Electrophoresis

CE is an excellent technique for the separation of charged molecules.[4] In CE, a capillary is filled with a background electrolyte (BGE) solution prior to a sample injection, which is done either hydrodynamically or electrokinetically. Hydrodynamic injections use pressure to force a sample into the capillary and electrokinetic injections use an electric field to force a sample into the capillary. Both injections only require nanoliter sample volumes. Once the sample is injected into the capillary the ends of the capillary are immersed in vials containing the BGE and electrodes. A voltage is then applied to the ends of the capillaries via the electrodes in the BGE vials, creating an electric field within the capillary. After the voltage is applied, ions move through the BGE solution based on their electrophoretic mobility. Electrophoretic mobility is based on the constant proportionality between speed of the ion and electric field strength.[4] Anions move in the direction of the anode, located at the inlet of the capillary and cations move in the direction of the cathode, located at the outlet of the capillary.

In addition to the electrophoretic mobility of the ions, the electroosmosis within the capillary must also be considered. The walls of the fused silica capillary are covered with silanol groups, which are deprotonated above pH 3. As a result of this, cations in the buffered solution form a diffuse layer against the silanol groups. The first layer of cations is tightly bound to the negatively charged silanol groups.

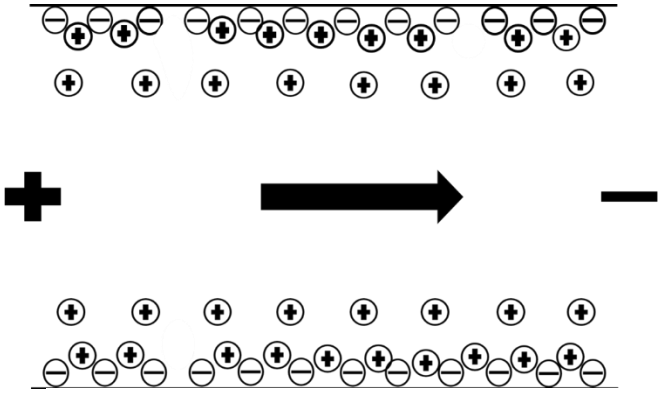

Figure 1-2. Electroosmotic flow through the capillary.

The second layer of cations is not as tightly bound. This allows the second layer of cations to migrate toward the cathode, thereby inducing a uniform bulk flow called electroosmotic flow (EOF), as seen in Figure 1-2. Unlike HPLC, which is pressure driven and has a parabolic flow profile, CE has a uniform flat flow profile that leads to greater separation efficiency. The EOF and the electrophoretic mobility of individual ions result in the systematic elution of cations, neutral analytes, and anions, as seen in Figure 1-3.

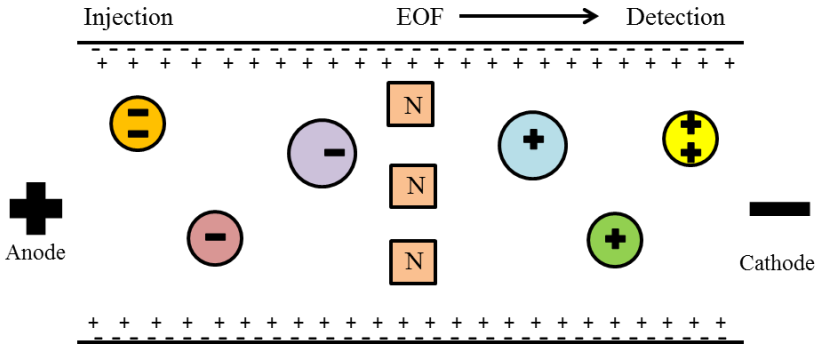

Figure 1-3. Systematic elution of cations, neutral analytes, and anions from the capillary.

Since cations have electrophoretic mobility in the direction of the cathode, they will migrate at the velocity of the EOF plus the mobility of the ion, and will elute first. Neutral analytes have no intrinsic mobility and will migrate at the same velocity as the EOF. The anions will elute last because their electrophoretic mobility is in the opposite direction of the EOF; leading them to have a slower velocity in the direction of the cathode and detector.

1.1.2 Electrokinetic Chromatography

Before 1984, neutral compounds could not be separated using capillary electrophoresis because they have no intrinsic electrophoretic mobility to induce a separation. This limitation was overcome by Terabe *et al.*[7] who demonstrated that neutral analytes could be separated using

anionic surfactants. Surfactants are organic compounds that contain a charged hydrophilic head group and a hydrophobic tail. Once the critical micelle concentration (CMC) of a surfactant is exceeded the surfactant condenses into micelles. Anionic micelles have a negative charge and will migrate in the opposite direction to the EOF. Although they have mobility in the opposite direction of the EOF, the electrophoretic mobility of the micelles is not greater than the mobility of the EOF. The micelles will migrate in the direction of the cathode, but with a net velocity less than that of the EOF. The difference in the migration times of the EOF and micelles leads to a separation window for neutral analytes, as seen in Figure 1-4.

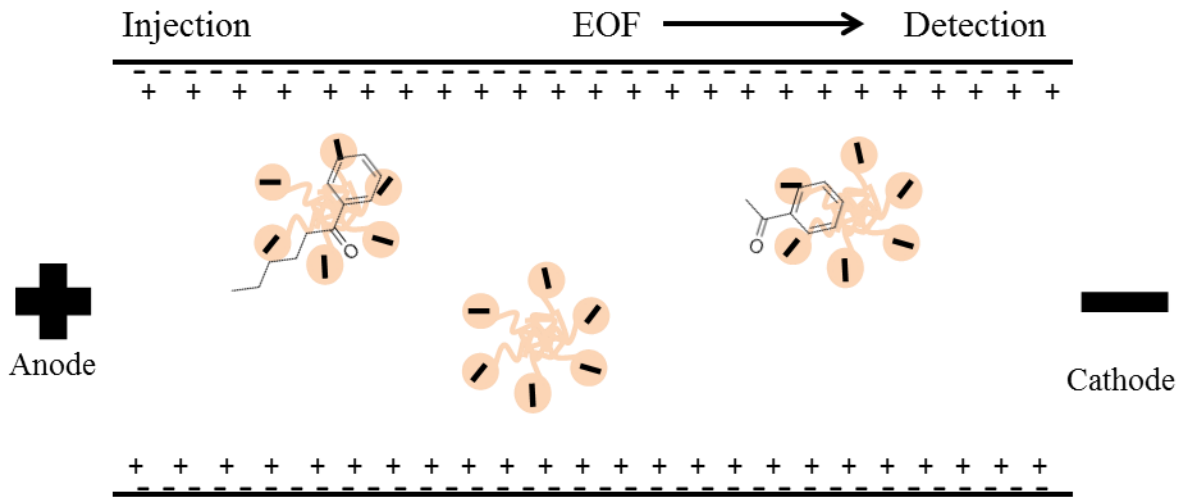

Figure 1-4. Separation of neutral analytes utilizing EKC.

Neutral analytes are separated by their interactions with the micellar pseudostationary phase: Terabe *et al.* demonstrated the separation of fourteen phenol derivatives in 19 minutes.[7] This process of separation is known as electrokinetic chromatography (EKC). The material that provides retention is analogous to that of a stationary phase in HPLC, but the materials are not affixed to the capillary, and elute from the system. They are therefore referred to as a pseudostationary phase (PSP). Since the development of EKC, numerous materials have been

developed as PSPs including micelles,[8,9] polymers,[10,11] vesicles,[12,13] microemulsions,[14,15] liposomes,[16–18] bicelles,[19,20] and nanoparticles,[21–23] either for analytical separations or to the study the PSP's unique solvent characteristics.

1.1.3 Affinity Capillary Electrophoresis

In nature, noncovalent interactions between small molecules and macromolecules are essential to many biological processes. As a result, understanding the strength of these interactions has become a key part of understanding the mechanisms of biological systems. One way to quantify these interactions is through the measurement of equilibrium constants, which are a measure of the equilibrium between ligand concentrations that are bound and unbound to a receptor. This equilibrium can prove to have valuable insight into the pharmacological activities.[24] The equilibrium between small molecule ligands and receptors, like macromolecules, is important to the regulation of physiological functions. Diseases, such as cancer, will affect the equilibrium between ligands and receptors in malign ways.[25] Affinity Capillary Electrophoresis, (ACE), is used to study ligand-receptor interactions with fast kinetics. A constant sample concentration of ligand is injected into the capillary and the electrophoretic mobility of the ligand is used as a measure of its affinity for the receptor. As the receptor concentration in the BGE is increased, the electrophoretic mobility of the ligand changes based on its affinity for the receptor. From the changes in the electrophoretic mobility, a dissociation constant, K_D, can be determined.

ACE has been used extensively to study the noncovalent interactions between pharmaceuticals and proteins, as well as between biomolecules and proteins in model systems. The binding of arylsulfonamides to carbonic anhydrase was one of the first systems to be studied using ACE. This was because carbonic anhydrase is a commercially available protein, with a known crystal structure.[26] In addition to studying the interactions between one ligand and a

receptor, ACE is capable of studying multiple ligand interactions with one receptor in a single experiment. Using peptides as ligands and vancomycin as a receptor, Chu and Whitesides were able to simultaneously measure the affinity of multiple peptides for the antibiotic.[27] Recently, ACE has been used for high-throughput screening in Fragmented Based Drug Discovery. The ability to detect small shifts in ligand electrophoretic mobility, is an attractive feature because these are indicative of weak noncovalent interactions with the receptor of interest.[28] Using this technique Farcaş *et al.* were able to measure the K_D's between thrombin and three known inhibitors of its activity that were comparable to previously published literature values. As a result of this proof of concept experiment the researchers were able to screen a small library of compounds with results comparable to spectroscopic studies.[28]

1.2 Theory

1.2.1 Electrophoresis

When an ion is placed in a solution with an applied electric field, it will migrate at a velocity known as its electrophoretic mobility, μ_{ep}. Electrophoretic mobility is constant proportionality between the speed of the ion and the electric field strength.[4] The mobility is proportional to the charge on the ion and inversely proportional to the friction coefficient, μ_{ep} is given by the following equation:

$$\mu_{ep} = \frac{qE}{6\pi\eta r} \tag{1-1}$$

Where q is the charge on the ion, E is the electric field strength, η is the viscosity of the solution, and r is the Stokes radius. For molecules of a similar size, mobility increases with the increasing number of charges. The Stokes radius for this equation is considered to be the hydrodynamic

radius of the molecule because most molecules are not spherical. The electric field strength results from the voltage applied, V, across the total length of the capillary, L_t.

$$E = \frac{V}{L_t} \tag{1-2}$$

In addition to electrophoretic mobility of analyte, the mobility of the electroosmotic flow, μ_{eo}, must also be considered. The μ_{eo} is the constant of the proportionality between electroosmotic velocity, u_{eo} and the electric field strength.

$$\mu_{eo} = \frac{u_{eo}}{E} \tag{1-3}$$

The surface charge density on the silica surface of the capillary effects the electroosmotic mobility of the solution. The μ_{eo} is proportional to the surface charge density on the silica surface of the capillary.[4] The μ_{eo} is faster at basic pH because the silanol groups on the silica surface are fully ionized and the fully ionized silica groups lead to a denser diffuse layer and uniform electroosmotic flow. Uniform electroosmotic flow contributes to separations with high resolution and theoretical plate counts. Deviations or instability in the electroosmotic flow can lead to a band broadening and decreased resolution.

The separations in CE result from the apparent mobility, μ_{app}, of the analytes, which is a sum of the electrophoretic mobility of the analyte and the electroosmotic mobility of the BGE.

$$\mu_{app} = \mu_{ep} + \mu_{eo} \tag{1-4}$$

An analyte with mobilities in the same direction will have a large μ_{app} and will reach the detector quickly. An example of this is when cations are analyzed in positive mode, where the cathode is at the terminal end of the capillary. When the anions are analyzed in positive mode the μ_{ep} is negative, the μ_{app} is small, and analysis times are considerably longer. If the μ_{app} is negative then

the analyte will never reach the detector. This would occur when an anion has a large negative μ_{ep} and the μ_{eo} is a small positive number, resulting from a slow EOF. The μ_{ep} can also be calculated from migration time of the analyte of interest (t_r) and a neutral marker which represents the EOF, (t_0) using the following equation:

$$\mu_{ep} = \frac{L_D * L_t}{V}\left(\frac{1}{t_0} - \frac{1}{t_r}\right) \quad (1\text{-}5)$$

L_D represents the length of the capillary from the injection end to the detector.

1.2.2 Electrokinetic Chromatography

Solutes are retained in EKC based on the magnitude of the partition coefficient, K, between the BGE and the PSP. K is an equilibrium constant that can be related to the change in the Gibbs free energy, ΔG^o, of the system:

$$\Delta G° = -RT \ln K \quad (1\text{-}6)$$

R is the gas constant and T is temperature in Kelvin. The ΔG^o of the system can also be related to the changes in enthalpy, ΔH^o, and entropy, ΔS^o, of the system.

$$\Delta G° = \Delta H° - T\Delta S° \quad (1\text{-}7)$$

Analytes will interact with the PSP when the ΔG^o of the interaction is negative. This is important because the noncovalent interactions that govern the partitioning between the BGE and PSP determine the entropy and enthalpy of the analyte partitioning. The retention factor, *k*, can be related to the partition coefficient by the following equation.

$$k = K\frac{V_s}{V_m} \quad (1\text{-}8)$$

V_s is the volume of the PSP and V_m is the volume of the BGE. Neutral analytes are separated based on their interactions with the PSP; the retention factor for the analytes can be determined using the following equation:[7]

$$k = \frac{\mu_{eo} - \mu_{sol}}{\mu_{sol} - (\mu_{eo} + \mu_{PSP})} \quad (1\text{-}9)$$

μ_{eo} is the electroosmotic flow during the analyte run, which is determined by the migration time of EOF marker; μ_{sol} is the total (observed) electrophoretic mobility of the analyte including the μ_{eo}; and μ_{PSP} is the electrophoretic mobility of the PSP determined separately.

The parameter that characterizes how well two analytes are separated is the resolution (R_s). The resolution between two closely eluting peaks can be calculated using the following equation:

$$R_s = \frac{\Delta t_r}{w_{av}} \quad (1\text{-}10)$$

Where Δt_r is the separation between peaks in units of time, and w_{av} is the average width of the two peaks in units of time[4]. The selectivity between two peak, α, is calculated from k_2/k_1. The greater selectivity the greater separation (Δt_r) between components. The peak efficiency, which is measured by the number of theoretical plates (N), calculated using the following equation:

$$N = 16\left(\frac{t_r}{w}\right)^2 \quad (1\text{-}11)$$

Where t_r is the analyte retention time and w is the peak width. Resolution is proportional to the square root of the number of theoretical plates.

1.2.3 Affinity Capillary Electrophoresis

In order to calculate an analyte's K_D, the analyte's electrophoretic mobility should be determined at each concentration of PSP in the BGE. The analyte's electrophoretic mobility is measured and calculated based on the following equation:

$$\mu_{ep} = \mu_{app} - \mu_{eo} \tag{1-12}$$

Using ACE, the relative affinity an analyte has for the PSP is determined using the change in the analyte's electrophoretic mobility as the concentration of PSP in the BGE is increased. Change in electrophoretic mobility allows for the percent bound of each probe to be determined using the following equation:[29]

$$\theta = \frac{bound}{unbound} = \frac{(\mu_{ep} - \mu_{ep,free})}{(\mu_{ep,max} - \mu_{ep,free})} \tag{1-13}$$

Where μ_{ep} is the electrophoretic mobility of the analyte at a given PSP concentration and $\mu_{ep,free}$ is the electrophoretic mobility of the analyte with no PSP in the BGE. $\mu_{ep,max}$ is the maximum change in electrophoretic mobility caused by the analyte-PSP interaction. The K_D can be determined using the following equation and nonlinear data fitting methods[29]:

$$\theta = \frac{[PSP]^n}{(K_d{}^n + [PSP]^n)} \tag{1-14}$$

Where K_D is the dissociation constant of the analyte-PSP interaction, and *n* is the measure of the cooperativity of the interaction. If $n > 1$ then a solute bound to the PSP will increase the PSP's affinity for a second solute and if $n = 1$ then a solute bound to the PSP does not affect future solute-PSP interactions. Lastly, if $n < 1$ then a solute bound to the PSP will decrease affinity for future solutes.

1.3 Lipid Bilayers

Lipid bilayers are thin sheets of amphiphilic biomolecules, which form the basis for cell membranes. These amphiphilic biomolecules, called lipids, form a compact double layer, where the hydrophilic head groups point outward to interact with the water molecules and the hydrophobic tails point inward to form a hydrophobic core.[30] Lipids constitute almost 50% of the mass of eukaryotic cell membranes and the remaining mass is attributed to proteins.[30] Phospholipids make up the largest portion of lipids in the cell membrane. Phosphatidylcholine shown in Figure 1-5[30], is composed of a choline head group and glycerophosphoric acid backbone, with two fatty acid tails. The lipid bilayer is an integral part of the cell membrane and many important biological interactions occur at or within the cell membrane surface.[31] Therefore, lipid bilayer properties have been subject to extensive study over the years.

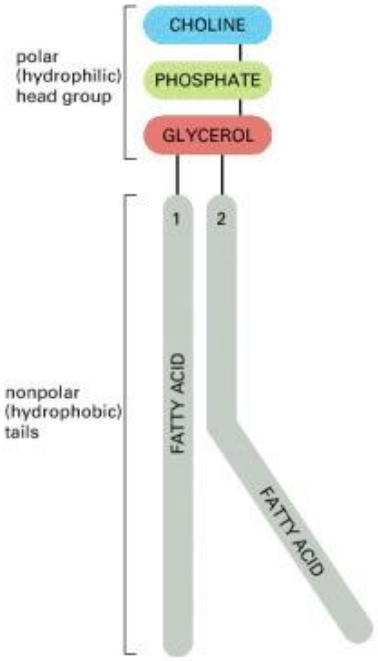

Figure 1-5. Structure of phosphatidylcholine.

1.3.1 Liposomes

Liposomes are one of the most prevalent model membrane systems. They are a form of phospholipid aggregate, seen in Figure 1-6,[32] that consist of concentric lipid bilayers that form around an aqueous core.

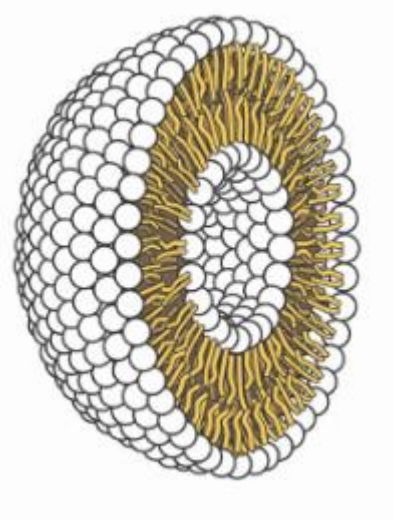

Figure 1-6. Liposome structure.

Liposomes form because it is energetically unfavorable to maintain a planar shape while the hydrophobic edges are exposed to the hydrophilic aqueous environment. Liposomes can range in size from 50 nm-5μm in diameter, depending on the technique used to prepare them.[33] Prior to their use as a PSP in EKC, liposomes were used in the cosmetics industry[34] and as a drug delivery system.[35]

The first use of liposomes in conjunction with CE was as a buffer additive. Zhang *et al.* utilized liposomes in order to study the free energy of pharmaceutical and peptide interactions with the model lipid bilayer.[36] In this experiment, the liposomes were composed of zwitterionic lipids and did not have intrinsic electrophoretic mobility. The anionic analytes and peptides provided the μ_{ep} for the separations. In order to impart electrophoretic mobility onto liposomes, anionic lipids need to be incorporated during the synthesis. Both 1-palmitoyl-2-oleoyl-sn-glycero-3-phospho-L-serine[37] and 1-palmitoyl-2-oleyl-sn-glycero-3-[phospho-rac-(1-glycerol)][38] have been incorporated into liposomes in order to impart electrophoretic mobility in the direction of the anode. Using liposomes a variety of interactions between small molecules and lipid bilayer systems have been studied. Vanova *et al.* determined that antioxidants such as phenolic acids and flavonoid glycosides have lower distribution constants than flavonoids, when they interact with the liposome PSPs.[39] Another report investigated the effects that ionic liquids have on the affinity of common pollutants for lipid bilayers. This research demonstrated that ionic liquids can reduce pindolol, metroprolol, and propranolol affinity for lipid bilayers, and this could have implications for cleaning toxic spills.[40]

1.3.2 Bicelles

In addition to liposomes, bicelles have also been used as a CE additive for the study of lipid bilayers. Bicelles seen in, Figure 1-7[41], are disk shaped aggregates that consist of a planar

phospholipid bilayer. The edges of the planar bilayer are covered by phospholipids with short alkyl tails, forming a disk shape. These were originally developed to study peptide-bilayer interactions using NMR.[42] Bicelles are compatible with solution state NMR because they can be made small enough to attain appropriate tumbling times[43] and they can also be analyzed using solid state NMR because they will spontaneously align in an electric field.[44]

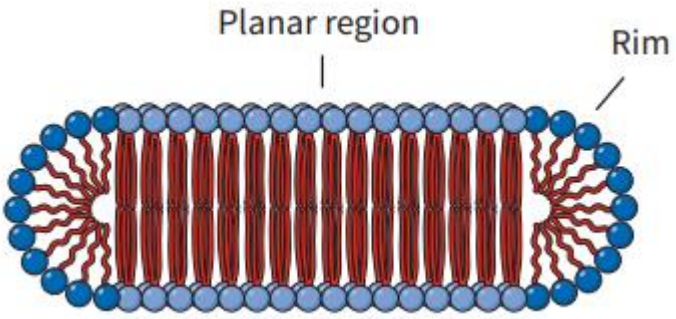

Figure 1-7. Bicelle structure.

Holland and Leigh were the first to report the use of bicelles as a CE additive.[20] Some of the major findings of that study were that bicelles produced separations with higher efficiencies than micelles of the same lipid composition.[20] The authors believe that the bicelle led to reduced interactions between the analytes and the capillary walls. Bicelles also allowed for the separation of proteins myoglobin and somatostatin, this separation that was not possible without the use of bicelles as a CE additive.[20] Interactions between the bicelles and the proteins prevented the proteins from absorbing to the surface of the capillary. This research was quickly followed by another report where the interaction between antimicrobial peptides and bicelles were studied. The results showed that as the 1,2-dimyristoyl-sn-glycero-3-phosphocholine content of the bicelle increased, the retention factor of antimicrobial peptides increased as well.[19] It was also determined that membrane fluidity also affected the interaction between antimicrobial peptides and bicelles.[19]

1.3.3 Nanodiscs

In order to study lipid bilayers and membrane bound protein, Bayburt *et al.*[45] and Denisov *et al.*[46] introduced the nanodisc. Nanodiscs are nanometer scale disc-shaped phospholipid bilayer assemblies encircled by two genetically engineered belt or scaffold proteins, as seen in Figure 1-8.[47] The belt proteins interact with the hydrophobic edges of the lipid bilayer on the inner side and the surrounding aqueous medium on the outer side, serving to stabilize the nanodiscs in aqueous dispersions. The belt proteins are based on human serum apolipoprotein, and can be generated in different lengths to create nanodiscs of different diameters. The phospholipid composition of the nanodiscs can also be varied to mimic specific biological systems. These phospholipid bilayer structures thus have extraordinary and unique potential to simulate biological membranes and could represent useful constructs to study membrane affinities by EKC. Unfortunately, it is prohibitively difficult to generate enough belt protein to produce nanodiscs in sufficient quantity to carry out EKC studies.

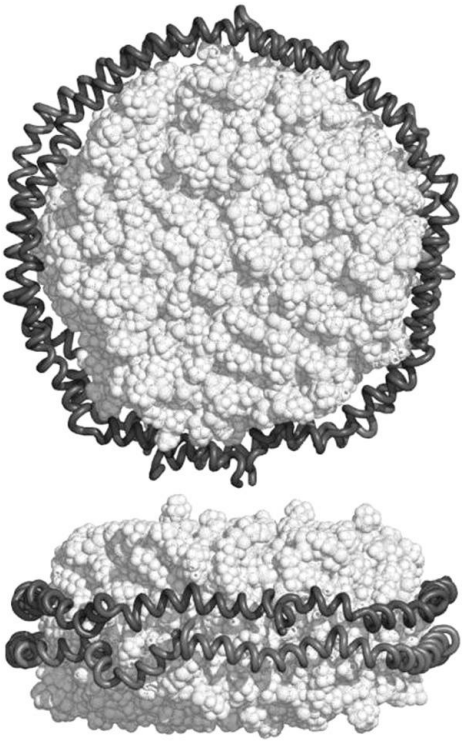

Figure 1-8. Nanodisc with protein belt.

The recent introduction of synthetic styrene maleic acid copolymer to stabilize lipid nanodiscs in solution has made these structures accessible as additives for CE measurements. The synthetic copolymer belts are inexpensive and are available commercially in large quantities. The structure of the copolymer lipid nanodisc was studied extensively by Jamshad *et al.*[48] using small angle neutron scattering and it was suggested that the copolymer belt takes the form of a bracelet encircling the lipid membrane with the styrene oriented parallel to the alkyl

chains of the lipid.[48] It is thought that the maleic acid portion of the polymer has the same orientation as the styrene groups, but instead interacts with the polar phospholipid head. This would suggest that the driving force behind the spontaneous formation of nanodiscs is the strong hydrophobic interactions between the styrene groups and the alkyl tails. It was thought that the electrostatic interactions between the anionic maleic acid and the zwitterion head groups could cause problems for copolymer insertion. However, work by Scheidelarr *et al.* showed the copolymer belt could readily insert into a membrane that contained a lipid composition of up to 20% mol. anionic lipid.[49] The anionic maleic acid group serves another purpose as well; it gives the nanodiscs electrophoretic mobility in the opposite direction of the EOF. This allows the nanodisc to operate as a PSP to effect the separation of neutral compounds in between the elution of the EOF and the elution of the nanodiscs. This copolymer belt also leads to uniform polydispersity among the size of the nanodiscs. For example, nanodiscs synthesized using this method yield a diameter around 10 nm with a standard deviation of usually $\pm$3 nm.[49]

1.4 Determination of Lipophilicity

Small molecule and pharmaceutical affinity is an important parameter in pharmaceutical development. Lipophilicity is a measure of a molecule's ability to dissolved nonpolar solvents and it is used as a proxy for a molecule's ability to partition into lipid bilayers. Log $P_{o/w}$ values are used as a measure of a molecule's lipophilicity. The log $P_{o/w}$ value is the logarithm of the partition coefficient based on a molecule's partitioning between the two immiscible solvents: n-octanol and water. Log *D* values have also been used to measure lipophilicity, they are computationally derived measures of lipophilicity at specific aqueous pH.[50] Molecules with a high lipophilicity value tend to have poor solubility and metabolic clearance.[51] As a result of the

implications of lipophilicity, the determination of a potential pharmaceutical's log $P_{o/w}$ value is an integral part of drug discovery and development. In addition to implications in pharmaceutical development, log $P_{o/w}$ values have implications in environmental science and the agricultural industry. There are established correlations between log $P_{o/w}$ values and pesticide soil sorption, water solubilities, and their bioaccumulation in aquatic and terrestrial life.[52]

The current industry standard for the determination of octanol-water partition coefficients is the shake-flask method. According to guidelines set up by the Organization of Economic Cooperation and Development (OECD), experiments must be completed with no more than 10 mM of analyte of interest in each experiment. Each set of experiments has two 1 liter stock bottles of n-octanol and water. One bottle has a higher ratio of n-octanol to water and the other contains a higher ratio of water to n-octanol. The bottles with 10 mM of analyte are shaken for 24 hours then allowed to stand until the phases separate. A second set of experiments is run at half the volume of liquid and a third is run at double the volume of liquid. After these six bottles have settled into equilibrium, the concentration of the analyte in the water portion is determined using GC or HLPC instrumentation[53]. After the concentration of analyte is determined in the aqueous portion, the ratio between the concentrations of the analyte in the aqueous portion and the organic portion can be calculated. In order for this to be considered successful, the log $P_{o/w}$ values derived for the 3 sets of experiments must be within ± 0.3; if this doesn't happen then one of the sets of the experiments must be redone. Not only is this process time consuming, but also it can require significant amounts of sample if experiments have to be redone. This also does not take into consideration what potential additional method development is needed in order to determine the analyte concentration.

In response to this laborious process, scientists have been working to develop faster methods for determining partition coefficients that require smaller amounts of sample. There have been attempts to study partitioning with reverse phase-high performance liquid chromatography (RP-HPLC), but that has been met with only limited success. There are several problems that have been associated with RP-HPLC such as size exclusion effects as a result of varying pore sizes among packed column beads. This is something that is not encountered in an octanol-water environment.[54] In addition, these coefficients can only be determined under isocratic conditions, which limits the window in which their coefficients can be determined.[54] Even under isocratic conditions with a binary stationary phase there are complications. It is thought that changing the ratio between organic and aqueous phases should lead to a linear change in the relationship between retention factor and partition coefficient. However, in RP-HPLC it seems that this is not true when the mobile phase has a low fraction of organic solvent. It is speculated that having close to a purely aqueous mobile phase leads to conformational changes in the stationary phase, which changes the retention factor of the analyte.[54] Reverse Phase-Thin Layer Chromatography (RP-TLC) was also developed as an alternative to the shake-flask method. However, after several studies, it was determined that this technique could not be used for aromatic and nitrogen heterocyclic bases. It was found that this technique mostly applied to compounds that are weakly polarizable.[54]

EKC methods have been developed in order to avoid the problems associated with the previously mentioned methods and because EKC allows for fast, selective, and efficient separations that require only nanoliter sample volumes. Log $P_{o/w}$ values have most often been correlated to retention factors in microemulsion EKC. Using microemulsion EKC, Ostergaard *et al*. were able to accurately correlate the logarithm of the retention factor, log *k,* of 38 solutes to

their log $P_{o/w}$ values.[55] Coated Capillaries have also been used in conjunction with microemulsion EKC for the indirect measure of log $P_{o/w}$ values. The anionic capillary coating was used to stabilize the EOF. Using this method, the correlation between log $P_{o/w}$ values and log k resulted in an r^2 value of 0.972.[14]

1.5 Linear Solvation Energy Relationship Analysis

Indirect measurement of log $P_{o/w}$ values can provide information about the hydrophobicity of a PSP, but it cannot provide information about the mechanisms of solute-PSP interactions. Linear Solvation Energy Relationship, LSER, analysis was developed in order to study the mechanisms of retention in chromatography.[56] This techique has been used to characterize PSP in EKC as well.[23,57] Noncovalent interactions determine selectivity in EKC, these interactions include dispersion forces, dipole-induced interactions, dipole-dipole interactions, and hydrogen bonding. Dispersion forces are caused by temporary fluctuations in charge distribution of a molecule. The charge distribution has an electric field associated with it and can induce a dipole moment in an adjacent molecule. Dipole-induced interactions occur when the permanant dipole of one molecule induces a dipole interaction in another molecule due to temporary fluctuations in the charge distribution.[56] Dipole-dipole interactions are caused by attractive forces between the positive end of one polar molecule and the negative end of another polar molecule, when the molecules are aligned in solution.[58] Hydrogen bonding is a unique dipole-dipole interaction that results from a hydrogen bonded to highly electronegative atom, with a lone pair of electrons, such as nitrogen or oxygen. The small size of the hydrogen and the large dipole moment allow for other electronegative atoms to get in close proximity to the hydrogen atom and results in strong attractive forces.[59]

Currently LSER analysis is focused on understanding solute interactions with stationary and pseudostationary phases, however LSER analysis was originally developed to understand the properties of bulk solvents. The original equation is shown below:

$$SP = c + s(\pi^* + d\delta) + a\alpha + b\beta \quad (1\text{-}15)$$

In this equation, SP represents a solvent dependant property such as the solvochromatic shift of a fluorescent probe.[56] Letters are measures of a solvent's polarity (Π^*), polarizeability (δ), hydrogen bond donating ability (α), and hydrogen bond accepting ability (β). This equation was adapted by Abraham to study solute interactions with chromatographic material and can be represented by the following equation:[60]

$$SP = c + eE + sS + aA + bB + vV \quad (1\text{-}16)$$

Where *SP* is any property which measures the free energy transfer of the solute from the mobile phase to the stationary phase. In the case of EKC, an analyte's log *k* value is used as a measure of the free energy of transfer between the BGE and the PSP. The letters *V, E, S, A,* and *B,* are related to individual solute parameters which are found in the literature.[57] These specific parameters are representative of a molecule's molar volume (V), excessive molar refraction (E), dipolarity/polarizability (S), hydrogen bond acidity (A), and hydrogen bond basicity (B).[56] The constant *c* accounts for the phase ratio and other interactions that cannot be explained by the previously mentioned solute descriptors. By using experimentally derived log *k* values and known solute descriptors the solvation characteristics of the PSP can be broken down into five different categorical interactions defined by the *v*,*e*, *s*, *a*, and *b* terms. The lower case letters represent the PSP solvation characteristics derived from the PSP interactions with solute probes that have defined partitioning parameters.

The solvation parameters are based on a cavity model of solvation. Figure 1-9[56] shows a visual representation of the model. First an cavity is formed in the PSP for the analyte.[61] The energy required to form the cavity depends on the intramolecular forces that stabilize PSP and the size of the analyte.[61] Then an equilibrium is established between the PSP's solvent environment and the analyte. In the final step, the analyte enters the cavity and noncovalent interactions occur between the analyte and the PSP's solvent environment.[61]

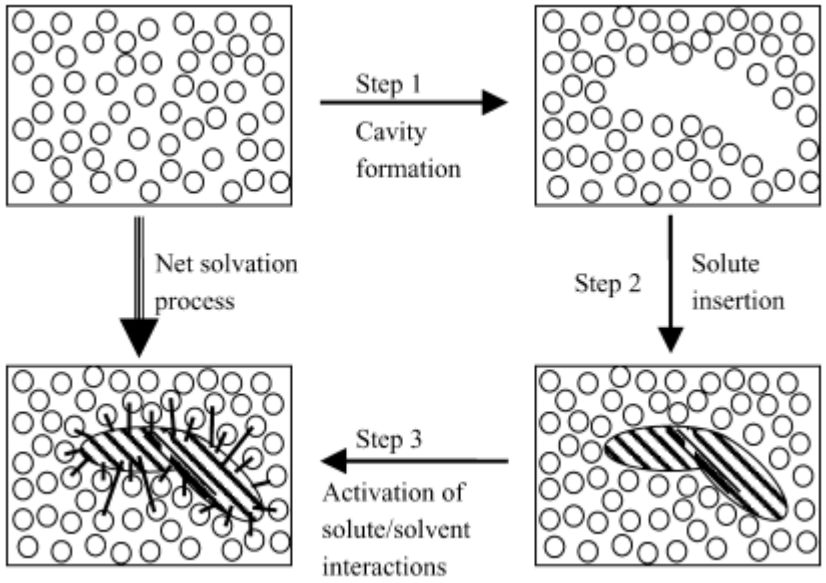

Figure 1-9. Cavity model of solvation.

The magnititude of the positive or negative system parameters describe difference in energy for this solvation process in the PSP relative to the BGE. The *v* term is used to account for cavity formation energy. A large positive *v* term indicates that the PSP is not as cohesive as the BGE and therefore less energy is required to break the interactions between the molecules of the PSP than to break the interactions between the molecules of the BGE to form a solvation pocket. The *a* term reflects a PSP's ability to accept a hydrogen bond from a solute probe relative to the BGE. Similarly, the *b* term reflects the nanodisc ability to donate a hydrogen bond to a solute probe relative to the BGE. It is characteristic of almost all PSPs in EKC to have a large negative *b* term because water is a superior hydrogen bond donor. The *s* term is a measure of a

solute's ability to interact with the PSP or BGE through a dipole moment.[56] Finally, the *e* term represents the PSP or BGE ability to interact with π or nonbonding electrons;[21] therefore a positive term would represent having a stronger interaction with a solute's nonbonding or π electrons. LSER analysis can provide insight into why changes in lipid chemistry affect small molecule solvation.

1.6 Chiral Separations

PSPs in EKC are constantly being developed to separate complex mixtures or to separate analytes of similar structure, but different toxicities. Chirality is the result of an asymmetric carbon on a molecule or due to sterically hindered rotation around a bond. Although two chiral molecules have the same molecular formula, they have different spatial arrangements.[62] The differences in the spatial arrangement between chiral molecules cause these molecules to have significantly different activity and toxicity. This is because stereochemistry, a molecules 3D arrangement, can greatly affect a pharmaceutical's absorption, distribution, metabolism, and excretion.[63,64] An atropisomer is a form of chirality that results from sterically hindered rotation around one or more single bonds.[65,66] Atropisomers can have significant differences in activity; the (R)-(+)/(S)-(−) configurations of Telenzepine, a selective muscarinic antagonist with a stereogenic C-N axis used for the treatment of peptic ulcers,[67] were found to have a 500-fold difference in activity.[66] As a result of these significant biological effects, most pharmaceuticals developed are achiral or are stereochemically pure.[68,69]

As a result of the important differences in pharmaceutical toxicity and activity, chiral separations have become a major field of study. Traditionally chiral molecules are separated when interacting with a chirally pure selector. The separation occurs because of a three-point interaction between the chiral analyte and chiral selector as seen in Figure 1-10. The three-point interaction leads to one chiral molecule to be more retained by the pseudostationary phase than the other chiral molecule that only has a two-point interaction. One of the interactions, whether it be based on pi-pi, hydrogen bonding or dipole-dipole, must be stereoselective.[70]

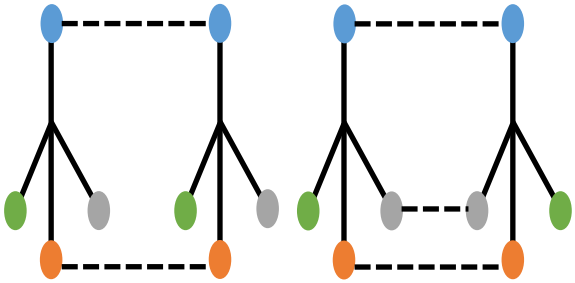

Figure 1-10. Comparison of two-point interactions and three-point interactions.

EKC has been used for the separation of chiral molecules because of it superior separation efficiencies. Crown ethers,[71,72] cyclodextrins, [62,73] and proteins[74,75] have been used as chiral selectors for the separation of enantiomers and other chiral molecules. Using crown ethers as a PSP, Schmid and Gübitz were able to separate the enantiomers of 12 glycyl-dipeptides in under 35 minutes.[76] While bovine serum albumin has been used for the separations of pantoprazole, omeprazole, and lansoprazole. Using bovine serum album as a chiral selector, the enantiomers of pantoprazole were separated with a resolution of 4.4.[75]

1.7 Conclusions

Capillary electrophoresis provides fast, and efficient separations that only require nanoliter sample volumes. The overall efficiency of CE instrumentation makes it an attractive technique for the study of biological systems and interactions. Techniques that utilize CE such as electrokinetic chromatography and affinity capillary electrophoresis expand the potential application of the instrumentation beyond the separation of charged molecules. In the next

chapter the synthesis of nanodiscs will be described, in addition to the methods and materials necessary for the completion of EKC, chiral separations, and ACE experiments using nanodisc PSPs or additives.

Chapter 2: Nanodisc Synthesis and Characterization

2.1 Introduction

This chapter will describe the methods used for synthesis and characterization of copolymer-stabilized nanodiscs. Methods will also include procedures followed for EKC and ACE experiments. The results of nanodisc characterization will be found in the appropriate chapters. This chapter includes work that was published in *Electrophoresis*, 2017, 38, 738-746,[77] *Electrophoresis*, 2018, 39, 844-852,[78] and *Chemistry and Physics of Lipids*, 2018, 214, 11-14.[79]

2.2 Styrene-Maleic Acid Copolymers

Styrene-maleic acid copolymers are used to stabilize cylindrical sections of lipid bilayer in solution. Not only does the copolymer stabilize the lipid bilayer, it provides the nanodiscs with electrophoretic mobility due to the negatively charged maleic acid moieties. Two copolymers, were used to synthesize nanodiscs, Xiran 30010 and Xiran 25010. The Xiran copolymers (Polyscope Polymers, Geleen, Netherlands), were a gift from Stefan Scheidelaar of Utrecht University, and came in their anhydride form. The Xiran 30010 contains a 2:1 styrene:maleic acid mole ratio and has a molecular weight of 6.0 kDa. Xiran 25010 is a larger copolymer, it contains a 3:1 styrene:maleic acid mole ratio and has a molecular weight of 10.0 kDa. Hydrolysis of the copolymers was necessary in order to make them negatively charged and soluble in aqueous solutions. The anhydride and hydrolyzed forms of the copolymers are shown in Figure 2-1.

2.2.1 Copolymer Hydrolysis

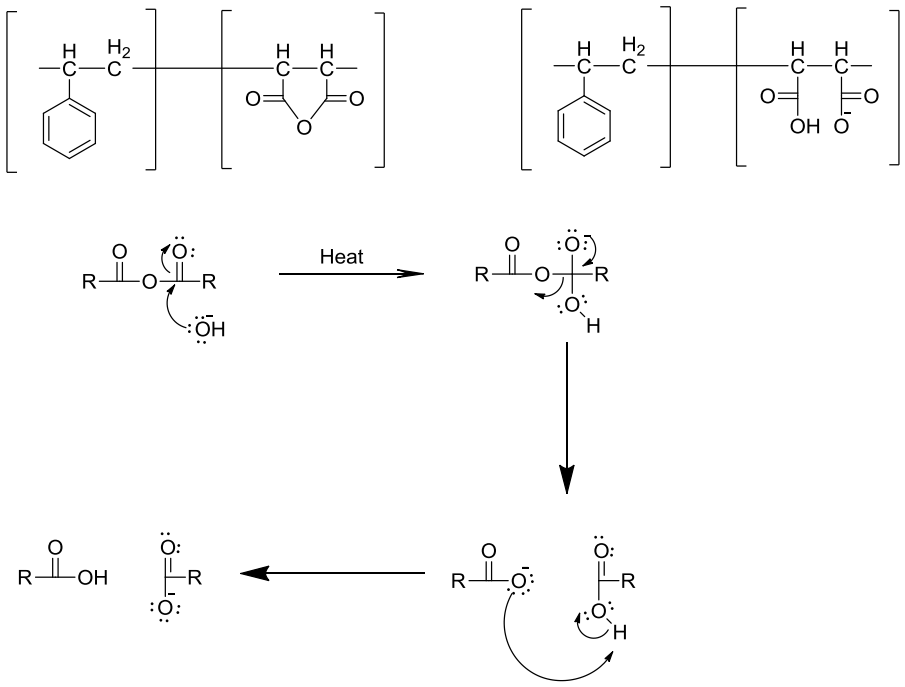

Figure 2-1. The anhydride (A) and hydrolyzed (B) forms of the Xiran copolymer. The mechanism of the base catalyzed hydrolysis.

The procedure for hydrolyzing the copolymers is based on procedures in the literature.[49,80] A 5% (w/v) solution of Xiran 30010 or Xiran 25010 is suspended in a 20 mL 1 M KOH solution and refluxed for 6-8 hours. After the reflux of the copolymer a 1.0 mL sample of the solution is frozen and freeze-dried overnight. To confirm reaction completion FTIR analysis is employed. FTIR is used to monitor the shift of the carbonyl signal from 1780 to 1560 cm^{-1}. The shift in the carbonyl signal confirmed the formation of a carboxylate salt from the ester ring. The results of FTIR analysis are shown in Figure 2-2. After FTIR analysis, the copolymer is precipitated using 3.48 mL 6 M HCl to create a 1.1 M HCl solution. The precipitate is then washed five times with 0.1 M HCl. After washing, the copolymer is freeze-dried and stored at −20°C. This procedure utilizes base catalyzed hydrolysis in order to break open the anhydride ring, the mechanism for the reaction can be seen in Figure 2-1.

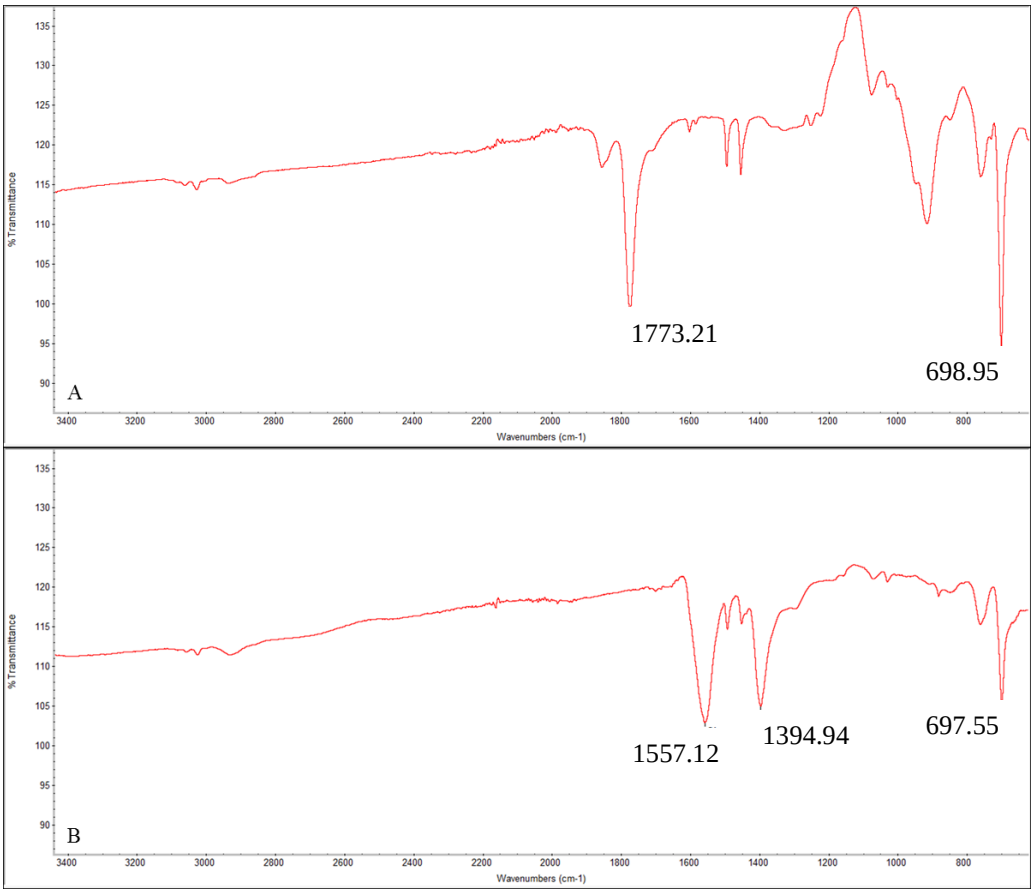

Figure 2-2. The spectra from the FTIR analysis. A) The spectrum of the Xiran copolymer before hydrolysis. B) The spectrum of the Xiran copolymer after hydrolysis. Axes: x- axis wavenumbers (cm^{-1}), y-axis % transmittance.

2.3 Synthesis of Copolymer Stabilized Nanodiscs

Nanodiscs were synthesized with seven different lipid compositions, drawn from the lipids in Figure 2-3, and all nanodiscs utilized in EKC analysis were prepared using the following procedure. Lipids dissolved in chloroform were dried using a rotary evaporator and rehydrated to 1 mM or 5 mM lipid concentration using either 10 mM or 25 mM phosphate pH 7.0 buffer. Ten freeze–thaw cycles were performed on the lipid solution using a dry ice-ethanol bath and a sonicator with a water temperature set 10°C above lipid gel-to-liquid crystalline phase transition temperature (T_m) to form multilamellar liposomes. A solution of Xiran 30010 or Xiran

25010 copolymer in 10 mM or 25 mM phosphate buffer was heated to 45°C to help solubilize the copolymer and then the solution was adjusted to pH 7.0. The copolymer was added to the lipid solution, so the multilamellar solution contained the desired (w: w) copolymer to lipid ratio. The combined solution mixture was then lightly vortexed for 5 min before being placed in a 45ºC heated bath for 30 minutes to complete nanodisc formation. The heated bath decreased the amount of time needed for complete liposome to nanodisc conversion. Once the conversion is complete, the nanodiscs are placed in the refrigerator for storage. Nanodiscs were generated using systematically varied copolymer to lipid ratios and copolymer belts of different molecular weight and chemical composition.

Figure 2-3. Structure of lipids used in analysis.

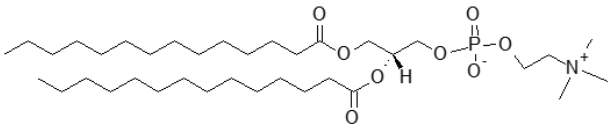

1,2-dimyristoyl-sn-glycero-3-phosphocholine (14:0 PC)

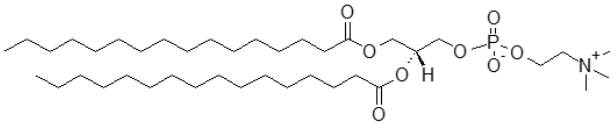

1,2-dipalmitoyl-*sn*-glycero-3-phosphocholine (16:0 PC)

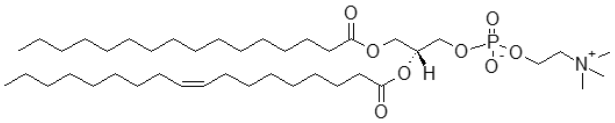

1-palmitoyl-2-oleoyl-*sn*-glycero-3-phosphocholine (16:0-18:1 PC)

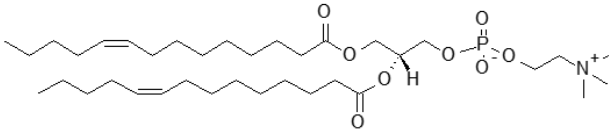

1,2-dimyristoleoyl-*sn*-glycero-3-phosphocholine (14:1 PC)

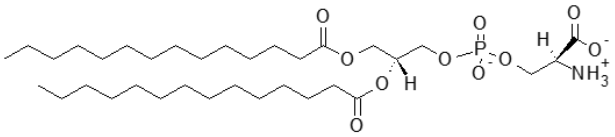

1,2-dimyristoyl-*sn*-glycero-3-phospho-L-serine (14:0 PS)

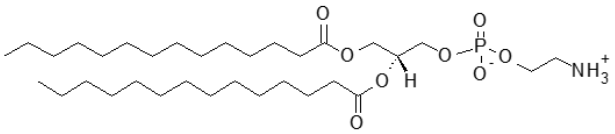

1,2-dimyristoyl-*sn*-glycero-3-phosphoethanolamine (14:0 PE)

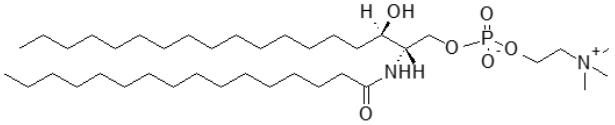

N-hexadecanoyl-D-*erythro*-sphingosylphosphorylcholine (16:0 SM)

2.4 Nanodisc Characterization

The size and polydispersity of the nanodiscs were obtained by dynamic light scattering at 1 mM or 5 mM phospholipid concentrations in 10 mM or 25 mM phosphate buffer, pH 7.0 with a Malvern Zetasizer Nano ZS. All Zetasizer samples were first filtered through a 0.45 μm pore sized filters to remove any potential artifacts, such as dust, that would skew the results. Each synthesis was measured in three separate trials that consisted of 13–15 measurements per trial.

2.5 Electrokinetic Chromatography Characterization

Phosphate buffers were prepared using sodium phosphate monobasic and sodium phosphate dibasic to create 10 mM or 25 mM concentrations in 18 MΩ nanopure water from an EMD Millipore system (Bedford, MA, USA). A 5 mM lipid concentration of nanodiscs in BGE was used for separations in the indirect measurement of Log $P_{o/w}$ or Log D values, LSER analysis, and chiral separations. For the indirect measurement of Log $P_{o/w}$ or Log D values and LSER analysis, stock solutions (25 mM) of each analyte were prepared in acetone. Analytical samples were prepared from stock solutions by dilution to 250 μM in BGE so that the injected samples contained only 1% acetone for LSER analysis. For chiral separations, analytical samples were prepared from stock solutions by dilution to 62.5 μM of each atropisomer in BGE so that the injected sample contained only 0.5% acetone. EKC experiments were performed on an Agilent 3D CE instrument with on-column DAD controlled by Agilent Chemstation software using 50 μm id fused-silica capillaries with either 50 μm path length cells or 150 μm extended path length cells (Agilent Technologies, Santa Clara, CA, USA).

Capillaries with total length of 48.5 cm and effective length of 40 cm were flushed at the beginning of every day and every five runs with 1.0 M NaOH. Between injections, the capillary was flushed with acetone, and nanopure water, to prevent absorption to the capillary wall, and buffered nanodisc solution. Analytes were injected individually by 35 mBar of pressure for 5 s and detected at 225, 245, and 254 nm. All EKC experiments were run at 15 kV applied voltage and between 18–30°C using 5 mM phospholipid concentration of nanodiscs in BGE.

The migration time and the electrophoretic mobility of the nanodiscs in the buffered solution were estimated by using the method developed by Bushey and Jorgenson.[81] This method calculates μ_{psp} using the negative water peak as the EOF marker and the migration times of six alkyl–phenyl ketone homologs: acetophenone, propiophenone, butyrophenone, valerophenone, hexanophenone, and heptanophenone. The Excel application solver was used to determine the μ_{psp} that gave the maximum r^2 for the plot of log retention factor versus homolog carbon number.

The logarithm of experimental $P_{o/w}$ and that of computationally derived $D_{pH7.0}$ were graphed against log of the respective retention factors for 38 probe solutes to determine the linear correlation. The log $D_{pH7.0}$ values were generated by ChemAxon software, the computational methods are based on work by Viswanadhan *et al.*,[50] who generated values through the combination of atomic physiochemical properties.

LSER characterization was performed using the 32 LSER probe solutes, which is similar to the list used in a recent study of a latex nanoparticle PSPs.[57] All solute probes were analyzed in triplicate for each LSER analysis. After measurement of k-values, Excel was used for multivariate linear regression to determine LSER coefficients. Each set of LSER coefficients were a result of 96 data points and the error bars in figures containing LSER data are the

standard error from the multivariate linear regression. Results for LSER analysis were considered significantly different if the standard error ranges did not overlap.

2.6 Affinity Capillary Electrophoresis Characterization

Ten different concentrations of sphingomyelin, 16:0 SM, nanodiscs were used in the BGE for affinity measurements. Stock solutions (5 mM) of each analyte were prepared in acetone. Analytical samples were prepared from stock solutions by dilution to 25 μM for pyrene and 3-(α-Acetonylbenzyl)-4-hydroxycoumarin, and 10 μM for rhodamine 123 in nanodisc buffer solution. ACE experiments were performed on an Agilent 3D CE instrument with on-column DAD controlled by Agilent Chemstation software using 50 μm id fused-silica capillaries with 150 μm extended path length cells (Agilent Technologies, Santa Clara, CA, USA).

Capillaries with total length of 48.5 cm and effective length of 40 cm were flushed at the beginning of every day and every five runs with 1.0 M NaOH. Between injections, the capillary was flushed with acetone, nanopure water, and buffered nanodisc solution. Analytes were injected individually by 35 mBar of pressure for 15 s and detected at 225, 245, and 254 nm. All analyses were run at 25 kV applied voltage and 20°C. For both probes ten different sphingomyelin nanodisc concentrations in the BGE were used in order to study how the electrophoretic mobility of the analyte changed with increasing sphingomyelin nanodisc concentrations. For pyrene and 3-(α-Acetonylbenzyl)-4-hydroxycoumarin lipid concentrations were used between 0-1000 μM and for rhodamine 123 lipid concentrations were used between 0-250 uM.

2.7 Conclusion

The nanodiscs used for EKC experiments were generated using systematically varied copolymer to lipid ratios, copolymer belts of different molecular weight and chemical composition, and seven different lipid compositions. The effects of nanodisc composition on size and PSP properties were studied using dynamic light scattering, EKC characterization methods, and LSER analysis. In the following chapters the results of nanodisc characterization will be described in detail, along with the effects of synthesis parameters on small molecule-nanodisc interactions. The nanodiscs used in ACE were synthesized based on optimized parameters in order to determine the accuracy of using nanodisc affinity capillary electrophoresis for the measurement of K_D values. These results are found in chapter 7.

Chapter 3: Phospholipid bilayer affinities and solvation characteristics by electrokinetic chromatography with a nanodisc pseudostationary phase

3.1 Introduction

Using the methods described in Chapter 2 nanodiscs were characterized as a PSP in EKC. The utility of EKC to characterize PSPs and PSP–solute interactions has been recognized since EKC was developed.[7] A major application of EKC has been to measure the affinity between solutes and a PSP as proxy for lipid bilayer affinity or as an indirect measurement of octanol–water partition coefficients ($P_{o/w}$). The measurement of lipophilicity, as described by log $P_{o/w}$ or log D values (measured or calculated under specific conditions), is important in pharmaceutical development because metabolic clearance rates [54]and biotransport properties can be correlated to lipophilicity.[12] The measurement of solute partitioning is a primary application of EKC with liposome PSPs,[16,82–85] and this approach has also been used to estimate steroid-skin permeability,[86,87] blood–brain barrier transport,[88] ecotoxicity,[89] and drug-induced phospholipidosis risk.[90]

In this study, phospholipid nanodiscs were evaluated as a representative model of a lipid bilayer to determine bilayer affinities by EKC. Nanodiscs are generated from 1,2-dimyristoyl-*sn*-glycero-3-phosphocholine (14:0 PC) lipids, shown in Figure 2-3, and the styrene–maleic acid copolymer, shown in Figure 2-1. 14:0 PC lipids were chosen for this initial study to generate lipid–copolymer discs with uniform composition. 14:0 PC is a net nonionic lipid with no carbon double bonds leading to a bilayer with minimal disorder.

The utility of these nanodiscs as EKC PSPs is demonstrated for the first time, and the retention factors of 38 compounds are correlated to their experimental log $P_{o/w}$ values. All of the

compounds were analyzed in phosphate BGE in the absence of PSP in order to confirm zero electrophoretic mobility. This allowed for the comparison of log *k* values to log $P_{o/w}$ values and confirmed that the compounds migrate with electroosmotic flow when not associated with the nanodiscs. LSER analysis was conducted to further understand the interactions between small molecules and the lipid bilayer. Analysis of the results indicates that interactions with the phosphocholine head groups contribute significantly to the affinities of solutes for the nanodiscs. This chapter includes work that was published in *Electrophoresis*, 2017, 38, 738-746.[77]

3.2 Results and Discussion

3.2.1 Nanodisc Characterization

The first reported use of copolymer stabilized nanodiscs was for solubilization of membrane-bound proteins for spectroscopic studies.[1] Those nanodiscs were synthesized using a higher ratio of 3:1 (w:w) of copolymer to lipid[49] than were used in the current study. For the purposes of EKC, large ratios of copolymer belt to lipid were avoided in order to decrease the background UV absorbance. A copolymer to lipid ratio of 0.85:1:00 was used and yielded nanodiscs that were on average less than 20 nm by *Z*-average diameter and intensity measurements (Table 3-1). For three of the four syntheses, the measured diameters were not significantly different ($\alpha < 0.05$) and averaged 17.8 nm, while the fourth synthesis yielded nanodiscs about 20% larger. According to the literature, decreasing the copolymer-to-lipid ratio may increase the size of the nanodisc[91]. The copolymer-to-lipid ratio used here was selected to provide nanodiscs of sufficiently small diameter to minimize light scattering while at the same time reducing background absorbance from the copolymer that would be observed at higher copolymer-to-lipid ratios.

Table 3-1. Results of 4 syntheses using 0.85:1.00 belt: lipid (w: w) ratio.

Sample 1	Z-Average (d.nm)	Intensity (d.nm)
Trial 1	21.6±6.0	23.0±10.3
Trial 2	21.7±6.0	23.8±10.8
Trial 3	21.6±5.4	24.4±11.4
Sample 2		
Trial 1	17.9±6.3	17.2±7.0
Trial 2	17.9±5.5	17.6±7.0
Trial 3	17.8±5.8	18.2±8.0
Sample 3		
Trial 1	18.0±5.9	16.8±6.2
Trial 2	17.7±5.3	18.7±8.6
Trial 3	17.7±5.0	18.6±8.2
Sample 4		
Trial 1	17.6±5.7	16.7±6.3
Trial 2	17.7±5.3	17.6±7.0
Trial 3	17.9±5.4	19.3±9.5

Separations of representative small molecule probes using the 0.85:1 nanodiscs as a PSP are presented in Figs. 3-1 and 3-2. Figure 3-1 shows a separation of alkyl-substituted phenones with good plate counts and selectivity. The results from the alkyl-substituted phenones separation were used to calculate a nanodisc electrophoretic mobility of $–3.44±0.10 \times 10^{–4}$ $cm^2/V·s$. The reported electrophoretic mobility of SDS micelles is $–4.05 \times 10^{–4}$ $cm^2/V·s$[92] ; nanodiscs have lower mobility and provide a narrower migration range than typical micellar PSPs. Still, the nanodisc electrophoretic mobility is sufficient to provide a useful migration range and allows measurable differences in migration time for solutes with differing affinities. The nanodisc generated an average of 230 000 theoretical plates for the compounds in Fig. 3-1. The separation in Figure 3-2 also illustrates the good performance of the nanodisc PSP, providing good resolution, sufficient differences in migration time, and an average of 180 000 theoretical plates. Both figures also show reproducible negative system peaks observed in this system. The belt polymers have significant absorbance at the wavelength of detection, and small changes in

the background concentration of nanodiscs or styrene-containing impurities may be the cause of these system peaks.

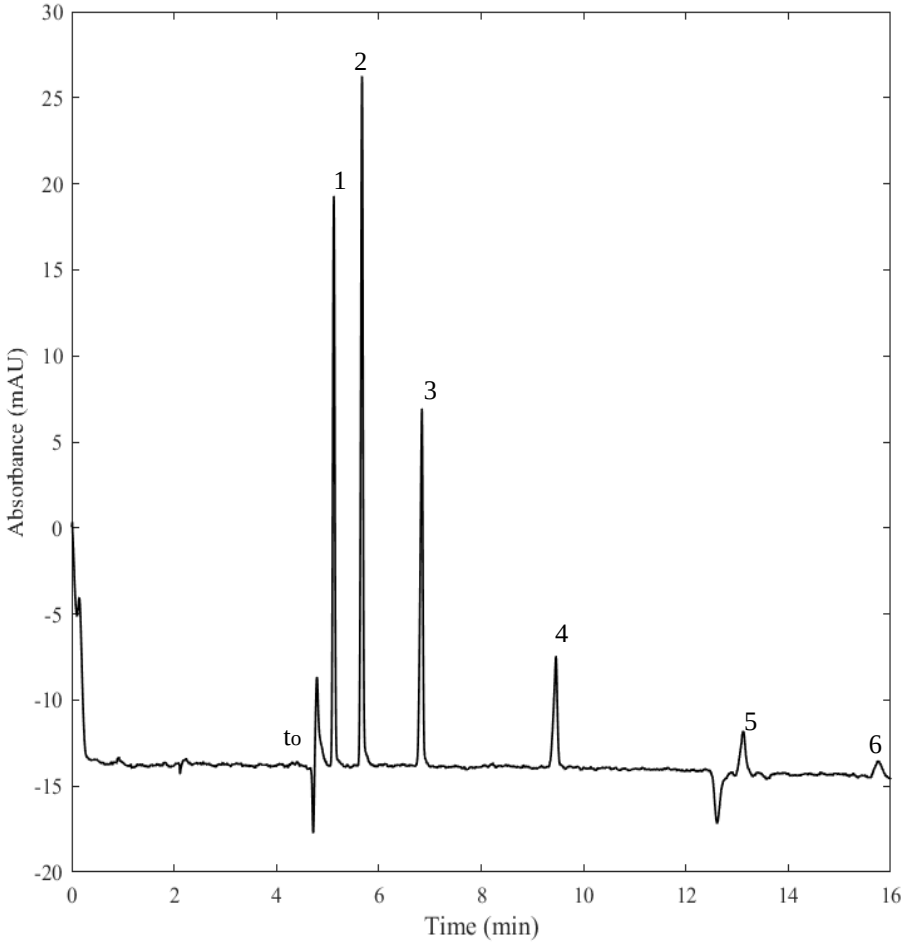

Figure 3-1: Separation of six alkyl-phenone solutes: (1) Acetophenone, (2) Propiophenone, (3) Butyrophenone, (4) Valerophenone, (5) Hexanophenone, and (6) Heptanophenone. Separation parameters: 5 mM phospholipid nanodisc with 1:0.85 (w:w) lipid to belt ratio, in a 25 mM phosphate pH 7.0. Capillary dimensions: 48.5 cm x 50µm I.D. with a 150µm extended cell pathlength. The injection was made with 35 mbar of pressure for 5 seconds. The operating voltage was 15 kV with detection at 245 nm. The negative peaks shown in the electropherogram are system peaks.

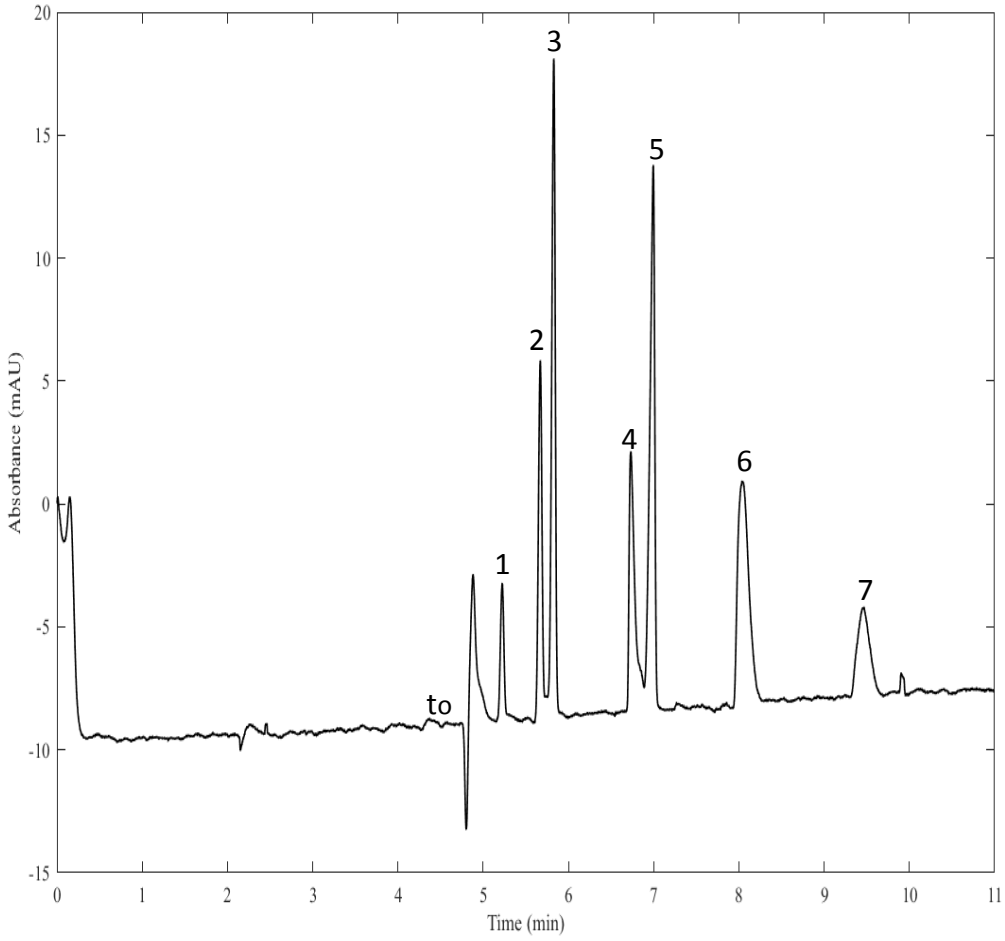

Figure 3-2. Separation of solutes: (1) Benzonitrile, (2) Nitrobenzene, (3) Methyl Benzoate, (4) 4-Nitroaniline, (5) Ethyl Benzoate, (6) Indole, and (7) 4-Chlorophenol. The analysis conditions were the same as in Fig. 3-2, with detection at 245 nm.

3.2.2 Comparison of octanol–water partition coefficients to retention factors

Thirty-eight compounds with varying functional groups and size and with published values for log $P_{o/w}$[12,93–96] (Table 3-2) were used to determine the effectiveness of these nanodiscs for indirect measurement of log $P_{o/w}$ and log $D_{pH7.0}$. Retention factors (k) for these were measured and are reported in Table 3-2.

Compound List[12,93–96]	Log $P_{o/w}$ Values	Log D Values	*k* value	Compound List	Log $P_{o/w}$ Values	Log D Values	*k* Value
Resorcinol	0.80	1.36	0.163 ±0.001	3,5-Dimethylphenol	2.35	2.70	0.858 ±0.002
Benzyl Alcohol	0.87	1.21	0.068 ±0.0001	4-Nitrotoluene	2.42	2.43	0.627 ±0.007
4-Nitroaniline	1.39	1.08	0.405 ±0.099	4-Chlorophenol	2.44	2.27	1.77 ±0.04
Phenol	1.46	1.67	0.197 ±0.0005	3-Chlorophenol	2.50	2.27	1.76 ±0.01
Phenyl Acetate	1.49	1.58	0.111 ±0.0007	4-Ethylphenol	2.50	2.63	1.12 ±0.03
Benzonitrile	1.56	1.83	0.121 ±0.0004	4-Bromophenol	2.59	2.43	2.86 ±0.015
3-Methyl Benzyl Alcohol	1.60	1.72	0.135 ±0.0009	3-Bromophenol	2.63	2.43	2.42 ±0.008
Acetophenone	1.63	1.53	0.116 ±0.0009	Butyrophenone	2.66	2.68	0.700 ±0.0009
4-Fluorophenol	1.77	1.81	0.390 ±0.002	Methyl-o-Toluate	2.75	2.49	0.789 ±0.003
4-Chloroaniline	1.83	1.75	0.559 ±0.0006	Chlorobenzene	2.84	2.58	1.25 ±0.01
Nitrobenzene	1.86	1.91	0.248 ±0.0004	Propylbenzoate	3.18	2.86	2.06 ±0.01
m-Cresol	1.96	2.18	0.396 ±0.004	Valerophenone	3.28	3.12	1.99 ±0.02
p-Cresol	1.97	2.18	0.448 ±0.001	4-Chlorotoluene	3.33	3.09	3.92 ±0.06
Anisole	2.11	1.82	0.321 ±0.001	Naphthalene	3.37	2.96	4.33 ±0.25
Methyl Benzoate	2.12	1.98	0.297 ±0.003	Hexanophenone	3.79	3.57	5.62 ±0.53
Indole	2.14	2.07	1.17 ±0.017	1-Methyl Naphthalene	3.95	3.48	15.4 ±3.4
Propiophenone	2.19	2.23	0.287 ±0.0006	Biphenyl	3.95	3.62	15.6 ±2.7
4-Chloroacetophenone	2.32	2.13	0.584 ±0.0009	Heptanophenone	4.32	4.01	12.5 ±0.7
Ethylbenzoate	2.33	2.33	0.692 ±0.005	Dibutyl Phathalate	4.50	4.63	16.8 ±0.5

Table 3-2. Probe solutes and their log $P_{o/w}$ values.

Correlations between log $P_{o/w}$ or log$D_{pH7.0}$ and log k were determined through linear regression. The data for log $P_{o/w}$ are plotted in Figure 3-3, and it is clear that there are at least two different classes of solute probes with different relationships between log $P_{o/w}$ and log k. The primary difference between the two groups of solutes was found to be their hydrogen bond donor strength. The upper group of 22 solutes, with an r^2 value of 0.973 and a slope of 1.24 ± 0.05, contains varying functionalities but none capable of donating a hydrogen bond. The second set of 16 solutes is hydrogen bond donors, and gave an r^2 value of 0.847 and a slope of 1.13 ± 0.13. Regression of all 38 compounds gave an r^2 value of 0.881 and a slope of 1.31 ± 0.08. There is not a single strong correlation for all solute chemistries, but good correlation and log $P_{o/w}$ determination could be achieved within particular solute categories, especially depending on solute hydrogen bond donor strength. It is possible that solutes with more acidic hydroxyl groups versus those with more basic amine groups may have slightly different trends, but more solutes with amine functionalities would need to be analyzed to determine if a significantly different trend is present.

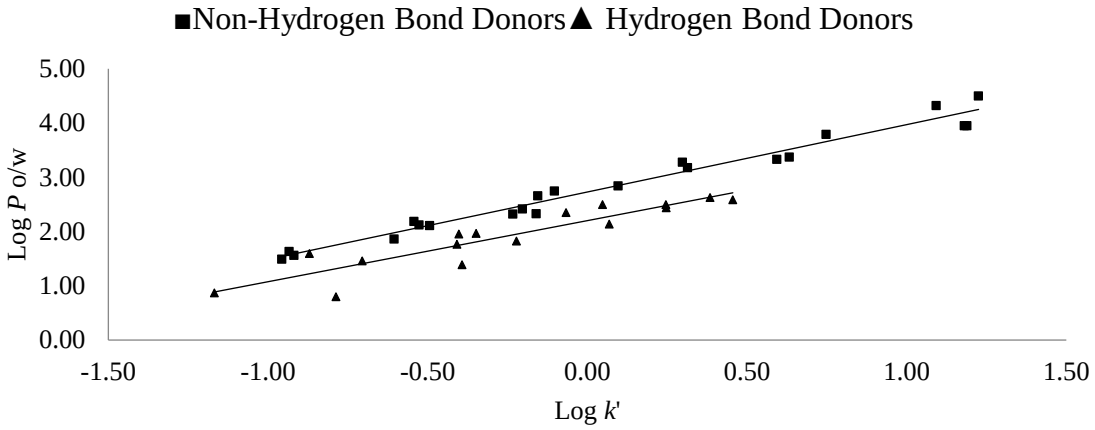

Figure 3-3: Plot of log $P_{o/w}$ versus log k for nanodisc system.

A plot of computationally derived log $D_{pH7.0}$ values versus log k is presented in Figure 3-5. Unlike Figure 3-4, there are no separate trends based on hydrogen bond strength. The r^2 value was 0.810 and the slope was 1.09 ± 0.09. In general, retention factor results correlate better with experimental log $P_{o/w}$ values than with computational log $D_{pH7.0}$ values.

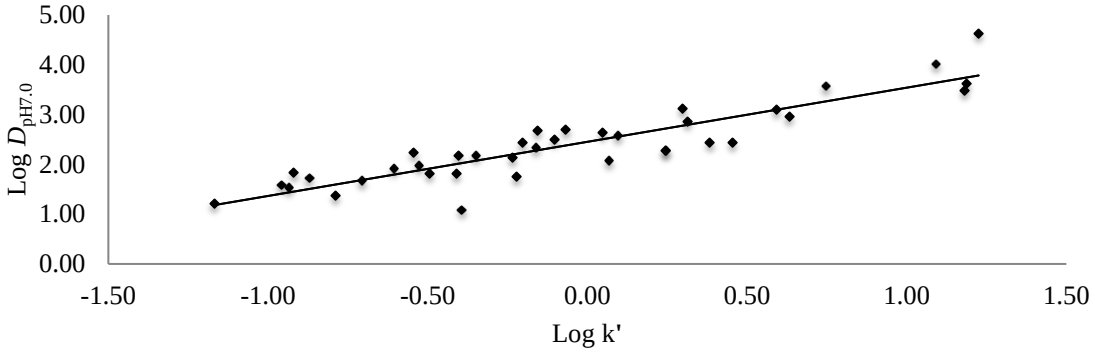

Figure 3-4: Plot of log $D_{pH7.0}$ versus log k for nanodisc system.

3.2.3 LSER Analysis

In order to gain a better understanding of why the affinities of different classes of compounds correlate separately with log $P_{o/w}$ values, LSER analysis was employed. The solutes used for this LSER analysis and their descriptors are provided in Table 3-3. This model, proposed and developed by Abraham *et al*.,[97] allows for the nanodiscs' solvation properties to be compared to other PSPs, octanol, and biological systems. The LSER coefficients for the phospholipid nanodiscs are presented in Table 3-4, along with the LSER coefficients for synthetic vesicles,[12] phospholipid vesicles,[98] cationic surfactants,[9] the octanol–water system, skin permeation studies, and transmission across the blood brain barrier. The skin permeation studies were completed using cadaver skin and stirred side by side in diffusion cells.[99] The blood–brain barrier is the interface between the walls of the capillaries and the neural tissue.[100] Neither the

skin permeation nor blood–brain barrier measurements represent similar processes to the aqueous-nanodisc partitioning measurements reported here. They do provide an indication of how these values are affected by solute chemistry for comparison with the model solvent systems, including nanodisc EKC or octanol/water partitioning.

Table 3-3: LSER Solutes and their solvation parameters.

Solute[57]	v	e	s	α	β	Solute[57]	v	e	s	α	β
1-Methyl Naphthalene	1.226	1.344	0.900	0.000	0.200	Benzonitrile	0.871	0.742	1.110	0.000	0.330
3-Bromophenol	0.950	1.060	1.150	0.700	0.160	Benzyl Alcohol	0.923	0.832	0.870	0.370	0.560
3-Chlorophenol	0.898	0.909	1.060	0.690	0.150	Biphenyl	1.324	1.360	0.990	0.000	0.220
3-Methyl Benzyl Alcohol	1.057	0.815	0.900	0.330	0.590	Chlorobenzene	0.839	0.718	0.650	0.000	0.070
3,5-Dimethylphenol	1.057	0.820	0.840	0.570	0.360	Ethylbenzoate	1.214	0.689	0.850	0.000	0.460
4-Bromophenol	0.950	1.080	1.170	0.670	0.200	Indole	0.946	1.200	1.120	0.440	0.220
4-Chloroacetophenone	1.136	0.955	1.090	0.000	0.440	m-Cresol	0.916	0.822	0.880	0.570	0.340
4-Chloroaniline	0.939	1.060	1.130	0.300	0.310	Methyl Benzoate	1.073	0.733	0.850	0.000	0.460
4-Chlorophenol	0.898	0.915	1.080	0.670	0.200	Methyl-o-Toluate	1.214	0.772	0.870	0.000	0.430
4-Chlorotoluene	0.980	0.705	0.670	0.000	0.070	Naphthalene	1.085	1.340	0.920	0.000	0.200
4-Ethylphenol	1.057	0.800	0.900	0.550	0.360	Nitrobenzene	0.891	0.871	1.110	0.000	0.280
4-Fluorophenol	0.793	0.670	0.970	0.630	0.230	p-Cresol	0.916	0.820	0.870	0.570	0.310
4-Nitroaniline	0.990	1.220	1.910	0.420	0.380	Phenol	0.775	0.805	0.890	0.600	0.300
4-Nitrotoluene	1.032	0.870	1.110	0.000	0.280	Phenyl Acetate	1.073	0.661	1.130	0.000	0.540
Acetophenone	1.014	0.818	1.010	0.000	0.480	Propiophenone	1.155	0.804	0.950	0.000	0.510
Anisole	0.916	0.708	0.750	0.000	0.290	Resorcinol	0.834	0.980	1.000	1.100	0.580

	Nanodiscs	O/W[97a]	CTAB-SOS[12]	POPC/PS[98]	C_{16}TAB[101]	Blood/Brain Barrier Rats[100a]	Skin Permation Studies[99a]
v	3.04 (0.10)	3.81 (0.12)	2.85 (0.16)	2.68 (0.25)	3.28 (0.22)	1.00 (0.20)	2.01 (0.20)
e	0.60 (0.07)	0.56 (0.12)	0.56 (0.13)	0.70 (0.22)	0.65 (0.13)	0.20 (0.20)	0.44 (0.20)
s	-0.36 (0.05)	-1.05 (0.12)	-0.57 (0.12)	-0.54 (0.18)	-0.58 (0.11)	-0.69 (0.20)	-0.41 (0.20)
a	0.57 (0.04)	0.03 (0.12)	0.23 (0.09)	0.02 (0.17)	1.06 (0.09)	-0.72 (0.20)	-1.63 (0.20)
b	-3.26 (0.08)	-3.46 (0.12)	-3.25 (0.18)	-2.90 (0.30)	-2.77 (0.18)	-0.70 (0.20)	-3.29 (0.20)

a - values in parenthesis are reported as standard deviation and not standard error
Table 3-4. LSER parameter results.

The *v* term is a measure of the increase in affinity of the PSP for solutes as the size of the solutes increases, and is a measure of the cohesiveness of the PSP relative to the BGE. The

aqueous BGE in EKC is a relatively cohesive solvent, like water in octanol–water systems, and so the value for *v* in the EKC and octanol–water systems is relatively large and positive. The relative magnitude of the values suggests that octanol is the least cohesive of the solvents or phases and that the nanodiscs are more cohesive and most similar to vesicles. No significant differences are observed among the nanodiscs, synthetic vesicles, and phospholipid vesicles.

All of the PSPs and octanol–water system have similar positive *e* terms, which represent the PSP's ability to interact with nonbonding and π electrons. The positive value for all systems indicates that they are more adept at interactions with nonbonding and π electrons than their aqueous counterparts. There are no statistically significant differences observed in the *e* values between different PSPs or octanol.

All of the systems shown have a negative *s* term signifying that more polar solutes are preferentially partitioned into the aqueous medium. The value for octanol is of significantly greater magnitude than for the EKC systems including the nanodiscs. This suggests that lipid bilayers and systems designed to model them are more polar than octanol, presumably because of the polar and ionic head groups. In this case, the model systems are more similar to the biological systems than is the octanol/water model.

The large negative *b* term for the nanodiscs, octanol, and the other PSPs indicates that they are less able to interact with hydrogen bond acceptors (are less acidic) than their aqueous counterparts. The skin permeation *b* value is also negative and of similar magnitude, while the blood/brain barrier *b* term is a much smaller negative value indicating that it responds very differently to more basic solutes.

The *a* term is positive and of relatively large magnitude for the nanodiscs, and it is this term that shows the greatest difference between the nanodiscs and other model systems. A positive *a* term means that a PSP has a greater ability to accept a hydrogen bond (is more basic) than the BGE. This is consistent with the observation relative to log $P_{o/w}$ above that hydrogen bond donor solutes behave differently as a class, with greater affinity for the nanodiscs than expected. The *a* terms for the octanol/water system and the phospholipid vesicles are not significantly different from 0, meaning solute acidity plays no measurable role in the solute partitioning in those systems. The nanodisc bilayer may be more able to accept hydrogen bonds because of the multiple carbonyls or the quaternary ammonium group located in the lipid head group, or the negative charge on the phosphate could allow for electrostatic interactions with an acidic hydrogen.

Norman *et al*.[102] demonstrated that indole partitions into lipid bilayers, near the hydrophobic/hydrophilic interface due to hydrogen bonding between indole's secondary amine and lipid carbonyl groups. The cationic surfactant micelles also have positive values for *a* of about unit magnitude, which is reported for all cationic micelles[9].This suggests that the positive *a* value for these nanodiscs is related to the presence of a quaternary amine in the head group. It should be noted that the *a* value for the nanodiscs could result from interactions with carbonyl groups on the copolymer belt, although a large positive *a* term is not typically associated with acrylate-containing polymeric PSPs.[101,103] Our preliminary experiments indicate weak or no interaction between probe solutes and the polymer alone as a PSP. Future experiments will probe this in greater detail as well as investigate and confirm the effect of lipid head group chemistry on the solvation environment.

3.3 Conclusions

Phospholipid bilayer nanodiscs with synthetic copolymer belts have, for the first time, been introduced as a PSP in EKC and demonstrated good performance. The use of a synthetic copolymer in place of belt proteins allows the nanodiscs to be generated affordably and in sufficient quantity for use in EKC. The nanodiscs have sufficient electrophoretic mobility to allow for a good migration range and generate high theoretical plate counts. Together, this results in high peak capacity and excellent ability to separate, resolve, and distinguish analytes of similar chemistry and structure.

More significantly, the nanodiscs offer a representative model of biological phospholipid bilayers that can be dispersed in BGE and studied by EKC. By this approach, the affinity of the bilayer structure for probe solutes can be determined and characterized.

One application of this method could be to calibrate retention versus log $P_{o/w}$ in order to estimate or determine log $P_{o/w}$ values quickly and inexpensively. Nanodisc retention factors for particular classes of compounds have been shown to correlate well with $P_{o/w}$, suggesting that this is a viable approach. However, it is clear that, due to specific localized interactions with the phospholipid used in this study, the method could not be applied generally and would require calibration with standards of similar chemistry to the compound of interest. Alternatively, other lipid structures incorporated into nanodiscs might provide better and more general correlation of retention with log $P_{o/w}$.

A potentially significant application of this technology relative to other PSPs could be to measure and characterize interactions between solutes and lipid bilayers directly. Nanodiscs with lipid composition similar to specific biological membranes could be generated and studied.

LSER analysis of the nanodisc–solute interactions in this study demonstrates that the nanodiscs provide a solvation environment with low cohesivity and weak hydrogen bond donating ability, similar in many respects to micelles, vesicles, and octanol. However, the nanodiscs also provide relatively strong hydrogen bond acceptor strength, similar to cationic micelles but significantly different from vesicles and octanol. This affinity for hydrogen bond donors is likely due to interactions with the phosphocholine head group, demonstrating that the approach is sensitive to specific localized interactions with the phospholipids and should be sensitive to changes in lipid composition.

Chapter 4: Optimization of the Synthesis, and Characterization of Copolymer Stabilized Nanodiscs

4.1 Introduction

Based on the results in Chapter 3 there remained some uncertainty on whether solute probes were interacting with the phospholipid head group or the styrene maleic acid copolymer. In this Chapter, we investigate more comprehensively the effects of nanodisc chemistry and composition on solvent characteristics in order to determine if these nanodiscs can be used in future work to study small molecule, peptide and protein interactions with lipid bilayers. In Chapter 3 the technique nanodisc electrokinetic chromatography was introduced,[104] but was unclear if the solute interactions with the nanodisc were solely or predominantly a solute-bilayer interaction. To determine the extent to which the styrene maleic acid, SMA, copolymers interact with the solute probes, nanodiscs were generated using systematically varied copolymer to lipid ratios, and copolymers of different molecular weight and chemical composition. Some significant differences are observed as a result of changes in copolymer to lipid ratio and copolymer chemistry that may be the result of changes in the nanodisc structure or to direct interactions with the copolymer. This chapter includes work that was published in *Electrophoresis*, 2018, 39, 844-852.[78]

4.2 Results and Discussion

4.2.1 Nanodisc Characterization

Over the course of this study, systematic changes were made to the structure and composition of the nanodiscs in order to understand how different factors affect PSP

performance and selectivity. This allowed for a systematic comparison of nanodiscs size, electrophoretic mobility, methylene selectivity, and theoretical plate count. Listed in Table 4-1 and 4-2 are the nanodiscs organized by SMA copolymer belt type and SMA belt to lipid ratio. All measurements had 3–7 replicates.

Copolymer	Copolymer: Lipid Ratio (w: w)	Nanodisc Lipid Composition	°C	μ_{eo} 10^4 ($cm^2/V*s$)	μ_{ep} 10^{-4} ($cm^2/V*s$)	α_{CH2}	N	n
30010[77]	0.85:1.00	14:0 PC	25	4.46±0.15	-3.44±0.10	2.59±0.12	253,000±40,100	5
30010	1.00:1.00	14:0 PC	25	4.41±0.15	-3.49±0.03	2.56±0.04	259,000±26,600	6
30010	1.43:1.00	14:0 PC	25	4.05±0.25	-3.79±0.06	2.38±0.03	260,000±34,700	6
30010	2.00:1.00	14:0 PC	25	4.22±0.10	-3.76±0.01	2.33±0.01	298,000±34,500	4
25010	2.00:1.00	14:0 PC	24	4.36±0.06	-3.70±0.08	2.45±0.05	165,000±50,500	6

Table 4-1. Nanodisc Parameters. The following table categorizes the nanodiscs by copolymer belt composition and copolymer to lipid ratio (w: w). In addition it also list the temperature at which the analysis was performed, the μ_{eo}, the μ_{ep}, the methylene selectivity, the average theoretical plate count of the phenones used in the analysis, and the number of replicates of the experimental runs.

4.2.1.1 Copolymer to lipid ratio

In Chapter 3 and published work,[104] nanodiscs composed of 14:0 PC were synthesized with a low copolymer (Xiran 30010) to lipid ratio, 0.85:1.00, for the purpose of decreasing background absorbance. This yielded nanodiscs on average that were 18 to 20 nm in diameter. Here, the results for 14:0 PC nanodiscs synthesized using Xiran 30010 ratios of 1.00:1.00, 1.43:1.00 and 2.00:1.00 are described. As the ratio of copolymer belt increased from 0.85 to 1.43:1.00, the diameter of the nanodiscs decreased from 20 to 10 nm, where it stabilized as the ratio was further increased to 2.00:1.00 (Table 4-2). Previous experiments in the literature show that 14:0 PC nanodisc will not shrink below approximately 10 nm even in an excess of SMA copolymer.[91] The smaller size of the nanodiscs with higher copolymer to lipid ratio suggests either that there are fewer lipids per nanodisc, that the higher copolymer content compresses the

lipid bilayer structure, or some combination of effects. Lipid bilayers are known to be fairly compressible.[105] As would be expected, the electrophoretic mobility increased as the anionic copolymer ratio increased and the size decreased (Table 4-1). The nanodiscs with 1.43:1.00 and 2.00:1.00 ratio showed statistically indistinguishable values of electrophoretic mobility. Methylene selectivity is a measure of hydrophobic selectivity, meaning it is a measure of how sensitive a PSP is to slight changes in a solute's hydrophobicity[10]. As the SMA ratio increased the methylene selectivity decreased from 2.59 ± 0.12 to 2.33 ± 0.01 (Table 4-1). All nanodiscs using the Xiran 30010 copolymer provided efficiency of 253 000-298 000 theoretical plates with no statistically significant differences observed (Table 4-1).

Copolymer	Copolymer: Lipid Ratio (w: w)	Nanodisc Lipid Composition	Diameter (nm)
30010	1.00:1.00	14:0 PC	16.1±6.93
30010	1.00:1.00	14:0 PC	16.0±7.00
30010	1.00:1.00	14:0 PC	14.7±5.51
30010	1.43:1.00	14:0 PC	10.3±3.22
30010	1.43:1.00	14:0 PC	10.5±3.43
30010	1.43:1.00	14:0 PC	10.0±2.76
30010	2.00:1.00	14:0 PC	10.4±4.22
30010	2.00:1.00	14:0 PC	10.1±3.74
30010	2.00:1.00	14:0 PC	10.8±4.51

Table 4-2. Nanodisc characteristics based on copolymer and lipid composition. Nanodiscs are organized by the copolymer chemistry and copolymer to lipid ratio (w: w). The diameter of the nanodisc is a result of 13-15 measurements.

4.2.1.2 Copolymer Chemistry

Nanodiscs composed of 14:0 PC lipids were synthesized with two different copolymer chemistries (Xiran 30010 and Xiran 25010) using 2.00:1.00 copolymer to lipid ratio and a 5 mM

lipid concentration. These nanodiscs, with the same ratio of copolymer to lipid, but different copolymer chemistry, have approximately the same diameter (Table 4-2).

The results in Table 4-1 show no statistically significant difference in the electrophoretic mobilities with the two belt chemistries, while a statistically significant difference is observed in the methylene selectivity ($p = 0.002$). The larger copolymer creates a slightly more hydrophobic environment. The efficiency was also significantly different ($p = 0.001$), with the Xiran 30010 generating significantly higher plate counts.

4.2.2 Comparison of octanol–water partition coefficients to retention factors

The log *k* values for a wide range of solutes were measured with nanodiscs of varied composition. Correlations between log $P_{o/w}$ and log *k* were determined through linear regression.

4.2.2.1 Copolymer to lipid ratio

Changes in the copolymer to lipid ratio were determined to have only minor effects on performance and selectivity. When the Xiran 30010 copolymer belt to lipid ratio was increased from 0.85:1.00 to 2.00:1.00 there was only a slight increase in the r^2 of the linear relationship between the log *k* values and the log $P_{o/w}$ from the literature. For 38 solute probes the r^2 increased from 0.881 to 0.904 as seen in Table 4-3. Plots of log $P_{o/w}$ vs. log *k* for three belt to lipid ratios appear very similar (Figure 4-1).

Table 4-3 Comparison of nanodiscs based on copolymer belt.

Copolymer Belt	**Copolymer Belt : Lipid Ratio (w: w)**	**Nanodisc Lipid Composition**	**Analysis Temperature °C**	**r^2 value relative to $P_{o/w}$**
Xiran 30010	0.85:1.00	14:0 PC	25	0.881
Xiran 30010	1.00:1.00	14:0 PC	25	0.891
Xiran 30010	2.00:1.00	14:0 PC	25	0.904
Xiran 25010	2.00:1.00	14:0 PC	24	0.941

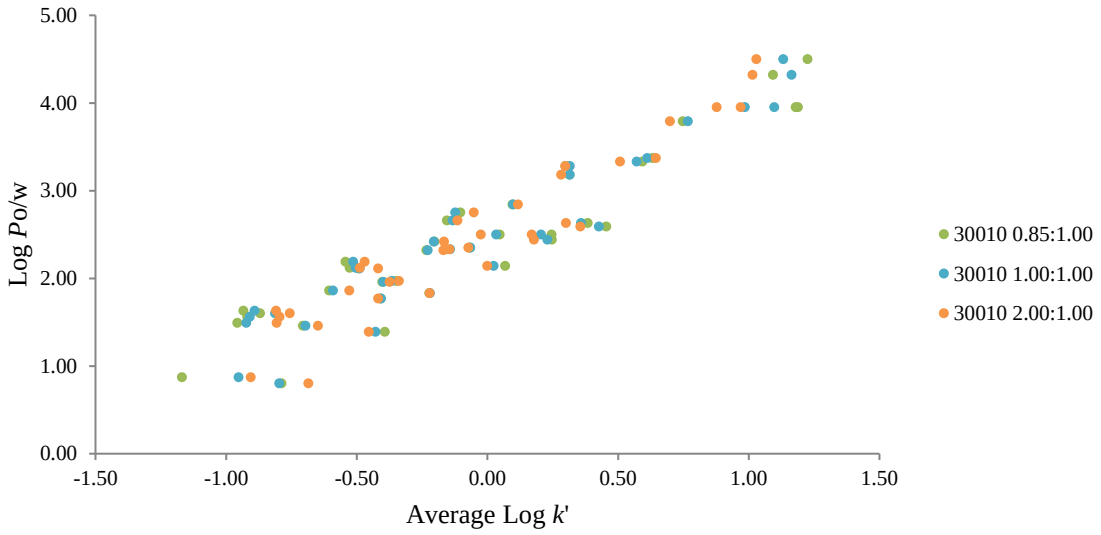

Figure 4-1.Plot of log $P_{o/w}$ vs log k for nanodiscs with different copolymer: lipid ratios.

In order to determine if there were changes in the selectivity of the solute-nanodisc interactions, the log *k* values obtained using nanodisc 1.00:1.00 and 2.00:1.00 Xiran 30010 copolymer to lipid ratios were graphed against each other. As presented in Table 4-4, the resulting r^2 for all solutes was 0.997, for hydrogen bond donating solutes was 0.997 and for non-hydrogen bond donors was 0.998. This demonstrates that there are no significant changes in the nanodisc-solute interactions when the copolymer to lipid ratio is increased. These results strongly suggest that interactions between solutes and the copolymer are not significant. If there were strong interactions between the solute probes and the copolymer portion of the nanodisc, one would expect that the r^2 value for the log *k vs* log $P_{o/w}$ plots would have decreased with increasing copolymer to lipid ratio and that the correlation between log *k* values that were graphed against each other would decrease as the difference in copolymer to lipid ratio increased.

	All Solutes			Hydrogen Bond Donors			Non Hydrogen Bond Donors	
Copolymer: Lipid	2:00:1:00	1:00:1.00		2:00:1:00	1:00:1.00		2:00:1:00	1:00:1.00
2:00:1:00	1.00	0.997		1.00	0.997		1.00	0.998
1:00:1:00	0.997	1.00		0.997	1.00		0.998	1.00

Table 4-4. Comparison of nanodisc interaction selectivity using correlation coefficients (r^2) for plots of log *k* on nanodiscs with different Xiran 30010 copolymer: lipid ratios (w: w).

4.2.2.2 Comparison of Xiran 30010 and Xiran 25010 Copolymers

The retention, selectivity and solvation characteristics of nanodiscs with copolymer belts of two different chemistries were also studied. The Xiran 25010 copolymer was introduced and compared with Xiran 30010 copolymer. Log *k* values from nanodiscs with Xiran 25010 copolymer were plotted vs. log $P_{o/w}$ values, resulting in an r^2 of 0.941 as compared to an r^2 value of 0.904 when using the Xiran 30010 copolymer (Table 4-3). In order to determine if there also was a change in nanodisc selectivity the log *k* values for the Xiran 25010 nanodiscs and the Xiran 30010 nanodiscs were graphed against each other and the r^2 values are presented Table 4-5. The r^2 for all solutes was 0.979, for hydrogen bond donating solutes was 0.937 and for non-hydrogen bond donors was 0.998. These results show that the chemical composition of the coolymer plays a more important role in nanodisc-solute interactions, particularly for hydrogen bond donors, than the copolymer to lipid ratio. It remains unclear whether this indicates a change in lipid bilayer structure with the different copolymers or is evidence of interactions of hydrogen bond donors with the copolymer.

	All Solutes			Hydrogen Bond Donors			Non Hydrogen Bond Donors	
Copolymer	30010	25010		30010	25010		30010	25010
30010	1.00	0.979		1.00	0.937		1.00	0.998
25010	0.979	1.00		0.937	1.00		0.998	1.00

Table 4-5. Comparison of nanodisc interaction selectivity using correlation coefficients (r^2) for plots of log *k* on nanodiscs with different Xiran copolymers.

4.2.3 LSER Analysis

In order to understand which chemical interactions determine nanodisc selectivity LSER analysis was employed. A detailed explanation of LSER analysis can be found in Chapter 2.

4.2.3.1 Xiran 30010 copolymer to lipid ratios

LSER analysis was conducted for three nanodiscs with ratios of Xiran 30010 copolymer to 14:0 PC lipid of 1.00:1.00, 1.43:1.00, and 2.00:1.00. These LSER results were also compared to LSER results of previously published nanodisc LSER data[104] with a 0.85:1.00 SMA:lipid ratio and can be seen in Fig. 4-2.

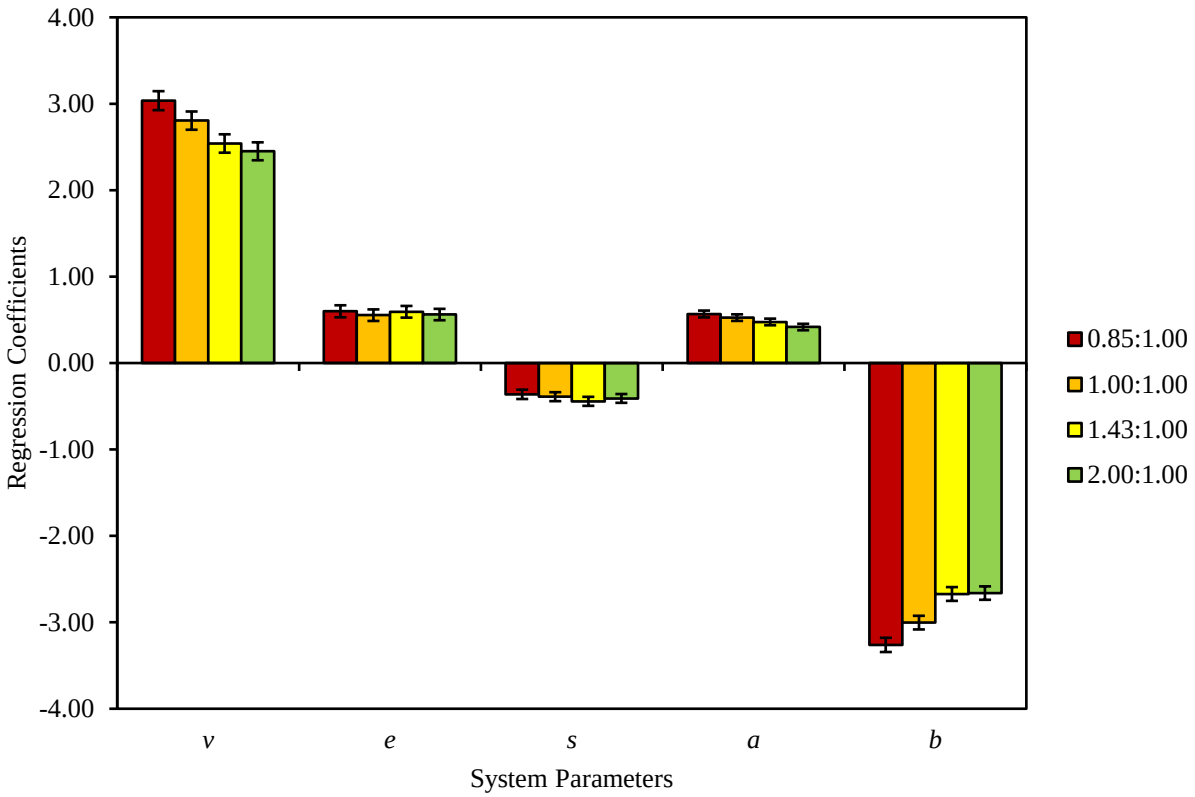

Figure 4-2. Comparison of LSER parameters based on Xiran 30010 to 14:0 PC ratio. LSER analysis was performed on nanodiscs that contained the same concentration of lipid, but varying (w: w) ratios of 30010 copolymer to lipid were using in the synthesis.

As the ratio of Xiran 30010 copolymer to lipid was increased and the nanodisc diameter decreased, the *v* term also decreased. The nanodiscs with a larger diameter and lower copolymer to lipid ratio would be less densely packed than nanodiscs of a smaller diameter and higher copolymer to lipid ratio. Formation of a solvation pocket is more energetically favorable in the less densely packed lipid bilayer. The *a* term also decreases with increases in copolymer to lipid ratio, which seems counterintuitive because increasing the copolymer to lipid ratio increases the number of maleic acid carbonyls capable of accepting hydrogen bonds. However, by increasing the amount of copolymer used in the synthesis, it appears that the lipids are packed more densely

and this increase in lipid packing density may sterically inhibit hydrogen bonding between the solutes and either the lipid head groups or the water molecules surrounding the lipid head groups. Lopez *et al*.[106] suggested that solvent accessibility was an important factor in hydrogen bonding and further analysis by Tejwani *et al*.[107] determined that hydrogen bonding with water molecules is the predominate mode of hydrogen bonding in the head group region. Increasing the packing density would reduce the amount or accessibility of water molecules in the head group region thereby reducing the *a* term. It is also possible that a less densely packed bilayer would allow greater access for hydrogen bond donating solutes to interact with the carbonyl groups of the ester near the hydrophilic/hydrophobic interface. This is the region where a bulk of the hydrophilic/hydrophobic partitioning occurs.[107] The *b* term also becomes less negative as the Xiran 30010 copolymer to 14:0 PC ratio increases; this could be a result of the PSP becoming a less effective hydrogen bond acceptor and therefore a more efficient hydrogen bond donor. The *s* and *e* parameters did not change within standard error meaning that the copolymer:lipid ratio and packing density of the lipid bilayer does not affect interactions with nonbonding, π-electrons, or polar solutes.

4.2.3.2 Comparison of Xiran 30010 and Xiran 25010 Copolymers

In order to further understand the role that the copolymer chemistry plays in solute-PSP interactions, LSER analyses were run on two sets of nanodiscs synthesized with Xiran 30010 and Xiran 25010 copolymers. The nanodiscs were generated using 5 mM lipid concentrations and a copolymer to lipid ratio of 2.00:1.00. Comparison of the LSER results in Figure 4-3, shows a statistically significant difference between the *s* and the *a* terms.

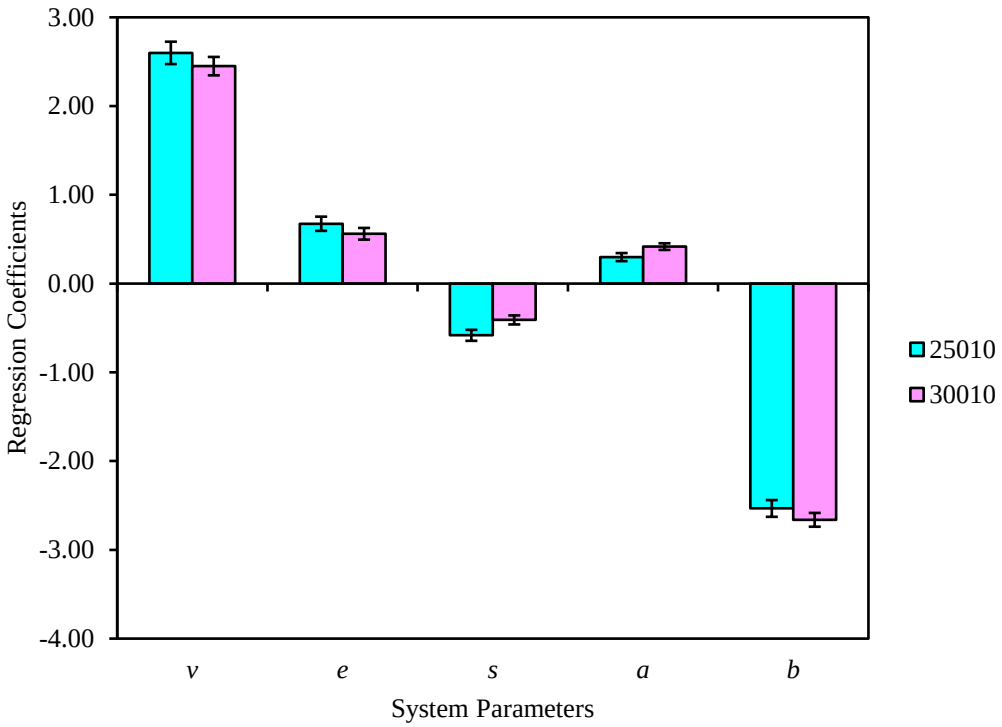

Figure 4-3**.** Comparison of Xiran copolymer using a 2.00:1.00 copolymer: lipid ratio. This LSER analysis compares two sets of nanodiscs that have the same lipid chemistry, the same concentration of lipid, and the same copolymer to lipid ratio (w:w). Two copolymers with different chemistries were used in the syntheses in order to compare how copolymer chemistry affects solute-nanodisc interactions.

The Xiran 30010 copolymer led to nanodiscs that had more favorable interactions with polar solutes, in addition to stronger interactions with molecules capable of donating hydrogen bonds. This change in the interactions could be a result of the chemistry of the copolymer or the different copolymer could cause structural changes to the lipid bilayer that encourage hydrogen bonding between solutes and the lipid head groups. Selectivity does change between nanodiscs with different stabilizing copolymers, which can be seen in Figure 4-4, where the hydrogen bond donor molecules are more retained by nanodiscs synthesized using the Xiran 30010 belt.

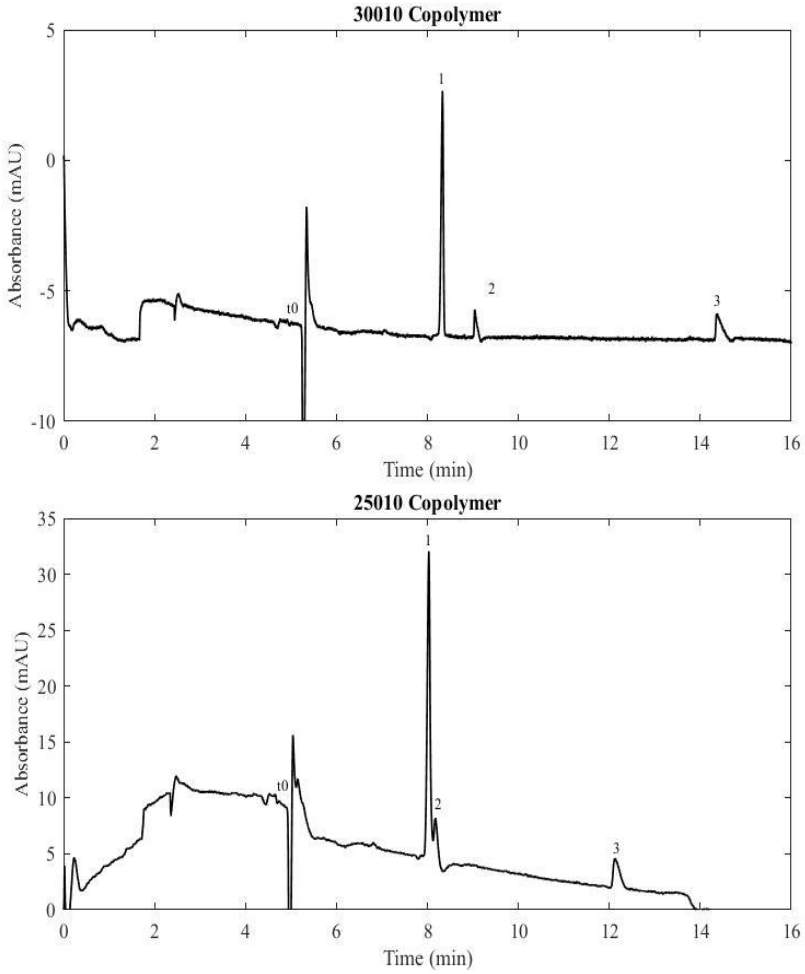

Figure 4-4. Separation of three solutes: (1) 4-Chloroacetophenone, (2) 3,5-Dimethylphenol, and (3) 4-Bromophenol. Separation parameters: 5 mM 14:0 PC phospholipid nanodiscs with 2.00:1.00 (w:w) Xiran copolymer belt:lipid ratio, in a 25 mM phosphate pH 7.0. Capillary dimensions: 48.5 cm x 50µm I.D. the top electropherogram utilized a 150µm extended cell pathlength, the bottom electropherogram did not. The injection was made with 35 mbar of pressure for 5 seconds. The operating voltage was 15 kV with detection at 245 nm. These separations averaged 179,000 theoretical plates.

4.3 Conclusions

Increasing the Xiran 30010 to lipid ratio resulted in smaller, more cohesive nanodiscs with reduced retention of hydrogen bond donor solutes. Comparison of nanodiscs formed with two copolymer, Xiran 30010 and Xiran 25010, determined either Xiran 30010 has greater affinity for hydrogen bond donating solutes or that Xiran 30010 produces structural changes in

the bilayer that promote interaction with hydrogen bond donor molecules and polar molecules. As a result of these experiments, nanodiscs in chapter 5 and the following chapters were synthesized using the Xiran 25010 copolymer. It is unclear if hydrogen bond donating solute probes are interacting with the Xiran 30010 copolymer if the Xiran 30010 copolymer induces a structural change in the lipid bilayer leading to an increase in the potential for hydrogen bonding.

Chapter 5: Determination of lipid bilayer affinities and solvation characteristics by electrokinetic chromatography using copolymer-bound lipid bilayer nanodiscs

5.1 Introduction

Following the results of Chapter 4, nanodiscs were synthesized using the Xiran 25010 at higher copolymer to lipid ratios. Since the parameters of the nanodisc synthesis were optimized in Chapter 4, the focus of this chapter is to study lipid bilayers with different bilayer chemistries. The performance, selectivity and solvation characteristics of nanodiscs with seven different lipid compositions, represented in Figure 2-3, were studied and compared to each other and to prior LSER analysis with liposomes.[37] Significant differences were observed in the solvent characteristics between nanodiscs with different lipid composition. LSER results that compared nanodisc solvent character with that of liposomes of similar lipid composition showed there were only minor differences in solute-bilayer interactions.[98] This strongly suggests that solute interactions with the lipid bilayer are dominant when using a nanodisc PSP. The nanodisc EKC approach is demonstrated to allow the determination of subtle differences in solvent characteristics between lipid bilayers of different composition. This chapter includes work that was published in *Electrophoresis*, 2018, 39, 844-852.[78]

5.2 Results and Discussion

5.2.1 Nanodisc Characterization

Seven different nanodiscs of varied lipid composition were generated from the seven lipids shown in Figure 2-3. Five contained uniform bilayers, and two contained mixed lipid bilayers. In order to form stable nanodiscs for all lipid compositions, a ratio of 2.50:1.00 Xiran 25010 copolymer to lipid was required. The lipid concentration for all the nanodiscs was 5 mM.

This led to a range of nanodisc diameters from 8–13 nm (Table 5-1). Nanodiscs composed of lipids containing double bonds were larger because unsaturated lipids are not able to pack as efficiently as those with fully saturated alkyl tails. As presented in Table 5-2, there was a large range in electrophoretic mobilities from $-3.89 \pm 0.07 \times 10^{-4}$ cm^2 $V^{-1}s^{-1}$ for 16:0 PC to $-4.12 \pm 0.03 \times 10^{-4}$ cm^2 $V^{-1}s^{-1}$ for 14:0 PC. With the exception of 16:0 PC nanodiscs, it does appear that on average larger nanodiscs have lower electrophoretic mobility and a smaller migration range than smaller nanodiscs, as might be expected. Nanodiscs that contained unsaturated alkyl tails had higher methylene selectivity than nanodiscs that had saturated alkyl tails. Changes to the head group chemistry in the 0.75:0.25 16:0 PC: 14:0 PE nanodisc led to higher methyl selectivity than would be expected for lipids with saturated alkyl tails.

Copolymer	Copolymer: Lipid Ratio (w: w)	Nanodisc Lipid Composition	Diameter (nm)
25010	2.50:1.00	0.75 16:0 PC 0.25 14:0 PE	11.5±4.86
25010	2.50:1.00	0.75 16:0 PC 0.25 14:0 PE	11.6±5.12
25010	2.50:1.00	0.75 16:0 PC 0.25 14:0 PE	11.5±5.15
25010	2.50:1.00	14:0 PC	8.85±2.86
25010	2.50:1.00	14:0 PC	9.09±3.20
25010	2.50:1.00	14:0 PC	9.38±3.54
25010	2.50:1.00	16:0 PC	9.76±4.10
25010	2.50:1.00	16:0 PC	9.55±3.84
25010	2.50:1.00	16:0 PC	9.74±4.17
25010	2.50:1.00	16:0 SM	10.1±3.66
25010	2.50:1.00	16:0 SM	10.2±3.83
25010	2.50:1.00	16:0 SM	10.5±3.95
25010	2.50:1.00	16:0-18:1 PC	12.2±4.95
25010	2.50:1.00	16:0-18:1 PC	12.5±5.59
25010	2.50:1.00	16:0-18:1 PC	12.5±5.78
25010	2.50:1.00	0.8 14:0 PC 0.2 14:0 PS	8.57±2.85
25010	2.50:1.00	0.8 14:0 PC 0.2 14:0 PS	8.57±2.70
25010	2.50:1.00	0.8 14:0 PC 0.2 14:0 PS	8.42±2.42
25010	2.50:1.00	14:1 PC	13.4±6.70
25010	2.50:1.00	14:1 PC	13.1±6.19
25010	2.50:1.00	14:1 PC	13.8±7.69

Table 5-1**.** Nanodisc diameter based on lipid composition. The diameter of the nanodisc is a result of 13-15 measurements.

Copolymer	Copolymer: Lipid Ratio (w: w)	Nanodisc Lipid Composition	°C	μ_{eo} 10^4 ($cm^2/V*s$)	μ_{ep} 10^{-4} ($cm^2/V*s$)	α_{CH2}	N	n
25010	2.50:1.00	14:0 PC	30	5.20±0.15	-4.12±0.03	2.37±0.03	256,000±39,300	6
25010	2.50:1.00	0.8 14:0 PC 0.2 14:0 PS	30	4.68±0.17	-4.10±0.05	2.39±0.06	201,300±34,200	6
25010	2.50:1.00	16:0 PC	30	4.53±0.08	-3.89±0.07	2.30±0.08	178,000±17,900	6
25010	2.50:1.00	0.75 16:0 PC 0.25 14:0 PE	30	5.00±0.06	-4.10±0.02	2.47±0.04	237,000±27,000	7
25010	2.50:1.00	16:0 SM	30	4.96±0.09	-4.09±0.03	2.37±0.03	232,000±24,300	7
25010	2.50:1.00	16:0-18:1 PC	30	4.89±0.09	-4.01±0.02	2.51±0.05	281,000±62,100	6
25010	2.50:1.00	14:1 PC	30	4.77±0.06	-4.02±0.04	2.44±0.03	222,000±9,600	5

Table 5-2. Results of EKC characterization. The following table lists the temperature at which the analysis was performed, the μ_{eo}, the μ_{ep}, the methylene selectivity, the average theoretical plate count of the phenones used in the analysis, and the number of replicates of the experimental runs.

5.2.2 Comparison of octanol–water partition coefficients to retention factors

The selectivity and solvation characteristics of the seven nanodiscs synthesized with different lipid compositions were compared to determine how changes in head and tail chemistry affect nanodisc-solute interactions. The log *k* values were graphed against log $P_{o/w}$ for each of the nanodiscs and the results are presented in Table 5-3.

Copolymer Belt	Copolymer Belt : Lipid Ratio (w: w)	Nanodisc Lipid Composition	Analysis Temperature °C	r^2 value relative to $P_{o/w}$
Xiran 25010	2.50:1.00	16:0 PC	30	0.933
Xiran 25010	2.50:1.00	14:0 PC	30	0.942
Xiran 25010	2.50:1.00	16:0 SM	30	0.954
Xiran 25010	2.50:1.00	0.75 16:0 PC 0.25 14: PE	30	0.960
Xiran 25010	2.50:1.00	14:1 PC	30	0.961
Xiran 25010	2.50:1.00	0.8 14:0 PC 0.2 14:0 PS	30	0.961
Xiran 25010	2.50:1.00	16:0-18:1 PC	30	0.962

Table 5-3. Comparison of nanodiscs r^2 values based on lipid composition.

16:0-18:1 PC nanodiscs resulted in the closest correlation to log $P_{o/w}$ values with an r^2 value of 0.962. This could be because 16:0-18:1 PC lipids contain a double bond and as a result 16:0-18:1 PC nanodiscs contain a more disordered bilayer. A disordered bilayer may be a better representation of octanol when compared to 14:0 PC or 16:0 PC lipids, which form more ordered bilayers. An example of the separations with different nanodisc lipid chemistries can be seen in Figure 5-1, which illustrates minor changes in selectivity as a function of lipid composition.

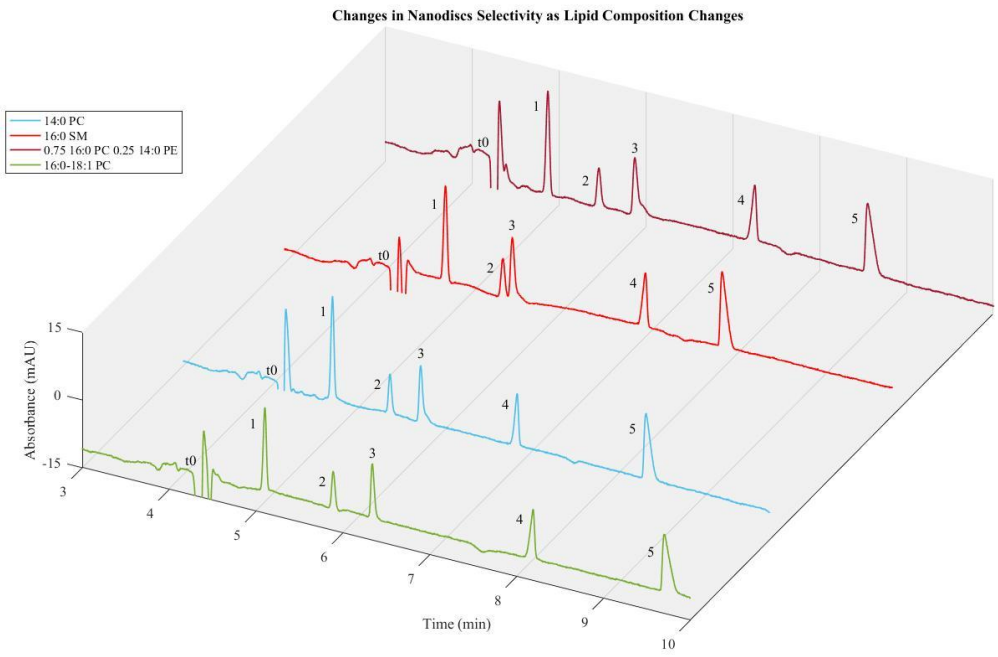

Figure 5-1. Separation of five solutes: (1) Benzonitrile, (2) p-Cresol, and (3) 4-Chloroaniline, (4) Butyrophenone, and (5) 3-Bromophenol. Separation parameters: 5 mM lipid nanodiscs with 2.50:1.00 (w: w) copolymer belt to lipid ratio, in a 25 mM phosphate pH 7.0. Capillary dimensions: 48.5 cm x 50µm I.D. the top electropherogram utilized a 150µm extended cell pathlength. The injection was made with 35 mbar of pressure for 5 seconds. The operating voltage was 15 kV with detection at 225 nm.

Using 16:0 SM nanodiscs the α between 4-Chloroaniline and p-Cresol was 1.36 ± 0.006 and using 14:0 PC nanodiscs the α was 1.32 ± 0.002, demonstrating quantitatively that there is significantly different selectivity between the two nanodiscs composed of different lipids. Both lipids contain saturated alkyl tails, but differ in head-group structure; 14:0 PC contains a glycerol group, while 16:0 SM contains a ceramide group. Figure 5-1 also demonstrates that nanodiscs are capable of producing separations with good peak symmetry and high separation efficiency, the average theoretical plate count of the 4 runs was 197,000±36,100 theoretical plates.

5.2.3 LSER Analysis

LSER analyses were run on seven different nanodiscs with varied lipid composition to determine how structural changes in lipid head and tail chemistry affect solute-lipid bilayer interactions. Figure 5-2 displays the LSER parameters for the seven different nanodiscs, and shows that the head group chemistry is much more influential in affecting bilayer-solute interactions than alkyl tail chemistry. There were no statistically significant differences between the *v* term for the seven nanodiscs analyzed even though there were lipids with varying alkyl tail length and degrees of unsaturation. Other studies have shown that water molecules only penetrate as far as the carbonyl atoms of the ester groups on the head group of the lipid,[108,109] which limits the number of solute probes that interact in the hydrophobic region of the nanodisc. There are also no significant differences between the *e* terms of any of the nanodiscs, indicating that changes to the lipid structure do not affect its ability to interact with nonbonding or π electrons.

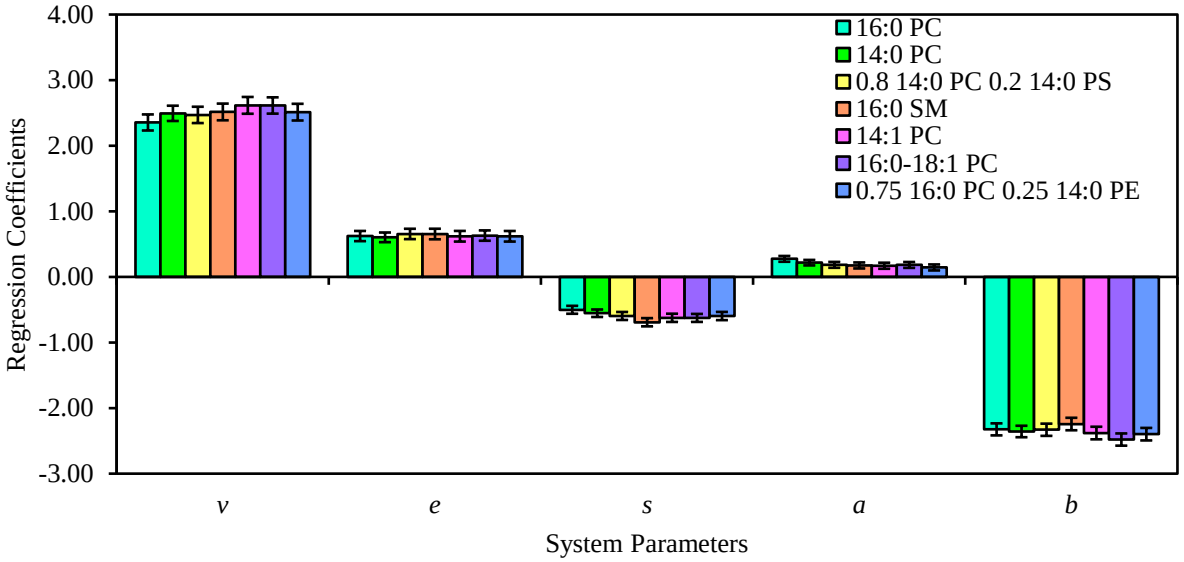

Figure 5-2**.** LSER results for nanodiscs of varied lipid composition. All nanodiscs were synthesized using the same concentration of lipid and ratio of 25010 copolymer to lipid. Five nanodiscs contained a single lipid chemistry and two contained mixed bilayers of two different lipid chemistries.

There were several significant differences between the *s* terms for the nanodiscs with different lipid compositions. The *s* term for 16:0 SM was significantly more negative than the *s* terms for 14:0 PC and 16:0 PC. Since the alkyl tails for 14:0 PC, 16:0 PC, and 16:0 SM are similar lengths and saturated, the difference in the *s* term must be the result of the changes to the head group chemistry. It should be mentioned that 16:0 SM was extracted from an egg and is actually 86% 16:0 SM, 6% 18:0 SM and 8% other alkyl chain variation. Unlike phospholipids, which have a glycerol backbone, sphingomyelin contains a sphingosine backbone and as a result it contains two polar groups: one hydroxyl and one amide[110] at the hydrophobic/hydrophilic interface. Both are capable of hydrogen bonding. According to simulations, 57% of sphingomyelin molecules intramolecularly hydrogen bond creating essentially a six-membered ring[110]. A side effect of this intramolecular hydrogen bond is that it reduces the water hydration in the head group region of the lipid. Sphingomyelin nanodiscs are less capable of interacting with polar solutes because the polar region is less hydrated[110] corresponding to a more negative *s* term. There is also a significant difference between 16:0 PC and 16:0-18:1 PC. This could be because 16:0 PC is in the gel phase at the temperature of analysis, whereas 16:0-18:1 PC is in the liquid crystalline phase. LSER data presented in Figure 5-4 shows the solvation characteristics of 14:0 PC nanodiscs, for which the transition temperature is 24°C, at various temperatures. These analyses were conducted with 14:0 PC in the gel phase, liquid crystalline phase, and a mixture of the two phases because nanodiscs have a broad transition unlike liposomes[48]. As the nanodiscs transition from a liquid phase to a gel phase the only LSER parameter to change within standard error is the *s* term, which became more negative. These experiments suggest that the differences in the ability to interact with polar solutes observed

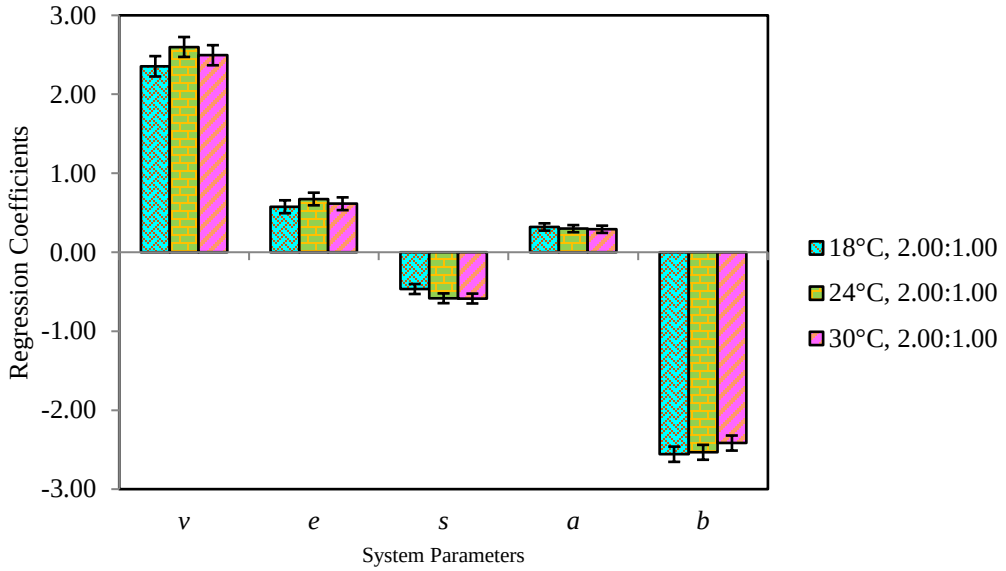

Figure 5-3**.** Comparison of Xiran 25010 14:0 PC nanodisc LSER temperature dependence. A series of LSER analysis was performed on a set of nanodiscs with a 2.00:1.00 copolymer: lipid ratio (w: w) at different temperatures. 14:0 PC has a transition temperature at 24ºC so altering the temperature allowed for the study of how lipid phase transition effected lipid-solute.

between 16:0 PC and 16:0-18:1 PC can be attributed to the phase state of 16:0 PC which is considered to be a more ordered bilayer.[111]

The *a* term for all of nanodiscs was positive implying that nanodiscs are more efficient hydrogen bond acceptors than the BGE. The structure of the polar head group must be considered to explain these results. Although the PC and SM head groups are polar, they each contain a quaternary ammonium with nonpolar methyl groups. As a result of these hydrophobic moieties, clathrate-like structures form wherein the polar water molecules form a lattice around the hydrophobic head groups.[108,112,113] This creates a hydration layer that can accept hydrogen bonds. In addition to this hydration layer the carbonyls on the phosphate and the ester groups are capable of accepting hydrogen bonds as well.[102,106–108] The *a* term for the nanodiscs composed of 16:0 PC was significantly more positive than all of the other nanodiscs with the exception of the nanodiscs composed of 14:0 PC. The *a* terms are not significantly different between 16:0 PC and 14:0 PC because they have the same head group chemistry and have saturated alkyl tails of a similar length. As can be seen in Figure 5-4, there is no difference between the *a* term of a lipid

in the gel phase and a lipid in the liquid crystalline phase. The *a* terms for 14:1 PC and 16:0-18:1 PC are smaller than 16:0 PC. Fluorescence studies have shown that increased unsaturation in the alkyl tail region leads to weakened hydrogen bond interaction between the head groups,[112] explain our observations. The 16:0 SM had significantly lower *a* term than 16:0 PC because of its ability to form intramolecular hydrogen bonds, reducing the ability of the carbonyls on the phosphate group to accept hydrogen bonds. The 0.8 14:0 PC 0.2 14:0 PS nanodisc has a significantly lower *a* term most likely due to the addition of 14:0 PS to the bilayer. Interestingly, there was a dramatic difference in the *a* term between the nanodisc that had a uniform 16:0 PC bilayer and the nanodisc of the mixed 0.75 16:0 PC and 0.25 14:0 PE. Phosphoethanolamine (PE) contains a primary ammonium instead of a quaternary ammonium. As a result of this change to the head group, PE lipids are capable of engaging in hydrogen bond donating with water and nonesterified oxygen on the phosphate group[108] and do not lead to formation of the clathrate structure. In addition to not forming a clathrate, PE head groups will break hydrogen bonds to undergo rotational motion.[113] These factors lead to a reduced ability to accept a hydrogen bond. The effects of changes in the *a* term on separation selectivity can be seen visually in the electropherograms in Figure 5-4.

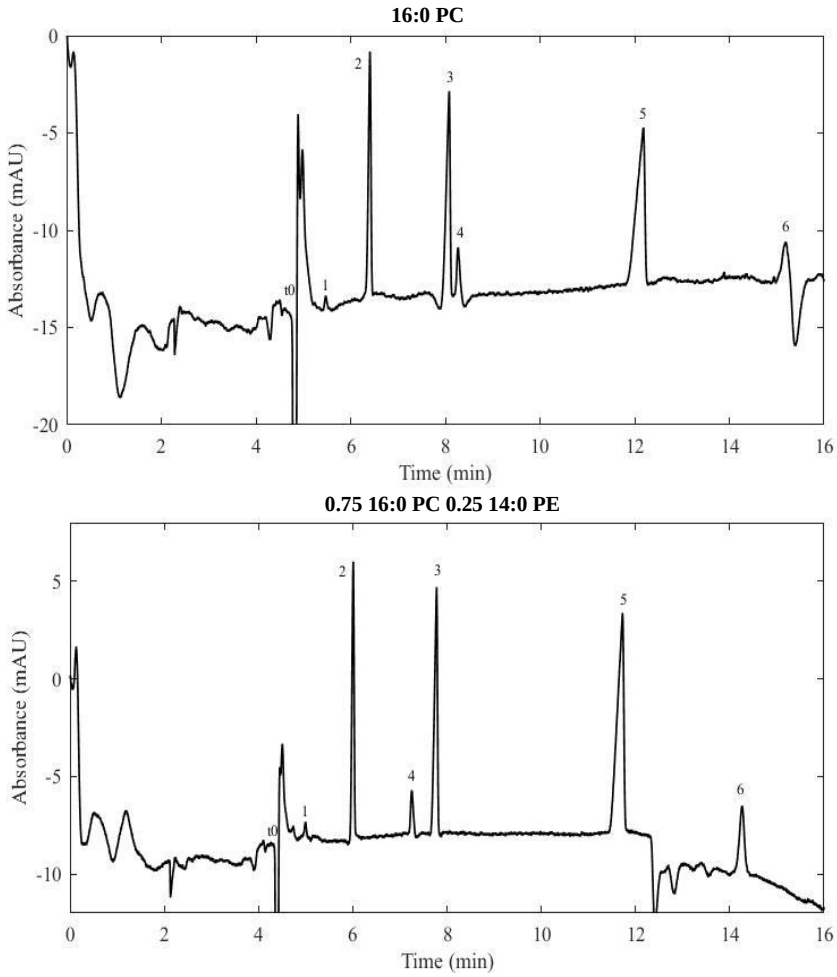

Figure 5-4. Separation of six solutes: (1) Benzyl Alcohol, (2) Methyl Benzoate, (3) Ethyl Benzoate, (4) 4-Ethylphenol, (5) Propyl Benzoate, and (6) 4-Chlorotoluene. Separation parameters: 5 mM phospholipid nanodiscs with 2.50:1.00 (w: w) Xiran 25010 copolymer belt to lipid ratio, in a 25 mM phosphate pH 7.0. Capillary dimensions: 48.5 cm x 50μm I.D. with a 150μm extended cell pathlength. The injection was made with 35 mbar of pressure for 5 seconds. The operating voltage was 15 kV with detection at 245 nm. These separations averaged 169,000 theoretical plates.

Lastly, the *b* term for all of the nanodiscs is negative because water in the BGE is a superior hydrogen bond donor. The only significant differences in the nanodisc LSER values were between 16:0-18:1 PC and 16:0 SM. The 16:0 SM *b* term was less negative than the 16:0-18:1 PC value and this is likely because of the structural differences between the head groups of the two lipids. At the interface between the hydrophobic and hydrophilic portion of the bilayer,

16:0 SM contains two moieties that are capable of donating a hydrogen bond[114], while the 16:0-18:1 PC contains only ester groups capable of accepting hydrogen bonds.

To further probe whether the predominant interactions with nanodiscs are with the lipid bilayer rather than the belt polymer, LSER results were compared to liposome LSER analysis reported by Pascoe *et al*.[98] The nanodiscs used for comparison were synthesized using a 2.50:1.00 Xiran 25010 copolymer belt to 16:0-18:1 PC ratio, while the liposomes were composed of a 0.80:0.20 molar ratio of 16:0-18:1 PC to 16:0-18:1 PS. The nanodisc electrophoretic mobility was $-4.01 \pm 0.02 \times 10^{-4}$ cm^2 $V^{-1}s^{-1}$ and provided a larger migration range than liposome that had an electrophoretic mobility of -3.87×10^{-4} cm^2 $V^{-1}s^{-1}$. The nanodiscs' peak efficiency was also superior; Pascoe *et al*. reported that the average theoretical plates per meter (N/m) for propiophenone was 75,100[98] while the average N/m for propiophenone on the nanodiscs was 712,000. LSER results were the same within standard error for four of the five system descriptors as seen in Figure 5-5. The difference in the *b* term is small but statistically significant, with the liposome value more negative than the nanodisc value. This could be a result of differences in bilayer-water interface. The nanodisc is a planar bilayer, while the liposome is a spherical bilayer. Analysis of the thermodynamics of peptide partitioning by Kim *et al*. determined that the curvature of the membrane surface may play a significant role in peptide partitioning,[42] and this could apply to other solute partitioning as well. Overall, these results demonstrate that the nanodisc bilayer solvation environment is very similar to that of liposomes, suggesting that copolymer belt-solute interaction plays a minimal, if any, role in the overall nanodisc-solute interaction.

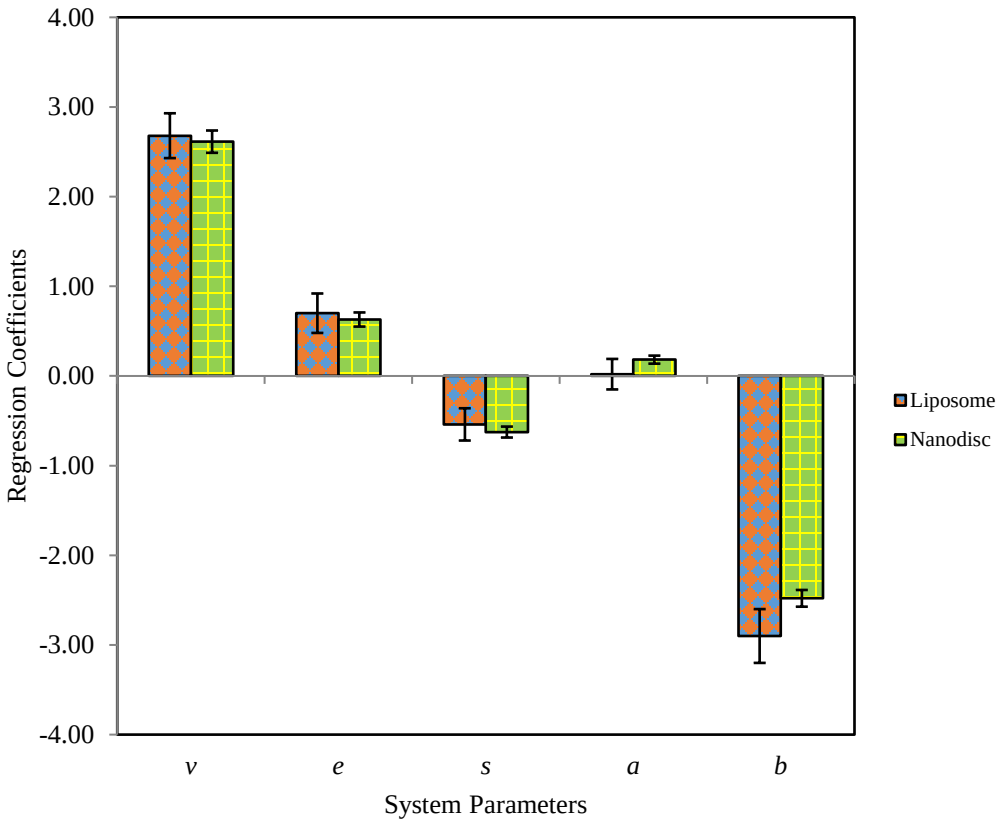

Figure 5-5. Comparison of liposome and nanodisc LSER results. Nanodiscs LSER results were compared to LSER results in the literature of liposomes, which contained similar lipid chemistry.

5.3 Conclusions

The properties of phospholipid and sphingomyelin nanodiscs were characterized using nanodisc EKC. For the indirect measurement of log $P_{o/w}$ values 16:0-18:1 PC lipids provided a solvent environment that was most analogous to octanol. LSER analysis showed that nanodisc EKC is sensitive to slight structural changes in lipid head group chemistry. Changes to in alkyl tail chemistry did not lead to significant changes in the bilayer-solute interactions because polar solutes rarely penetrate deep into the hydrophobic region. Comparison of LSER results for a nanodisc bilayer to published results for a lipid vesicle showed only minor differences that are likely due to differences in the lipid composition and bilayer curvature. Together, these results

demonstrate that solute interactions with polymer-bound nanodiscs are primarily with, and representative of, interactions with the lipid bilayer. Nanodisc EKC has been shown as a reliable method for the measurement and characterization of bilayer-solute interactions.

Chapter 6: Sphingomyelin ability to act as chiral selector using nanodisc electrokinetic chromatography

6.1 Introduction

Chapters 3 and 4 focused on developing and altering nanodisc synthesis, in order to optimize solute-bilayer interactions. Chapter 5, compared nanodiscs with different chemistries in order to understand how lipid structure affected nanodisc solvent environment. The focus of Chapter 6, is the study novel solute-bilayer interactions. This chapter includes work that was published in *Chemistry and Physics of Lipids*, 2018, 214, 11-14.[79]

Due to the inherent cost of pharmaceutical development, it is important to have fast, efficient, and relatively inexpensive techniques to study drug absorption, distribution, metabolism, and excretion. CE is a separation and analysis technique, which allows for quick analysis, high theoretical plate counts and resolution using nanoliter sample volumes. CE has become a valuable technique for studying biomolecule affinity,[115–117] and membrane characterization,[19,78,82,118] as well as pharmaceutical absorption,[18,119,120] and metabolism.[121–123] Nanodisc electrokinetic chromatography (NEKC), the focus of my research, is an adaptation of CE using lipid bilayer nanodiscs as additives, as a technique for the study of small molecule interactions with lipid bilayers.[78,118] Using this technique it was demonstrated that solvation of small molecules into lipid bilayers was sensitive to slight structural changes in lipid head group chemistry.[78] The sensitivity of this approach to observe and characterize small differences in affinity for the lipid bilayer nanodiscs should render it sensitive to differences in affinities between stereoisomers.

There is significant disagreement among previous studies of the effects of lipid stereochemistry on bilayer properties and affinities. Some studies have shown that phospholipids showed no preferential interaction with either R or S chiral molecules and that the changing the stereocenters of the lipids did not affect bilayer physical properties.[124–126] While more recent work has shown that after 24–48 hour incubation periods enantiomerically pure liposomes could preferentially absorb L-amino acids and preferentially absorb higher concentrations of one ibuprofen enantiomer over the other.[127,128]

A pair of papers published in 2001 suggested that sphingomyelin bilayers could distinguish between nat-cholesterol and ent-cholesterol, its unnatural enantiomer.[129,130] These findings were rebuked by the extensive analysis of Mannock *et al.* in 2003 who concluded that significant enantioselective cholesterol-sphingolipid interactions do not occur in model membrane systems.[131] Although the properties of sphingomyelin have been studied extensively in the literature,[110,132–134] there has not been extensive work on the interaction between atropisomers and sphingomyelin. Understanding if the stereochemistry of an atropisomer affects affinity for sphingomyelin has the potential for implications in drug development and in the study of membrane function.

The conflicting results in the literature regarding the chiral selectivity of sphingomyelin lipid bilayers led to us to apply NEKC to characterize enantiomer, diastereomer and atropisomer interactions with these bilayers. In general, no detectable enantiomer or diastereomer selectivity was observed, but significant selectivity was observed in the separation of (R)-(+)/(S)-(−)-1,1′-Bi-2-naphthol, an atropisomer shown in Figure 6-1. The successful separation demonstrates that NEKC is a sensitive technique for measuring small molecule bilayer interactions and provides tangible evidence of atropisomer selectivity in sphingomyelin bilayers.

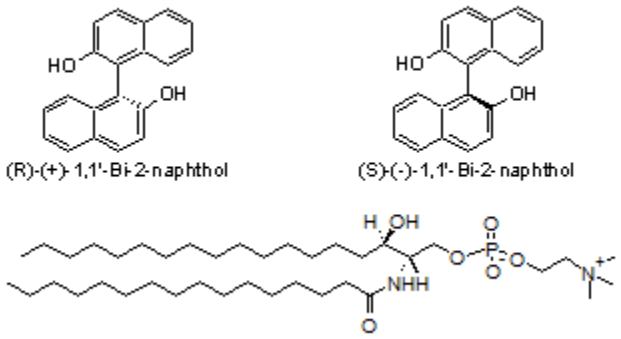

Figure 6-1. Atropisomers and sphingomyelin.

Sphingomyelin, seen in Figure 6-1, is a class of sphingolipids that contain a phosphocholine head group, sphingosine base and the acyl group linked to the amide nitrogen.[114] The sphingosine base contains two chiral centers with a D-*erythro* or 2S, 3R configuration, which differentiates it from other phosphocholine lipids, which only contain one chiral center. The stereochemistry of sphingomyelin has been shown to play an important role in its biophysical properties, when enantiomerically pure sphingomyelin is compared to its racemate.[135] Sphingomyelin is a major lipid component of cell membranes and studies have shown that sphingomyelin distribution in membranes of the aorta and arteries increases with age.[114]

6.2 Results and Discussion

6.2.1 Nanodisc Characterization

The nanodiscs used for the analysis of atropisomer interactions with sphingomyelin are similar in composition to sphingomyelin nanodiscs analyzed in Chapter 5.[78] The nanodisc properties are reported in Table 6-1. The different ratios of copolymer to lipid used in synthesis 2.50:1.00 (w:w) vs 2.00:1:00 (w:w) led to small but statistically significant ($p = 0.002$) differences in methylene selectivity, a measure of hydrophobicity.

Table 6-1. Nanodisc electrokinetic properties. μ_{ep} is the electrophoretic mobility, α_{CH2} is the methylene selectivity, and N is the theoretical plate count from the phenone separation. All values reported +/- one standard deviation for n measurements.

Copolymer	**Copolymer: Lipid Ratio (w: w)**	**Nanodisc Lipid Composition**	**°C**	**μ_{ep} 10^{-4} (cm^2/V*s)**	**α_{CH2}**	**Nx10^3**	n
25010	2.00:1.00	Sphingomyelin	30	-4.17±0.09	2.26±0.06	214±33	8
25010	2.50:1.00	Sphingomyelin	30	-4.09±0.03	2.37±0.03	232±24	7

The more hydrophobic environment with higher copolymer ratio is contrary to previous results with 1,2-dimyristoyl-sn-glycero-3-phosphocholine lipid nanodiscs.[78] In the current experiments, the nanodisc with lower ratio of copolymer to lipid was used to decrease the background absorbance and allow detection of analytes at low concentrations.

6.2.2 Separation of (R)-(+) & (S)-(−)-1,1′-Bi-2-naphthol

Using 5 mM concentration of sphingomyelin nanodiscs in the BGE, atropisomers of 1,1′-Bi-2-naphthol were separated. The resolution parameters are listed in Table 6-2, average resolution was 2.41 ± 0.34 with an average theoretical plate value of $889 \times 10^3 \pm 429 \times 10^3$. As shown in Figure 6-2 the (R)-(+) stereochemistry of 1,1′-Bi-2-naphthol was less retained than the (S)-(−) stereochemistry.

Table 6-2. 1,1'-bi-2-napthol Separation results. k is the retention factor, α the chromatographic selectivity, F_{ND} is fraction of the analyte bound to the nanodisc during the separation, N is the number of theoretical plates, and R_s the chromatographic resolution.

Atropisomer	**k_R**	**k_S**	**$k_{average}$**	**α**	**F_{ND}**	**$Nx10^3$**	**Rs**	**n**
(R)-(+)/(S)-(-)1,1'-bi-2-napthol	9.77±0.79	10.07±0.83	9.92±0.81	1.03±0.00	0.908±0.007	889±429	2.41±0.34	3

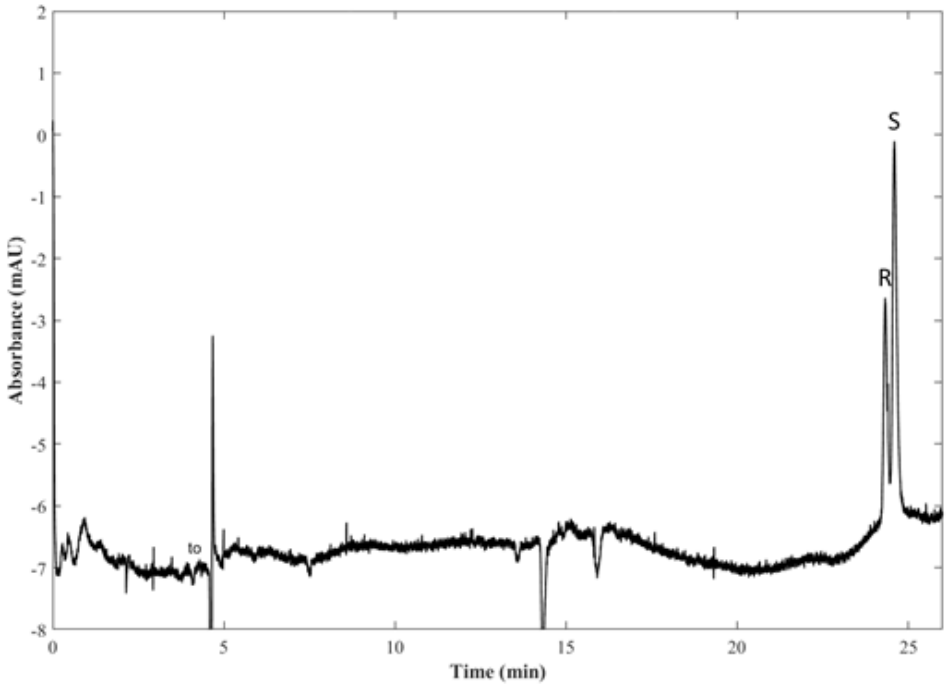

Figure 6-2. Separation of (R)-(+) / (S)-(-)-1,1'-Bi-2-naphthol . Separation parameters: 5 mM 16:0 SM nanodiscs with 2.00:1.00 (w:w) Xiran 25010 copolymer belt to lipid ratio, in a 25 mM phosphate pH 7.0. Capillary dimensions: 48.5 cm x 50µm I.D. The injection was made with 35 mbar of pressure for 5 seconds. The operating voltage was 15 kV with detection at 245 nm. This separation averaged $102x10^4$ theoretical plates.

The selectivity of 1.03 ± 0.00 represents consistent difference in affinity for the R and S configurations. The F_{ND} of 0.908 indicates that 90.8% of the analytes were bound to the nanodiscs during separation. The number of analyte molecules bound per nanodisc during separation was determined from the known analyte and lipid concentrations as well as the following equation:

$$F_{ND} = \frac{k}{k+1} \tag{6-1}$$

Where *k* is the retention factor and F_{ND} is the fraction of the analyte which is bound to the nanodiscs during the separation.

Based on previous measurements of the size of similar nanodiscs[48] and the molecular area of sphingomyelin, 52.5 Å^{2},[136] it can be approximated that there are between 156 and 192 lipids per nanodisc. Using this information and the F_{ND} of analyte bound to nanodisc it can be estimated that there are approximately 4 analytes bound per nanodisc during the separation.

In order to confirm that this separation was result of the chiral selectivity of sphingomyelin and not the result of an artifact each atropisomer was run as a single standard to determine that the compound was pure. The retention order of the atropisomers was determined by spiking the racemic mixture with one of the atropisomers and observing the changes in peak area. The racemic mixture was run in BGE without nanodiscs and in a solution of belt polymer in BGE with no separation observed. 1,2-Dimyristoyl-sn-glycero-3-phosphocholine nanodiscs were synthesized using the same synthesis parameters as the sphingomyelin nanodiscs. When 1,2-dimyristoyl-sn-glycero-3-phosphocholine nanodiscs were utilized as a pseudostationary phase no atropisomer separation was observed, as seen in Figure 6-3. Combined, these results demonstrate

that sphingomyelin, and not the copolymer belt, is responsible for the observed atropisomer selectivity.

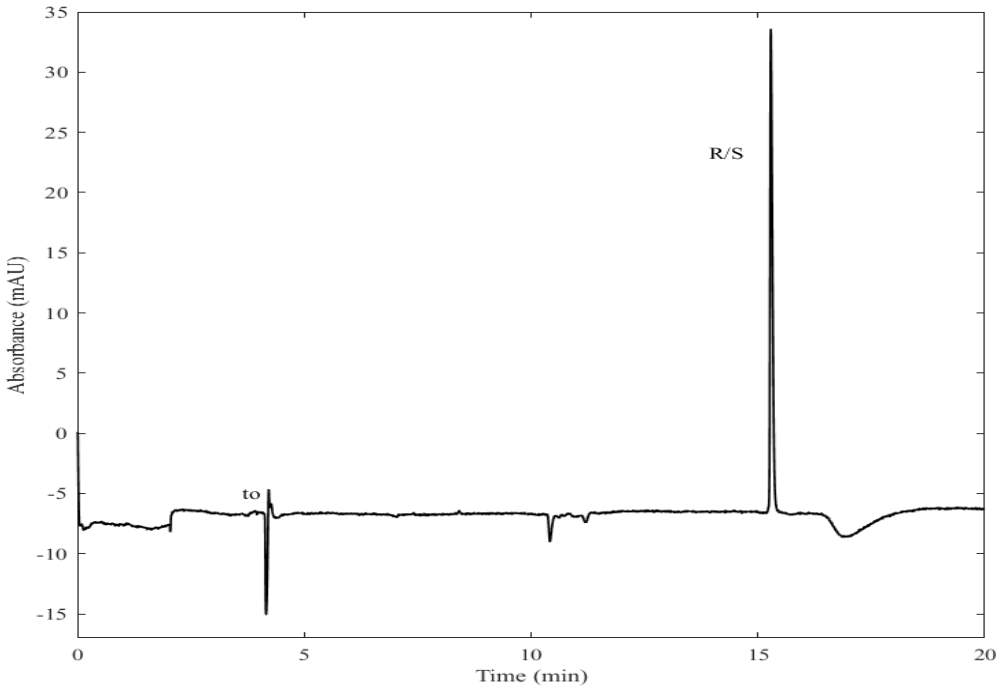

Figure 6-3. Separation of (R)-(+) / (S)-(-)-1,1'-Bi-2-naphthol using 14:0 PC nanodiscs . Separation parameters: 5 mM 14:0 PC nanodiscs with 2.00:1.00 (w: w) Xiran 25010 copolymer belt to lipid ratio, in a 25 mM phosphate pH 7.0. Capillary dimensions: 48.5 cm x 50µm I.D. The injection was made with 35 mbar of pressure for 5 seconds. The operating voltage was 15 kV with detection at 245 nm. The efficiency of this peak was $969x10^3$ theoretical plates.

Sphingomyelin contains two chiral centers in a 2S,3R configuration at the hydrophilic/hydrophobic interface, where previous analysis has shown that a majority of the hydrophilic/hydrophobic partitioning occurs[107]. The separation of the (R)-(+)/(S)-(−) atropisomers could be a result of a cooperative interaction between the two chiral centers or the configuration produces a sterically selective interaction with the atropisomers in the same way that dipeptide polymerized surfactants have for the separation of 1,1′-Bi-2-naphthol in EKC[137].

After successful separation of the atropisomers a series of chiral compounds of varied chemistry and structure were analyzed to determine if sphingomyelin nanodiscs were more generally enantiomer or diastereomer selective. The compounds that were analyzed are listed in Table 6-3. These compounds were chosen because they were of varying hydrophobicities with different levels of acidity and basicity. No resolution was observed for any of these enantiomers or diastereomers using sphingomyelin nanodiscs. These results confirmed previously published analysis by Mannock et al. that sphingomyelin did not have strong selectivity in interactions with enantiomers[131].

Analytes	Form of stereochemistry
1-Phenyl-2-propyn-1-ol	Enantiomer
3-(∝-Acetonyl-4-chlorobenzyl)-4-hydroxylcourmarin	Enantiomer
Chlorthalidone	Enantiomer
Ephedrine	Diastereomer
Flavanone	Enantiomer
Furoin	Enantiomer
Homatropine Hydrobromide	Enantiomer
Hydrobezoin	Diastereomer
Ketoprofen	Enantiomer
Methyl DL mandelate	Enantiomer
Norphenylephrine Hydrochloride	Enantiomer
Omeprazole	Enantiomer
Pseudoephedrine	Diastereomer
Propranolol Hydrochloride	Enantiomer
Salbutamol	Enantiomer
Verapamil	Enantiomer

Table 6-3. Chiral analytes that showed no evidence of selectivity using sphingomyelin nanodiscs as a chiral selector.

6.3 Conclusion

In conclusion, the chiral selectivity of sphingomyelin bilayers was studied using NEKC analysis. It was determined that (S)-(−)-1,1′-Bi-2-naphthol had measurably stronger affinity for

the sphingomyelin nanodisc than that (R)-(+)-1,1′-Bi-2-naphthol, to the point where the two atropisomers were successfully resolved. Sphingomyelin bilayers are shown to have selective interactions with an atropisomer, but not enantiomers or diastereomers. This result also demonstrates the high sensitivity of nanodisc electrokinetic chromatographyto small differences in affinity between bilayers and ligands, and that axial chirality might influence passive diffusion into sphingomyelin bilayers.

Chapter 7: Cross Correlational Study of K_D values derived using Nanodisc Affinity Capillary Electrophoresis and Steady State Fluorescence

7.1 Introduction

In the previous chapters styrene-maleic acid copolymer stabilized nanodiscs have been used to study interactions between small molecules and lipid bilayers using electrokinetic chromatography.[77] The retention factor (*k*) was determined and used as a measure of the affinity and relative affinity of various molecules for the nanodisc. Using this technique, it has been demonstrated that head group chemistry has a greater effect than alkyl tail chemistry on the thermodynamics of small molecule solvation in lipid bilayers.[78] As well, sphingomyelin bilayers have been shown to be stereoselective, when interacting with atropisomers.[79] Overall this work has demonstrated that the copolymer, which stabilizes the lipid bilayer, has minimal effect on small molecules interactions with the lipid bilayer nanodiscs.

There are many instances in which it would be useful and informative to measure actual equilibrium dissociation constant (K_D) values for the dissociation of small molecules or biomolecules with lipid bilayers; dissociation constants represent when 50% of the ligands in solution are associated with the receptor. For example, antimicrobial peptides are currently being developed as alternatives to traditional antibiotics because it is less likely that bacteria will develop resistance to peptides, like it has done to small molecule antibiotics[138]. These peptides are able to partition into cell membranes without the need of a receptor[43] and determination of their binding constants is important for design and evaluation. The protein cytochrome-c is also known to associate specifically with cardiolipin lipids in mitochondrial membranes, and this association is the first step in an apoptotic pathway.[139,140] Measuring dissociation constants for

cytochrome-c, particularly in combination with specific mutations to the protein, would lead to greater understanding of the binding process.

In this chapter, nanodisc affinity capillary electrophoresis (ACE) techniques are used to obtain direct measures of equilibrium dissociation constants (K_D) for the affinity of small molecules for lipid nanodiscs. The retention factors determined in previous chapters are proportional to K_D by the ratio of volumes of the PSP to BGE (equation 1-8), but difficulties in accurately determining this volume ratio make it difficult to determine or calculate actual K_D values by EKC. Affinity Capillary Electrophoresis techniques have been developed to allow for the measurement of K_D values, and are developed and applied here to determine the K_D values for the non-specific association of small molecules with lipid bilayer nanodiscs. The K_D's for rhodamine 123 and pyrene, seen in Figure 7-1, were determined using sphingomyelin nanodiscs and ACE. It was not possible to measure the K_D for 3-(α-Acetonylbenzyl)-4-hydroxycoumarin, Figure 7-1. The measured K_D's were then compared to K_D's measured using steady-state fluorescent techniques and nanodiscs of the same composition. The comparative measurements were possible due to solvatochromatic properties of analytes,[141–143] as the polarity of the solvent environment changed the emission of the fluorophores shifted.

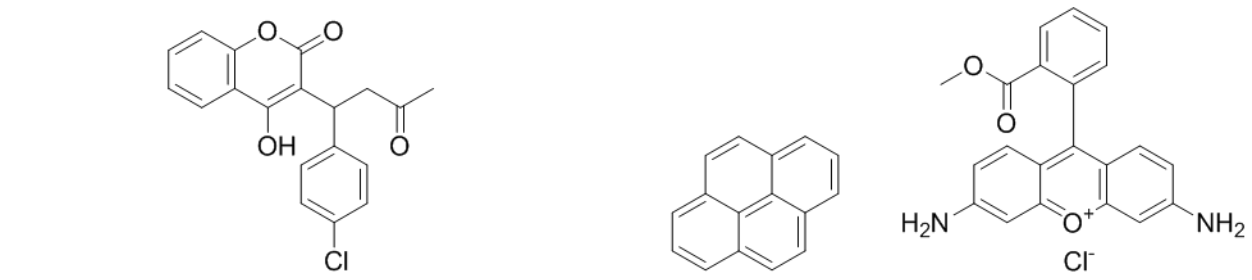

Figure 7-1. Analytes with solvatochromatic properties.

7.2 Experimental

7.2.1 Steady-State Fluorescence Measurements

Fluorescence measurements were carried out using pyrene and rhodamine 123 to determine their affinity for sphingomyelin nanodiscs. Emission spectra of the fluorescent probes were measured at varying sphingomyelin nanodisc concentrations on a fluorimeter (Agilent Technologies, Santa Clara, CA, USA). Both probes were dissolved in nanodisc buffer solution and allowed to equilibrate over night at room temperature. Pyrene, at a concentration of 5 µM, was incubated in sphingomyelin nanodisc solutions at ten different lipid concentrations ranging from 0 µM-1000 µM. Rhodamine 123, at a concentration of 1 µM, was incubated in sphingomyelin nanodisc solutions at ten different lipid concentrations ranging from 0 µM-250 µM. Pyrene measurements were made with excitation wavelength of 335 nm and an emission wavelength scanning range from 350-500 nm. Excitation and emission bandwidths were both 2.5 nm. For rhodamine 123, excitation was carried out at 505nm and the emission wavelength scanning range was 515-550nm. Excitation and emission bandwidths were 2.5 nm. All experiments were done at 25 °C.

Using steady-state fluorescence, the pyrene-sphingomyelin nanodiscs affinity was determined by changes in the fluorescent emission ratio of peaks I_1 and I_3, as the concentration of nanodisc in the cuvette was increased. The fluorescent intensity of peaks I_1 and I_3, 374 nm and 384 nm respectively, greatly depend on the polarity of pyrene's microenvironment.[144] Changes in I_1/I_3 ratio allowed for the percent bound of each probe to be determined using equation 7-1:

$$\theta = \frac{bound}{unbound} = \frac{\left(I_1/I_3 - I_1/I_{3_{free}}\right)}{\left(I_1/I_{3_{max}} - I_1/I_{3_{free}}\right)} \quad (7\text{-}1)$$

Where I_1/I_3 is the peak ratio of pyrene fluorescence intensity at a given sphingomyelin nanodisc concentration in the cuvette, I_1/I_{3free} is the peak ratio of pyrene fluorescence intensity with no nanodiscs in the cuvette, and I_1/I_{3max} is the max change in the ratio of fluorescence intensity at the highest concentration of nanodiscs in the cuvette. Once the percent bound/unbound was graphed the K_D was fit using equation 7-1 and Matlab.

Rhodamine 123 is a cationic fluorophore and its fluorescence experiences a red shift in hydrophobic environments.[145] The changes in the fluorescent emission wavelength were used to determine the cationic fluorescent probe's affinity for sphingomyelin nanodiscs. Using equation 7-2 the percent bound of rhodamine 123 to sphingomyelin nanodiscs was determined:

$$\theta = \frac{bound}{unbound} = \frac{(\Delta emission - emission_{free})}{(\Delta emission_{max} - emission_{free})} \quad (7\text{-}2)$$

Where Δemission is the change in the wavelength of fluorescent emission at a given sphingomyelin nanodisc concentration in the sample cuvette, $emission_{free}$ is the wavelength of the fluorescent emission of the fluorophore when there were no nanodiscs in the sample cuvette, and the $\Delta emission_{max}$ is the maximum shift in the emission wavelength to occur during the steady-state experiments. Once the percent bound/unbound was graphed the K_D was fit using equation 7-2 and Matlab.

7.3 Results and Discussion

7.3.1 ACE

The exchange between the 16:0 SM nanodiscs and the fluorophore analytes is relatively fast; the distribution equilibrium results in a change in the electrophoretic mobility of the analytes, but no separation of the bound and unbound fractions. The interactions between nanodiscs and analytes were investigated using ACE by increasing the concentration of

nanodiscs in the BGE and sample vial. As increasing concentrations of nanodiscs were added to the BGE and sample vial, the changes in electrophoretic mobility of the analytes increased; until at higher nanodisc concentrations the changes electrophoretic mobility did not increase significantly. The changes in electrophoretic mobility vs sphingomyelin concentration for both analytes can be seen in Figures 7-2. Representative electropherograms of the affinity measurements can be seen for both probes in Figures 7-3. A third probe was initially studied in order to look at neutral, cationic, and anionic probe interactions with sphingomyelin nanodiscs. However, the anionic 3-(α-Acetonylbenzyl)-4-hydroxycoumarin did not show any interactions with the nanodiscs during affinity measurements, as seen in Figure 7-3. The log $D_{ph7.0}$ for 3-(α-Acetonylbenzyl)-4-hydroxycoumarin is 1.31, compared to its log P value of 2.70[146]. Its reduction in hydrophobicity due to its negative charge at pH 7 made it an ineffective probe for ACE measurements.

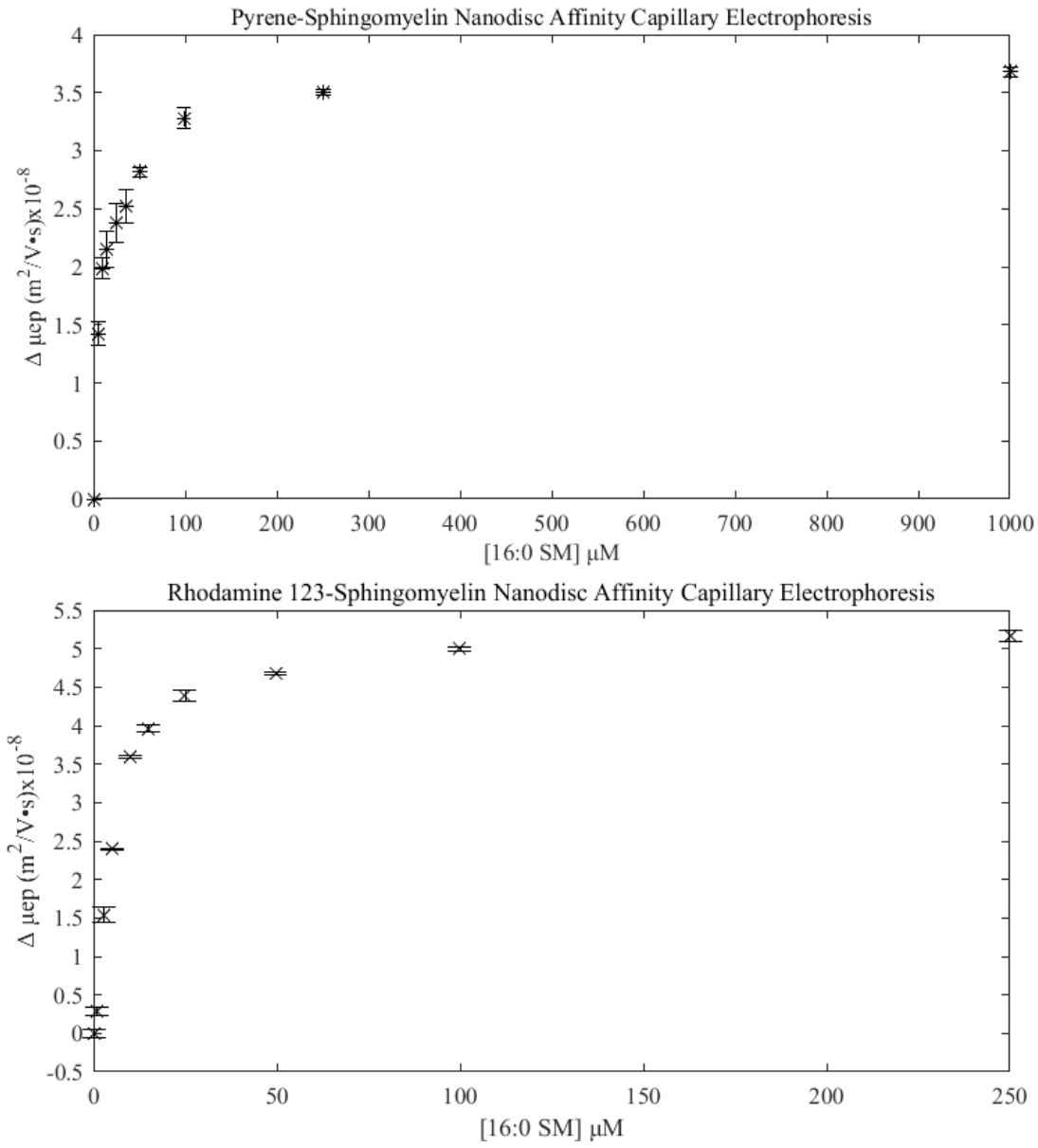

Figure 7-2. Changes in electrophoretic mobility of analytes as lipid nanodisc concentration is increased in the BGE.

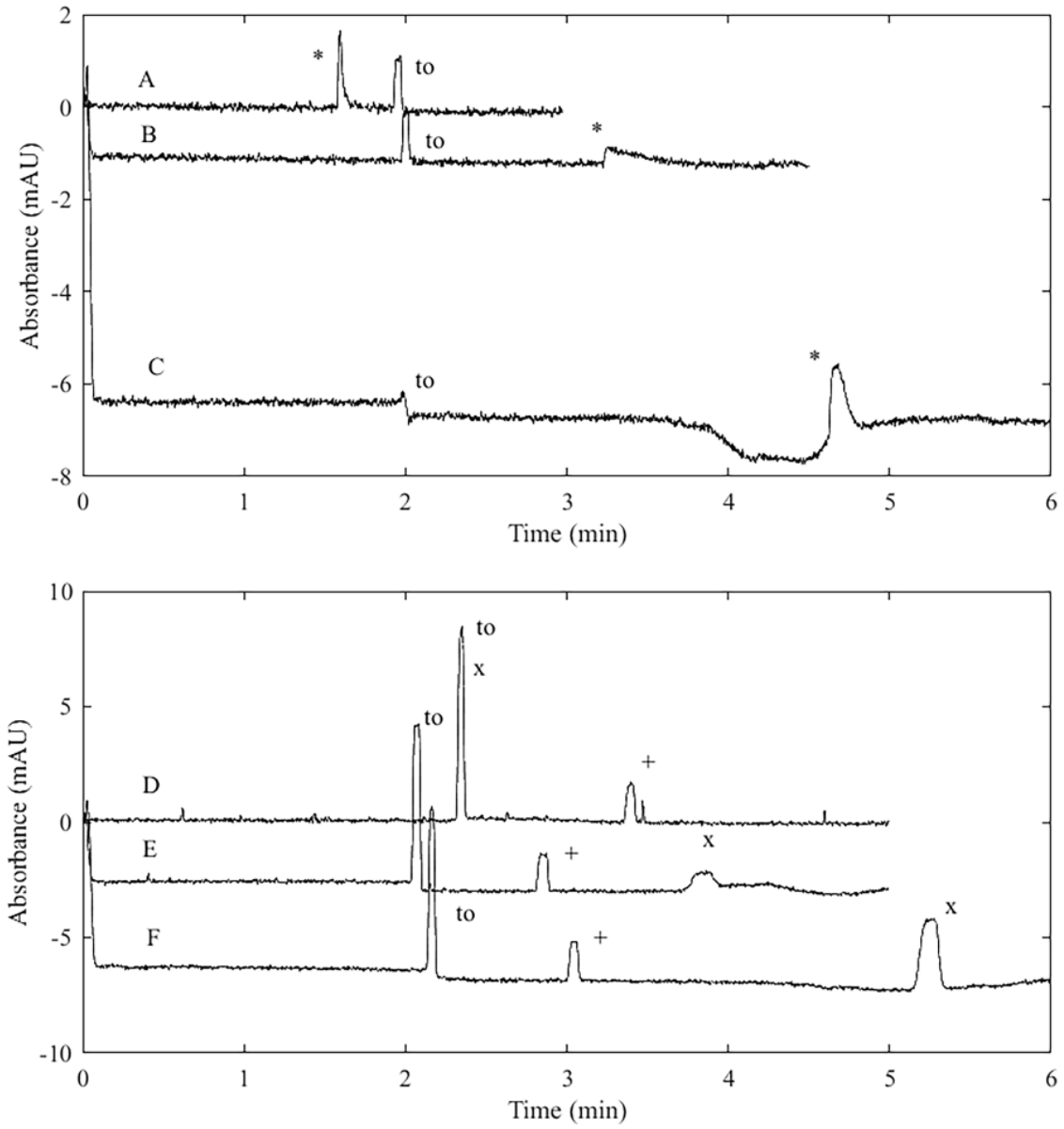

Figure 7-3. Nanodisc affinity capillary electrophoresis measurements. Experimental conditions: 10mM phosphate buffer (pH 7.0) capillary dimensions: 48.5 cm × 50 µm I.D. with a 150 µm extended cell pathlength. The injection was made with 35 mbar of pressure for 15 seconds. The operating voltage was 15 kV with detection at 225 nm for top electropheragram and 245 nm for bottom electropheragram. A, B, C, D, E, F represents the sphingomyelin concentrations in the BGE of 0 µM, 10 µM, 250 µM, 0 µM, 50 µM, and 250 µM. Analyte 10 µM rhodamine 123 (*), 25 µM pyrene (x) and 3-(α-Acetonylbenzyl)-4-hydroxycoumarin (+).

7.3.2 Steady-State Fluorescence

The changes in the emission ratio of peaks I_1/I_3 as the 16:0 SM nanodisc concentration in the sample cuvette can be seen in Figure 7-4. The steady-state measurements demonstrated the same trend that was seen with the affinity measurements; gradual increases in the 16:0 SM nanodisc concentrations lead to continually smaller incremental changes changes in I_1/I_3, as seen in Figure 7-5. The changes in the emission of the rhodamine 123 were unexpected because the emission shift hit a maximum change and then change started to slightly decrease with increasing 16:0 SM lipid concentrations, although the decrease in the change of the maximum emission was not significantly different within error, as seen in Figure 7-6.

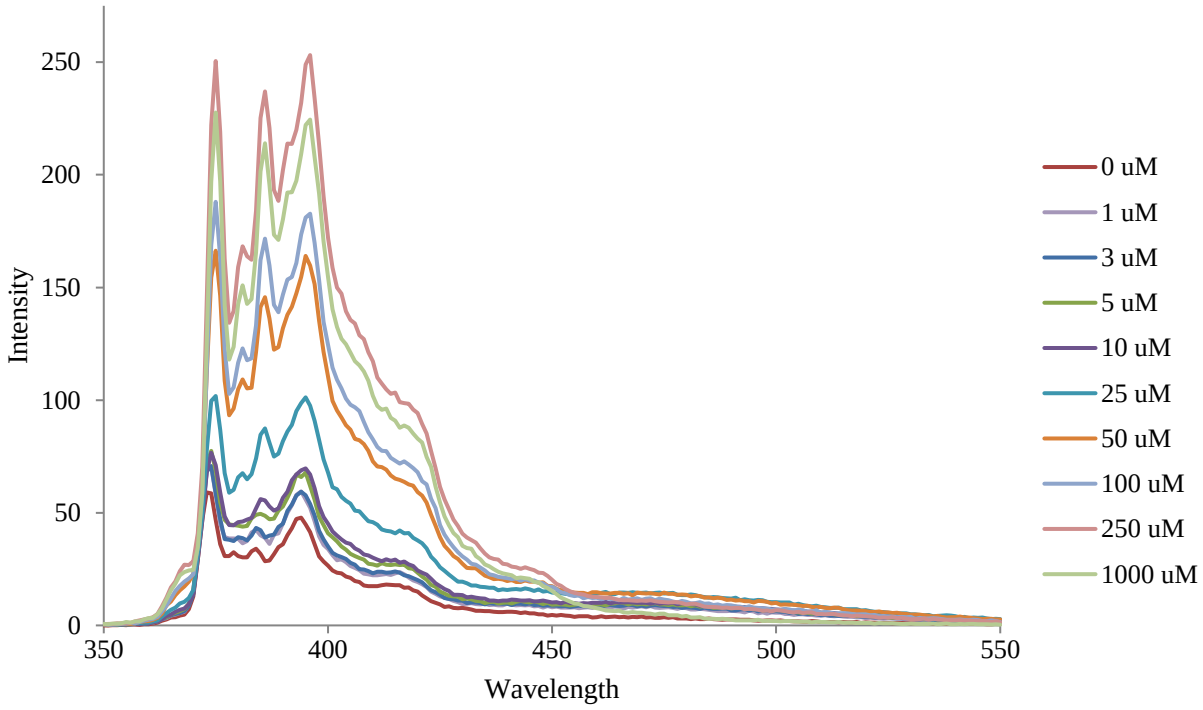

Figure 7-4. Change in fluorescence emission with increasing sphingomyelin concentrations in the sample curvette. 5µM Pyrene and sphingomyelin concentrations ranged from 0-1000µM.

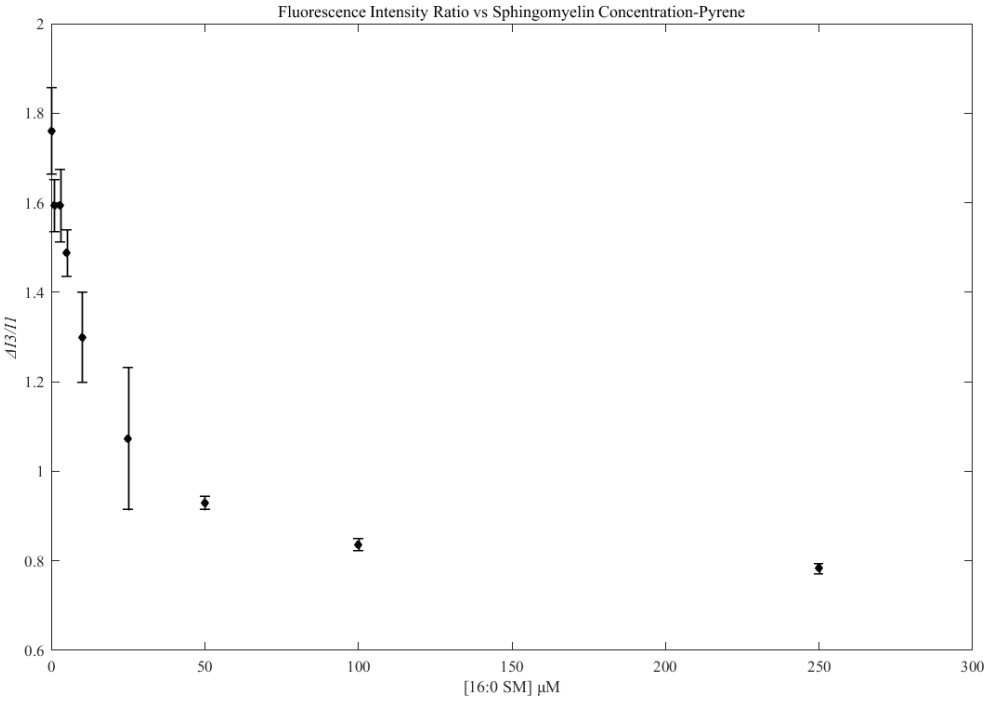

Figure 7-5. Change in I_1/I_3 ratio with increasing sphingomyelin concentrations in the sample curvette. 5µM Pyrene and sphingomyelin concentrations ranged from 0-1000µM.

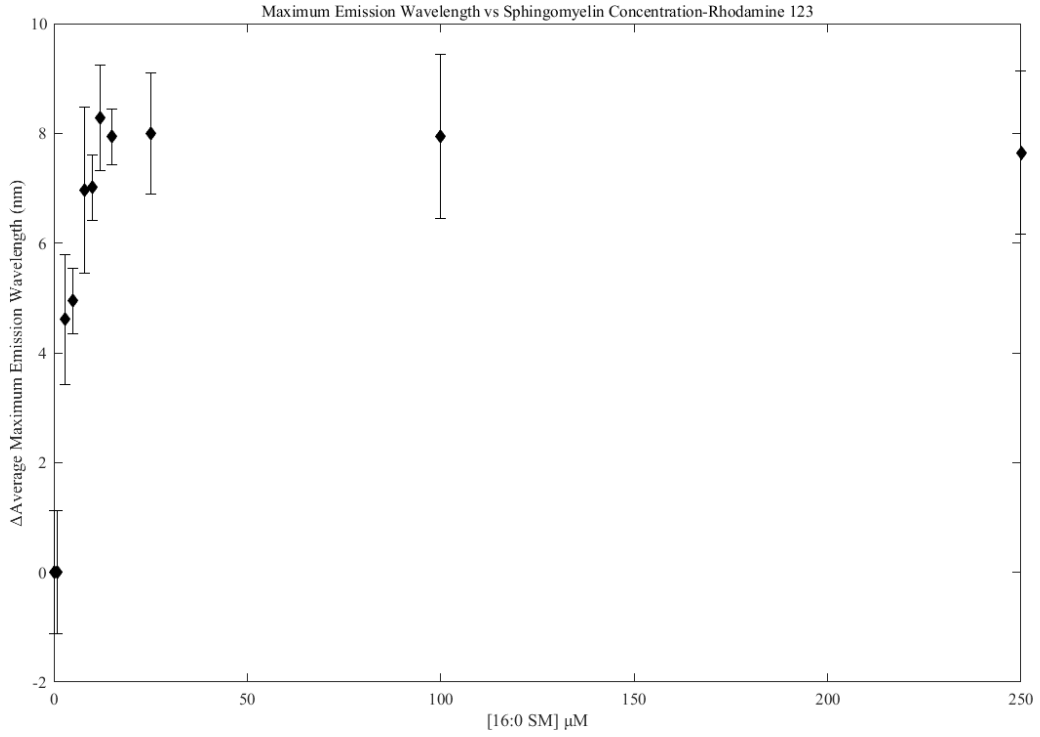

Figure 7-6. Change in maximum emission wavelength with increasing sphingomyelin concentrations in the sample curvette. 1µM Pyrene and sphingomyelin concentrations ranged from 0-250µM.

7.3.3 Comparison of Affinity Capillary Electrophoresis and Steady-State Fluorescence Measurements.

The K_D values for both the ACE and steady-state fluorescent measurements are shown in Table 7-1. These were a result of nonlinear curve fitting seen in Figure 7-7 for CE measurements and 7-8 for steady-state fluorescence measurements. For the pyrene ACE measurements, the K_D was 9.45 µM with a cooperativity of 0.787 and the steady-state fluorescence measurements K_D was measured to be 11.5 µM with a cooperativity of 1.06. The 95% confidence intervals for measured K_D values overlap, making the measurements not significantly different at this level of

confidence. The cooperativity measurements also were the same within 95% confidence and demonstrated that having a pyrene molecule in the lipid bilayer does not affect the ability of another pyrene molecule to partition into the lipid bilayer.

There were differences outside the 95% confident intervals for rhodamine 123 partitioning to sphingomyelin nanodiscs. The K_D for the steady-state measurements of the interaction between rhodamine 123 and sphingomyelin nanodiscs was 3.32 µM with a cooperativity of 1.93. The K_D for the ACE measurements was 5.80µM with a cooperativity of 1.29. Although the K_D for the ACE measurements was higher, the cooperativity values had overlapping 95% confidence intervals. Both cooperativity values suggest that having a rhodamine 123 molecule in the bilayer may allow for easier insertion of another rhodamine 123 molecule into the bilayer.

Pyrene	K_D µM	n	R^2	Rhodamine 123	K_D µM	n	R^2
NACE	9.51 (7.70, 11.3)	0.758 (0.627, 0.888)	0.992	NACE	5.80 (5.26, 6.34)	1.29 (1.14, 1.44)	0.996
SS Fluorescence	11.5 (9.44, 13.6)	1.06 (0.875, 1.25)	0.991	SS Fluorescence	3.32 (2.54, 4.10)	1.93 (1.20, 2.65)	0.969

Table 7-1. K_D measurements derived using ACE and Steady-State Fluorescence.

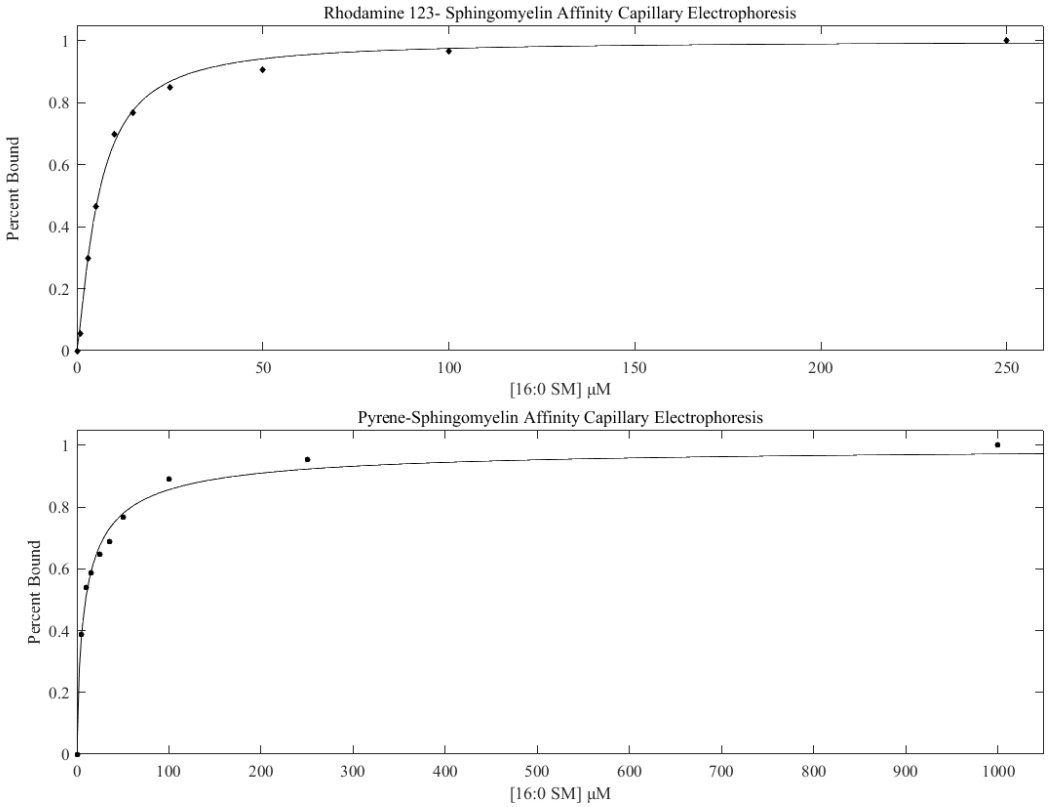

Figure 7-7. Nonlinear binding fits for analysis using ACE.

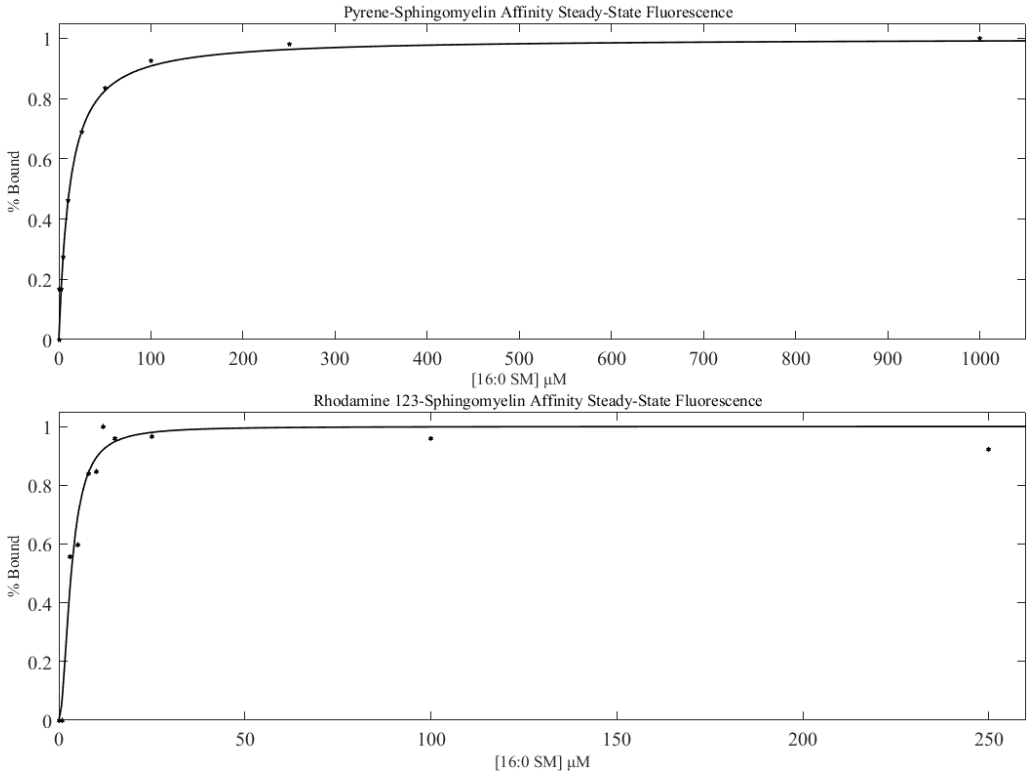

Figure 7-8. Nonlinear binding fits for analysis using steady-state fluorescence.

7.4 Conclusion

It was demonstrated that nanodisc affinity capillary electrophoresis can be employed for the study of quantitative interactions between neutral and cationic molecules and lipid bilayers. Interactions between pyrene and sphingomyelin nanodiscs were validated using steady-state fluorescence measurements and K_Ds derived using both methods were the same within 95% confidence interval. The K_D between rhodamine 123 and sphingomyelin nanodiscs were not the same within 95% confidence when CE and steady-state measurements were compared. Steady-state measurements resulted in a K_D that was 1.75 times lower than the ACE measurement. Overall, these measurements demonstrate that nanodisc affinity capillary electrophoresis is a relatively facile and useful technique for the measurement of lipid bilayer K_D values. ACE has the advantage that it can be applied with solutes that do not have a spectroscopic response to

binding. Peptide and protein interactions with lipid bilayer of interest should be explored using nanodisc affinity capillary electrophoresis.

Chapter 8: Conclusions and Preliminary Data

8.1 Conclusions

The research presented in this dissertation has explored the synthesis, characterization, and application of copolymer stabilized nanodiscs in electrokinetic chromatography and affinity capillary electrophoresis.

In chapter 3 phospholipid bilayer nanodiscs with synthetic copolymers were introduced as a PSP in EKC and demonstrated good performance. The use of a synthetic polymer in place of belt proteins allowed the nanodiscs to be generated affordably and in sufficient quantity for use in EKC. The nanodiscs have sufficient electrophoretic mobility to allow for a good migration range and generate high theoretical plate counts. Together, this results in high peak capacity and excellent ability to separate, resolve, and distinguish analytes of similar chemistry and structure. The results in Chapter 3 left open the question of whether the solute probes were interacting with the lipid bilayer of the nanodiscs, or with the copolymer belt that stabilized the lipid bilayer.

In order to determine the role the copolymer plays in solute-nanodisc interactions, LSER analysis was employed in Chapter 4 to characterize the changes in solvation environment of nanodiscs of varied belt to lipid ratio, belt polymer chemistry and molecular weight. Increases in the lipid to copolymer ratio resulted in smaller, more cohesive nanodiscs with greater electrophoretic mobility. Nanodisc structures with copolymers of different chemistry and molecular weight were compared. After LSER analysis it was determined that the Xiran 30010 copolymer had greater affinity for hydrogen bond donating solutes or that Xiran 30010 produces structural changes in the bilayer that promote interaction with hydrogen bond donor molecules.

As a result, all future syntheses utilized the Xiran 25010 copolymer. Xiran 25010 lead to the formation of nanodiscs which performed better in the indirect measurement of log $P_{o/w}$ values.

After the optimization of synthesis parameters in Chapter 4, Chapter 5 focused on the effects of lipid chemistry on solute-probe nanodisc interactions. LSER analysis showed that nanodisc EKC was sensitive to slight structural changes in lipid head group chemistry. Changes to in alkyl tail chemistry did not lead to significant changes in the bilayer-solute interactions. It is believed that changes in alkyl tail chemistry did not lead to significant changes in solute probe-nanodisc interactions because polar solutes rarely penetrate deep into the hydrophobic region. Comparison of LSER results of nanodisc and liposomes of similar chemistry showed only minor differences that are likely due to differences in the lipid bilayer curvature. Nanodisc EKC has been shown as a reliable method for the measurement and characterization of bilayer-solute interactions.

In Chapter 6 the stereochemistry of sphingomyelin bilayer were studied in order to understand how the chirality of sphingomyelin could influence passive diffusion through the lipid bilayer. It was determined that (S)-(−)-1,1′-Bi-2-naphthol had measurably stronger affinity for the sphingomyelin nanodisc than that (R)-(+)-1,1′-Bi-2-naphthol, to the point where the two atropisomers were successfully resolved. Sphingomyelin bilayers are shown to have selective interactions with an atropisomer, but not enantiomers or diastereomer. This result also demonstrates that axial chirality might influence passive diffusion into sphingomyelin bilayers.

Lastly, in Chapter 7 the equilibrium coefficients for partitioning of two fluorophores between sphingomyelin nanodiscs and aqueous buffer were measured using nanodisc affinity capillary electrophoresis. Using this technique the K_D values for the two interactions were verified by using steady-state fluorescence to study the same interactions. The independent

validation was possible because of the solvatochromatic properties of the analytes. For pyrene the K_D values derived from the two techniques were the same within 95% confidence, while for rhodamine 123 the K_D values for steady-state measurements was 1.75 times lower than the ACE measurement. These results demonstrate that nanodiscs are a valuable CE additive for studying membrane properties and interactions and that ACE measurements using nanodiscs provide an alternative means to measure dissociation constants.

8.2 Preliminary Data

Using nanodiscs to measure interactions between lipid bilayers and macromolecules shows promise after demonstrating the accuracy of the affinity measurements using small molecules. The next series of experiments was focused on studying cytochrome c interactions with cardiolipin using Frontal Analysis.

Cytochrome *c* is peripheral electron transport protein found in the mitochrondria[140], which is also believed to play an integral part in initiating cell death. The first step in cell death is cytochrome *c* binding to cardiolipin lipids[139]. The relative importance of cytochrome *c*-cardiolipin binding and the extensive literature on the interaction make it a model protein for studying protein-nanodisc affinity.

Frontal analysis (FA) is based on the separation of free ligand from the ligand receptor complex due to their respective differences in electrophoretic mobility after the introduction of a large volume of equilibrated sample mixture into a buffer filled capillary[147]. Dissociation constants can be determined from the change in the plateau height/peak height of the unbound ligand. Using frontal analysis and nanodiscs with 0.8 14:0 PC: 0.2 cardiolipin (14:0 CL) affinity was demonstrated between cytochrome *c* and the nanodisc, seen in Figure 8-1.

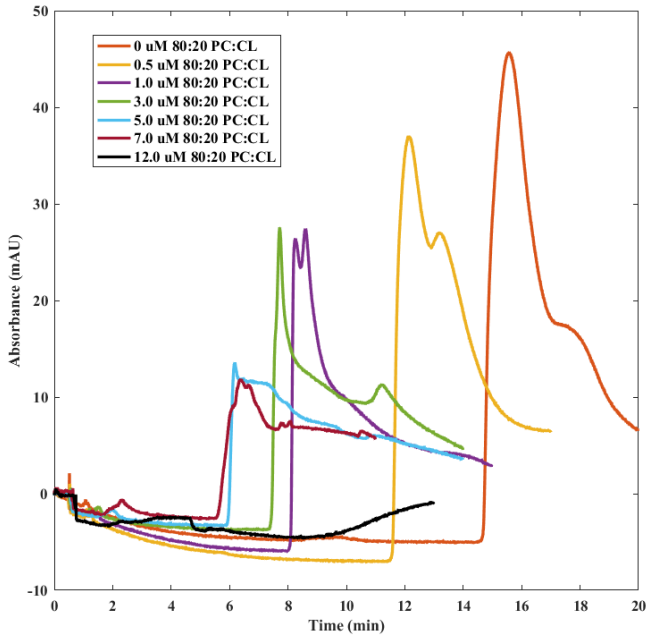

Figure 8-1. Change in the height of the unbound cytochrome *c* peak height with increasing concentrations of PC:CL nanodiscs in the sample vial.

As can been seen in Figure 8-1, as the concentration of PC:CL nanodisc increased in the sample vial the peak height of the unbound fraction of cytochrome *c* to decreased. Further experiments need to be completed in the analysis of the cytochrome *c*-nanodisc binding. The linearity between peak height and concentration in the absence of nanodiscs, must be validated using a calibration curve. To further demonstrate that binding is occurring because of the cytochrome *c*-cardiolipin interaction and not because of electrostatics interactions because of the low salt buffer, a control will be required. As a control, binding between cytochrome *c* and 14:0 PC nanodiscs should be measured, with the expectation that interactions between cytochrome *c*-14:0 PC nanodiscs should results in a significantly higher K_D.

References:

(1) Knowles, T. J.; Finka, R.; Smith, C.; Lin, Y. P.; Dafforn, T.; Overduin, M. *J. Am. Chem. Soc.* **2009**, *131* (22), 7484–7485.

(2) Tiselius, A. *Biochem. J.* **1937**, *31*, 313–317.

(3) Tiselius, A. *Biochem. J.* **1937**, *31* (9), 1464–1477.

(4) Harris, D. c. *Quantitative Chemical Analysis*; 2007; Vol. 42.

(5) Hjertén, S. *Chromatogr. Rev.* **1967**, *9* (2), 122–219.

(6) Jorgenson, J. W.; Lukacs, K. D. A. *Anal. Chem.* **1981**, *53* (8), 1298–1302.

(7) Terabe, S.; Otsuka, K.; Ichikawa, K.; Tsuchiya, A.; Ando, T. *Anal. Chem.* **1984**, *56*, 111–113.

(8) Terabe, S.; Otsuka, K.; Ando, T. *Anal. Chem.* **1985**, *57* (4), 834–841.

(9) Schnee, V. P.; Palmer, C. P. *Electrophoresis* **2008**, *29* (4), 767–776.

(10) Rauk, E.; Kotzev, A.; Laschewsky, A.; Palmer, C. P. *J. Chromatogr. A* **2006**, *1106* (1–2), 29–35.

(11) Kopecká, K.; Tesašová, E.; Pirogov, A.; Gaš, B. *J. Sep. Sci.* **2002**, *25* (15-17), 1027–1034.

(12) Klotz, W. L., Schure, M.R., F. J. P. *J. Chromatogr. A* **2002**, *962*, 207–219.

(13) Mohanty, A.; Dey, J. *J. Chromatogr. A* **2005**, *1070* (1–2), 185–192.

(14) Poole, S. K.; Patel, S.; Dehring, K.; Workman, H.; Dong, J. *J. Chromatogr. B Anal. Technol. Biomed. Life Sci.* **2003**, *793* (2), 265–274.

(15) Pomponio, R.; Gotti, R.; Luppi, B.; Cavrini, V. *Electrophoresis* **2003**, *24* (10), 1658–1667.

(16) Ruokonen, S. K.; Duša, F.; Lokajová, J.; Kilpeläinen, I.; King, A. W. T.; Wiedmer, S. K. *J. Chromatogr. A* **2015**, *1405*, 178–187.

(17) Wang, Y.; Sun, J.; Liu, H.; He, Z. *Electrophoresis* **2007**, *28* (14), 2391–2395.

(18) Ruokonen, S.-K.; Duša, F.; Rantamäki, A. H.; Robciuc, A.; Holma, P.; Holopainen, J. M.; Abdel-Rehim, M.; Wiedmer, S. K. *J. Chromatogr. A* **2017**, *1479*, 194–203.

(19) Mills, J. O.; Holland, L. A. *Electrophoresis* **2004**.

(20) Holland, L. A.; Leigh, A. M. *Electrophoresis* **2003**, *24* (17), 2935–2939.

(21) Palmer, C. P.; Keeffer, A.; Hilder, E. F.; Haddad, P. R. *Electrophoresis* **2011**, *32* (5), 588–594.

(22) Hua, X.; Du, Y.; Chen, J.; Xu, G.; Yu, T.; Zhang, Q. *Electrophoresis* **2013**, *34* (13), 1901–1907.

(23) McGettrick, J. R.; Williamson, N. H.; Sutton, A. T.; Palmer, C. P. *Electrophoresis* **2017**, *38* (5), 730–737.

(24) Popplewell, J. F.; Swann, M. J.; Freeman, N. J.; McDonnell, C.; Ford, R. C. *Biochim. Biophys. Acta - Biomembr.* **2007**, *1768* (1), 13–20.

(25) Olabi, M.; Stein, M.; Wätzig, H. *Methods*. 2018.

(26) Chu, Y.; Avial, L. Z.; Gao, J.; Whitesides, G. M. *Acc. Chem. Res.* **1995**, *28* (11), 461–468.

(27) Chu, Y. H.; Whitesides, G. M. *J. Org. Chem.* **1992**, *57* (13), 3524–3525.

(28) Farcaş, E.; Bouckaert, C.; Servais, A. C.; Hanson, J.; Pochet, L.; Fillet, M. *Anal. Chim. Acta* **2017**, *984*, 211–222.

(29) Li, N.; Zeng, S.; He, L.; Zhong, W. *Anal. Chem.* **2010**, *82* (17), 7460–7466.

(30) Alberts, B.; Johnson, A.; Lewis, J.; Raff, M.; Roberts, K.; Walter, P. *Molecular Biology of the Cell*; 2002.

(31) Elderdfi, M.; Sikorski, A. F. *Chemistry and Physics of Lipids*. 2018, pp 61–72.

(32) Zeineldin, R. Liposomes http://www.reemazeineldin.com/Liposome.html.

(33) Owen, R. L.; Strasters, J. K.; Breyer, E. D. *Electrophoresis*. 2005, pp 735–751.

(34) Alves, D. S.; Pérez-Fons, L.; Estepa, A.; Micol, V. *Biochem. Pharmacol.* **2004**, *68* (3), 549–561.

(35) Ruozi, B.; Forni, F.; Battini, R.; Vandelli, M. A. *J. Drug Target.* **2003**, *11* (7), 407–414.

(36) Zhang, Y.; Zhang, R.; Hjerten, S.; Lundahl, P. *Electrophoresis* **1995**, *16* (8), 1519–1523.

(37) Pascoe, R. J.; Foley, J. P. *Electrophoresis* **2003**, *24* (24), 4227–4240.

(38) Lokajová, J.; Pukkila, J.; Holopainen, J. M.; Wiedmer, S. K. *Eur. J. Pharm. Sci.* **2010**, *41* (3–4), 515–522.

(39) Váňová, J.; Liimatta, L. J.; Česla, P.; Wiedmer, S. K. *Cogent Chem.* **2017**, *3* (1), 1–11.

(40) Ruokonen, S.-K.; Duša, F.; Lokajová, J.; Kilpeläinen, I.; King, A. W. T.; Wiedmer, S. K. *J. Chromatogr. A* **2015**, *1405*, 178–187.

(41) Technical Bulletin 121 https://www.anatrace.com/getfile/f7f5b9c2-dfb8-41b9-8031-64897736f35b/Technical-Bulletin-121-Bicelles.aspx?chset=cdf38ec3-6fdc-4c98-9506-0b4975440585.

(42) Kim, C.; Baek, S. Bin; Kim, D. H.; Lim, S. C.; Lee, H. J.; Lee, H. C. *J. Pept. Sci.* **2009**, *15* (5), 353–358.

(43) Lind, J.; Gräslund, A.; Mäler, L. *Biochemistry* **2006**, *45* (51), 15931–15940.

(44) Prosser, R. S.; Evanics, F.; Kitevski, J. L.; Al-Abdul-Wahid, M. S. *Biochemistry*. 2006, pp 8453–8465.

(45) Bayburt, T. H.; Grinkova, Y. V.; Sligar, S. G. *Nano Lett.* **2002**, *2* (8), 853–856.

(46) Denisov, I. G.; Grinkova, Y. V; Lazarides, A. A.; Sligar, S. G. *J. Am. Chem. Soc* **2004**, *126*, 3477–3487.

(47) Ritchie, T. K.; Grinkova, Y. V.; Bayburt, T. H.; Denisov, I. G.; Zolnerciks, J. K.; Atkins, W. M.; Sligar, S. G. *Methods in Enzymology*; Nejat, D., Ed.; Academic Press, 2009.

(48) Jamshad, M.; Grimard, V.; Idini, I.; Knowles, T. J.; Dowle, M. R.; Schofield, N.; Sridhar, P.; Lin, Y.; Finka, R.; Wheatley, M.; Thomas, O. R. T.; Palmer, R. E.; Overduin, M.; Govaerts, C.; Ruysschaert, J. M.; Edler, K. J.; Dafforn, T. R. *Nano Res.* **2015**, *8* (3), 774–789.

(49) Scheidelaar, S.; Koorengevel, M. C.; Pardo, J. D.; Meeldijk, J. D.; Breukink, E.; Killian, J. A. *Biophys. J.* **2015**, *108* (2), 279–290.

(50) Viswanadhan, V. N.; Ghose, A. K.; Revankar, G. R.; Robins, R. K. *J. Chem. Inf. Comput. Sci.* **1989**, *29*, 163–172.

(51) Arnott, J. A.; Planey, S. L. *Expert Opin. Drug Discov* **2012**, *7* (10), 863–875.

(52) Noble, A. *J. Chromatogr. A* **1993**, *642* (1–2), 3–14.

(53) OECD. *OECD guideline for the testing of chemicals*; 1995.

(54) Poole, S. K.; Poole, C. F. *Journal of Chromatography B: Analytical Technologies in the Biomedical and Life Sciences*. 2003.

(55) Øtergaard, J.; Honore Hansen Steen, S.; Larsen, C.; Schou, C.; Heegaard, N. H. H. *Electrophoresis* **2003**, *24* (6), 1038–1046.

(56) Vitha, M.; Carr, P. W. *J. Chromatogr. A* **2006**, *1126* (1–2), 143–194.

(57) Hyslop, J. S.; Hall, L. M. G.; Umansky, A. A.; Palmer, C. P. *Electrophoresis* **2014**, *35* (5), 728–735.

(58) Anslyn, E. V; Dougherty, D. A. *Modern Physical Organic Chemistry*; 2006; Vol. 69.

(59) Hassan, P. A.; Verma, G.; Ganguly, R. In *Functional Materials*; 2012; pp 1–59.

(60) Abraham, M. H.; Ibrahim, A.; Zissimos, A. M. *Journal of Chromatography A*. 2004, pp 29–47.

(61) Pyell, U. *Electrokinetic Chromatography: Theory, Instrumentation and Applications*; 2007.

(62) Vespalec, R.; Boček, P. *Chem. Rev.* **2000**, *100* (10).

(63) Zhou, Q.; Yu, L.-S.; Zeng, S. *Drug Metab. Rev.* **2014**, *46* (3), 283–290.

(64) Lu, H. *Expert Opin. Drug Metab. Toxicol.* **2007**, *3*, 149–158.

(65) Glunz, P. W. *Bioorganic Med. Chem. Lett.* **2018**, *28* (2), 53–60.

(66) Clayden, J.; Moran, W. J.; Edwards, P. J.; Laplante, S. R. *Angew. Chemie - Int. Ed.* **2009**, *48* (35), 6398–6401.

(67) Eveleigh, P.; Hulme, E. C.; Schudt, C.; Birdsall, N. J. *Mol Pharmacol* **1989**, *35* (4), 477–483.

(68) Agranat, I.; Caner, H.; Caldwell, J. *Nature Reviews Drug Discovery*. 2002, pp 753–768.

(69) Smith, S. W. *Toxicological Sciences*. 2009, pp 4–30.

(70) Gübitz, G.; Schmid, M. G. *Molecular Biotechnology*. 2006, pp 159–179.

(71) Kuwahara, Y.; Nagata, H.; Nishi, H.; Tanaka, Y.; Kakehi, K. *Chromatographia* **2005**, *62* (9–10), 505–510.

(72) Kuhn, R.; Erni, F.; Bereuter, T.; Haeusler, J. *Anal. Chem.* **1992**, *64* (22), 2815–2820.

(73) Mayer, S.; Schurig, V. *Electrophoresis* **1994**, *15* (6), 835–841.

(74) Taga, A.; Du, Y.; Suzuki, S.; Honda, S. *J. Pharm. Biomed. Anal.* **2003**, *30* (5), 1587–1593.

(75) Haginaka, J. *Journal of Chromatography A*. 2000, pp 235–254.

(76) Schmid, M. G.; Gübitz, G. *J. Chromatogr. A* **1995**, *709* (1), 81–88.

(77) Penny, W. M.; Steele, H. B.; Ross, J. B. A.; Palmer, C. P. *Electrophoresis* **2017**, *38* (5), 738–746.

(78) Penny, W. M.; Palmer, C. P. *Electrophoresis* **2018**, *39*, 844–852.

(79) Penny, W. M.; Palmer, C. P. *Chem. Phys. Lipids* **2018**, *214*, 11–14.

(80) Swainsbury, D. J. K.; Scheidelaar, S.; Van Grondelle, R.; Killian, J. A.; Jones, M. R. *Angew. Chemie - Int. Ed.* **2014**, *53* (44), 11803–11807.

(81) Bushey, M.; Jorgenson, J. *Anal. Chem.* **1989**, *61*, 491–493.

(82) Burns, S. T.; Agbodjan, A. A.; Khaledi, M. G. *J. Chromatogr. A* **2002**, *973* (1–2), 167–176.

(83) Burns, S. T.; Khaledi, M. G. *J. Pharm. Sci.* **2002**, *91* (7), 1601–1612.

(84) Carrozzino, J. M.; Khaledi, M. G. *Pharm. Res.* **2004**, *21* (12), 2327–2335.

(85) Wiedmer, S. K.; Kulovesi, P.; Riekkola, M. L. *J. Sep. Sci.* **2008**, *31* (14), 2714–2721.

(86) Wang, Y.; Sun, J.; Liu, H.; Liu, J.; Zhang, L.; Liu, K.; He, Z. *Analyst* **2009**, *134* (2), 267–272.

(87) Xian, D. L.; Huang, K. L.; Liu, S. Q.; Xiao, J. Y. *Chinese J. Chem.* **2008**, *26* (4), 671–676.

(88) Wang, Y.; Sun, J.; Liu, H.; He, Z. *Electrophoresis* **2007**, *28* (14), 2391–2395.

(89) Xian, D.-L.; Huang, K.-L.; Liu, S.-Q.; Xiao, J.-Y. *Chromatographia* **2008**, *67* (5/6), 407–412.

(90) Wang, T.; Feng, Y.; Jin, X.; Fan, X.; Crommen, J.; Jiang, Z. *J. Pharm. Biomed. Anal.* **2014**, *96*, 263–271.

(91) Dörr, J. M.; Scheidelaar, S.; Koorengevel, M. C.; Dominguez, J. J.; Schäfer, M.; van Walree, C. A.; Killian, J. A. *European Biophysics Journal*. 2016, pp 3–21.

(92) Schulte, S.; Palmer, C. P. *Electrophoresis* **2003**, *24* (6), 978–983.

(93) Cabot, J. M.; Subirats, X.; Fuguet, E.; Rosés, M. *Admet Dmpk* **2014**, *2* (2), 98–106.

(94) Ellington, J. J. *J. Chem. Eng. Data* **1999**, *44* (6), 1414–1418.

(95) Leo, a.; Hansch, C.; Elkins, D. *Chem. Rev.* **1971**, *71* (6), 525.

(96) Sangster, J. *J. Phys. Chem. Ref. Data* **1989**, *18* (3), 1111–1229.

(97) Abraham, M. H.; Chadha, H. S.; Martins, F.; Mitchell, R. C.; Bradbury, M. W.; Gratton, J. A. *Pestic. Sci.* **1999**, *55* (January 1998), 78–88.

(98) Pascoe, R. J.; Foley, J. P. *Electrophoresis* **2003**, *24* (24), 4227–4240.

(99) Johnson, M. E.; Blankschtein, D.; Langer, R. *J. Pharm. Sci.* **1995**, *84* (9), 1144–1146.

(100) Abbott, N. J.; Patabendige, A. A. K.; Dolman, D. E. M.; Yusof, S. R.; Begley, D. J. *Neurobiology of Disease*. 2010, pp 13–25.

(101) Yang, S.; Bumgarner, J. G.; Khaledi, M. G. *J. Chromatogr. A* **1996**, *738* (2), 265–274.

(102) Norman, K. E.; Nymeyer, H. *Biophys. J.* **2006**, *91* (6), 2046–2054.

(103) Palmer, C. P. *Electrophoresis* **2002**, *23* (22–23), 3993–4004.

(104) Penny, W. M.; Palmer, C. P. *Electrophoresis* **2018**.

(105) Hazel, J. *Prog. Lipid Res.* **1990**, *29* (3), 167–227.

(106) Lopez, C. F.; Nielsen, S. O.; Klein, M. L.; Moore, P. B. *J. Phys. Chem. B* **2004**, *108* (21), 6603–6610.

(107) Tejwani, R. W.; Davis, M. E.; Anderson, B. D.; Stouch, T. R. *Mol. Pharm.* **2011**, *8* (6), 2204–2215.

(108) Damodaran, K. V.; Merz, K. M. *Biophys. J.* **1994**, *66* (4), 1076–1087.

(109) Marrink, S. J.; Berendsen, H. J. C. *J. Phys. Chem.* **1996**, *100* (41), 16729–16738.

(110) Chiu, S. W.; Vasudevan, S.; Jakobsson, E.; Mashl, R. J.; Scott, H. L. *Biophys. J.* **2003**, *85* (6), 3624–3635.

(111) Essmann, U.; Perera, L.; Berkowitz, M. L. *Langmuir* **1995**, *11* (24), 4519–4531.

(112) Slater, S. J.; Ho, C.; Taddeo, F. J.; Kelly, M. B.; Stubbs, C. D. *Biochemistry* **1993**, *32* (14), 3714–3721.

(113) Damodaran, K. V; Merz, K. M. *Langmuir* **1993**, *9* (5), 1179–1183.

(114) Barenholz, Y.; Thompson, T. E. *Biochim. Biophys. Acta - Biomembr.* **1980**, *604* (2), 129–158.

(115) Qian, C.; Fu, H.; Kovalchik, K. A.; Li, H.; Chen, D. D. Y. *Anal. Chem.* **2017**, *89* (17), 9483–9490.

(116) El-Hady, D.; Kühne, S.; El-Maali, N.; Wätzig, H. *J. Pharm. Biomed. Anal.* **2010**, *52* (2), 232–241.

(117) Berezovski, M.; Krylov, S. N. *J. Am. Chem. Soc.* **2002**, *124* (46), 13674–13675.

(118) Penny, W. M.; Steele, H. B.; Ross, J. B. A.; Palmer, C. P. *Electrophoresis* **2017**, *38* (5).

(119) Escuder-Gilabert, L.; Martínez-Pla, J. J.; Sagrado, S.; Villanueva-Camañas, R. M.; Medina-Hernández, M. J. *Journal of Chromatography B: Analytical Technologies in the Biomedical and Life Sciences*. 2003, pp 21–35.

(120) Awadallah, B.; Schmidt, P. C.; Wahl, M. A. *J. Chromatogr. A* **2003**, *988* (1), 141–149.

(121) Baciu, T.; Botello, I.; Borrull, F.; Calull, M.; Aguilar, C. *TrAC - Trends Anal. Chem.* **2015**, *74*, 89–108.

(122) Zeisbergerová, M.; Řemínek, R.; Mádr, A.; Glatz, Z.; Hoogmartens, J.; Schepdael, A. Van. *Electrophoresis* **2010**, *31* (19), 3256–3262.

(123) Langmajerová, M.; Řemínek, R.; Pelcová, M.; Foret, F.; Glatz, Z. *Electrophoresis* **2015**, *36* (11–12), 1365–1373.

(124) Arnett, E. M.; Gold, J. M.; Harvey, N.; Johnson, E. A.; Whitesell, L. G. *Adv Exp Med Biol*. 1988, pp 21–36.

(125) Mehvar, R.; Brocks, D. R.; Vakily, M. *Clin. Pharmacokinet.* **2002**, *41* (8), 533–558.

(126) Rainier, S.; Jain, M. K.; Ramirez, F.; Ioannou, P. V.; Marecek, J. F.; Wagner, R. *BBA - Biomembr.* **1979**, *558* (2), 187–198.

(127) Ishigami, T.; Suga, K.; Umakoshi, H. *ACS Appl. Mater. Interfaces* **2015**, *7* (38), 21065–21072.

(128) Okamoto, Y.; Kishi, Y.; Ishigami, T.; Suga, K.; Umakoshi, H. *J. Phys. Chem. B* **2016**, *120* (10), 2790–2795.

(129) Lalitha, S.; Sampath Kumar, A.; Stine, K. J.; Covey, D. F. *J. Supramol. Chem.* **2001**, *1* (2), 53–61.

(130) Lalitha, S.; Kumar, A. S.; Covey, D. F.; Stine, K. J. *Chem. Commun.* **2001**, No. 13, 1192–1193.

(131) Mannock, D. A.; McIntosh, T. J.; Jiang, X.; Covey, D. F.; McElhaney, R. N. *Biophys. J.* **2003**, *84* (2), 1038–1046.

(132) Slotte, J. P. *Progress in Lipid Research*. 2013, pp 424–437.

(133) Nyholm, T. K. M.; Nylund, M.; Slotte, J. P. *Biophys. J.* **2003**, *84* (5), 3138–3146.

(134) Nakamura, H.; Wakita, S.; Yasufuku, K.; Makiyama, T.; Waraya, M.; Hashimoto, N.; Murayama, T. *J. Cell. Biochem.* **2015**, *116* (9), 1898–1907.

(135) Ramstedt, B.; Peter Slotte, J. *Biophys. J.* **1999**, *77* (3), 1498–1506.

(136) Li, X.-M.; Smaby, J. M.; Momsen, M. M.; Brockman, H. L.; Brown, R. E. *Biophys. J.* **2000**, *78* (4), 1921–1931.

(137) Billiot, E.; Macossay, J.; Thibodeaux, S.; Shamsi, S.; Warner, I. M. *Anal. Chem.* **1998**, *70*, 1375–1381.

(138) Henriksen, J. R.; Etzerodt, T.; Gjetting, T.; Andresen, T. L. *PLoS One* **2014**, *9* (3).

(139) Elmer-Dixon, M. M.; Bowler, B. E. *Biochemistry* **2017**, *56* (36), 4830–4839.

(140) Lei, H.; Bowler, B. E. *Journal of Inorganic Biochemistry*. 2018.

(141) Pandey, S.; Redden, R. A.; Hendricks, A. E.; Fletcher, K. A.; Palmer, C. P. *J. Colloid Interface Sci.* **2003**, *262* (2), 579–587.

(142) Akagi, T.; Piyapakorn, P.; Akashi, M. *Langmuir* **2012**, *28* (11), 5249–5256.

(143) Klymchenko, A. S. *Acc. Chem. Res.* **2017**, *50* (2), 366–375.

(144) Petit-Agnely, F.; Iliopoulos, I.; Zana, R. *Langmuir* **2000**, *16* (25), 9921–9927.

(145) Pal, P.; Zeng, H.; Durocher, G.; Girard, D.; Giasson, R.; Blanchard, L.; Gaboury, L.; Villeneuve, L. *J. Photochem. Photobiol. A Chem.* **1996**, *98* (1–2), 65–72.

(146) Remko, M.; Broer, R.; Remková, A. *RSC Adv.* **2014**, *4* (16), 8072–8084.

(147) Østergaard, J.; Heegaard, N. H. H. *Electrophoresis* **2003**, *24* (17), 2903–2913.